UNIVERSIDAD DE CHILE
FACULTAD DE CIENCIAS FÍSICAS Y MATEMÁTICAS
DEPARTAMENTO DE GEOLOGÍA

FLUIDOS MINERALIZANTES DEL DISTRITO MINERO ALHUÉ, CHILE.

TESIS PARA OPTAR AL GRADO DE MAGÍSTER EN CIENCIAS, MENCIÓN GEOLOGÍA

ANDRÉS ROBERTO GÓMEZ GAJARDO

PROFESOR GUÍA
DANIEL MONCADA DE LA ROSA

MIEMBROS DE LA COMISIÓN
CLAUDIA CANNATELLI
GREGORY DE PASCALE
STEPHEN MATTHEWS

Este trabajo ha sido financiado por los Proyectos Fondecyt de Iniciación N. 11170210, y Núcleo Milenio Trazadores de metales NC130065

SANTIAGO DE CHILE
2019

RESUMEN DE LA TESIS PARA OPTAR AL GRADO DE:
Magíster en Ciencias, Mención Geología.
POR: Andrés Roberto Gómez Gajardo
FECHA: 13/05/2019
PROFESOR GUÍA: Daniel Moncada De la Rosa

FLUIDOS MINERALIZANTES DEL DISTRITO MINERO ALHUÉ, CHILE.

El distrito minero de Alhué se ubica en la cordillera de la Costa de la región central de Chile, en donde secuencias estratigráficas Jurásicas y Cretácicas forman un cinturón norte-sur reconocible en la región central del país. Las estructuras mineralizadas reconocidas en el distrito están hospedadas en andesitas y tobas con un claro control estructural y siguiendo orientaciones preferenciales. Las estructuras tienen leyes promedio de 5 ppm de oro (Au) y 23 ppm de plata (Ag) acompañadas de metales base y conformando un ejemplo clásico de depósito hidrotermal relacionado a ambientes mesotermales con pulsos epitermales proveyendo un laboratorio natural en relación a estudios de inclusiones fluidas, paragénesis mineral y texturas minerales. Existe una gran variación interna en T_h y salinidades observadas a toda escala: desde distrital a muestra de mano, que debe estar reflejando la gran variabilidad de procesos y componentes geoquímicos actuando en la zona de estudio. Evidencias de mecanismos de ebullición y vaporización fueron encontradas en las tres zonas en estudio: Maqui, Lorena y Chilco pero estos pueden no ser los únicos mecanismos participando en la precipitación de metales. El uso de espectroscopía RAMAN y LA-ICP-MS en laboratorios de Virginia Tech permitió una mejor caracterización de la composición del fluido y la paregenesis mineral. La presencia de oro (hasta 3.8 ppm) y plata (hasta 1424 ppm) en IF ricas en vapor hospedads en cuarzo y ricas en líquido hospedads en esfalerita implica que el oro está siendo trasnportado como complejo clorurado y/o sulfurado dependiendo de la estructura mineralizada en cuestión. Estimaciones de la presión obtenidas mediante RAMAN en IF ricas en vapor (3.1 – 61.4 bars) confirman la importancia de intensas despresurizaciones en ciertos sitios estructurales (jogs dilatacionales por ejemplo) con respecto a la precipitación de metales en el distrito minero de Alhué.

A mis ancestros y abuelos…

A Treng-Treng filu y Kay-Kay filu…

AGRADECIMIENTOS

Este trabajo ha sido financiado parcialmente por Yamana Gold Ltd., Fondecyt de Iniciación concedido a D. Moncada en el marco de los proyectos Fondequip EQM140009, FONDECYT N° 11170210 y Núcleo Milenio Trazadores de Metales NC130065.

Agradezco en primer lugar a los miembros de la comisión del presente trabajo de tesis, Dr. Daniel Moncada, Dr. Stephen Matthews, Dr. Gregory De Pascale y Dra. Claudia Cannatelli. Gracias por la oportunidad de dejarme participar en sus proyectos, aprendí mucho de ustedes.

Agradezco a la compañía Minera Yamana Gold y a Minera Florida, especialmente a Mauricio Durán, Jacqueline Harris, Steve Matthews, Pedro Mundaca, Cristian Calderón, Hugo Gonzalez, Miguel Pérez, Patricio Castro, Macarena Flores, Ricardo Ríos, Leonel Contreras, Enrique Manzor. Ha sido un honor conformar parte de tan bello equipo.

Y por sobre todo, a mi familia y amigos.

TABLA DE CONTENIDO

ÍNDICE DE TABLAS

ÍNDICE DE FIGURAS

CAPÍTULO 1

INTRODUCCIÓN

1.1 Presentación

En la región central de Chile, entre los 32° y 35° 20’ de latitud sur, es posible encontrar afloramientos de la cordillera de la costa chilena, en donde secuencias estratificadas de origen principalmente volcánico y sedimentario y de edades Jurásicas a Cretácicas forman cinturones norte-sur debido a la progresiva migración del arco magmático hacia el este y en donde se alojan franjas metalogénicas de gran importancia para la región central del país.

A diferencia de las zonas más nortinas de Chile, la información geológica de la zona central de Chile es considerablemente menor, las cubiertas vegetales y arcillosas, la falta de mapas geológicos y públicos de detalle, la presencia de urbanizaciones y cultivos y en general, el relativo poco interés en la investigación metódica de la región, llevan a desestimar el potencial minero del sector (Gropper, 2011).

El distrito minero de Alhué, que inició sus actividades mineras en 1739 (Iglesias Patrimoniales, 2014) y las continua hasta el día de hoy, está precisamente emplazado en rocas estratificadas de la cordillera de la costa de la región central de Chile y representa un depósito de oro y plata de origen hidrotermal, siendo un laboratorio natural para el estudio de la formación y génesis de este tipo de yacimientos. Durante los últimos cincuenta años, se ha incrementado exponencialmente la exploración a nivel mundial de yacimientos polimetálicos y por tanto también aquellos yacimientos de origen hidrotermal que contengan mineralización de metales preciosos, desarrollándose nuevas técnicas de exploración en pos de encontrar nuevos yacimientos. Numerosos estudios de inclusiones fluidas de depósitos de mena se han realizado desde entonces, y mucho del entendimiento del transporte de metales en fluidos hidrotermales y precipitación mineral a partir de ellos se ha adquirido desde estos estudios. El estudio de los ambientes geológicos relacionados a la mineralización ha evolucionado para mejorar las herramientas de exploración de yacimientos en parte porque mientras mejor se conozca como se forman los depósitos, mejor sabremos donde buscarlos (Roedder, 1984). Durante las últimas décadas ha habido numerosos estudios de fluidos e inclusiones fluidas tanto en sistemas geotermales terrestres activos como en sus equivalentes fósiles (Roedder, 1984; Hedenquist et al., 2000; Simmons et al., 2005). El entendimiento de la naturaleza de los fluidos, desde el estudio de inclusiones fluidas, texturas y paragénesis mineral presentes en los cuerpos de mena podrían

proveer una herramiento poderosa para testear nuevos targets y por lo tanto ahorrar dinero y tiempo a las compañías relacionadas a esta actividad.

La presencia o ausencia de ciertos mecanismos de precipitación de metales preciosos, como la ebullición o la vaporización, pueden ser observadas a temperatura ambiente usando un microscopio óptico y conociendo la petrografía de inclusiones fluidas y texturas minerales comúnmente asociados a estos mecanismos. La ebullición, o la inmiscibilidad de fluidos es comúnmente asociada a la deposición de metales preciosos y podría controlar la distribución mineral de un sistema (Buchanan, 1981; Vikre, 1985; Brown, 1986; Clark and Williams-Jones, 1990; Hedenquist et al, 2000; Simmons et al., 2005). Debajo del horizonte de ebullición, muchos sistemas se caracterizan por ser estériles, con un contenido de metales bajo (o ausente), mientras que por sobre este nivel, los metales preciosos tienden a ser más comunes. (Buchanan 1981, Cline et al. 1992, Hedenquist et al. 2000, Moncada et al., 2012).

Dado que los mecanismos de ebullición y/o vaporización son muy importantes en términos de desestabilizar la solubilidad de oro en un fluido hidrotermal (y hacerlo precipitar en respuesta a esto) y dado que la evidencia de estos procesos es relativamente fácil de observar mendiante la utilización de un microscopio óptico convencional, el objetivo de tesis esta relacionado al estudio de los mecanismos activos que influenciaron los fluidos hidrotermales del distrito minero de Alhué. Además, con esta tesis se pretende averiguar si estos mecanismos, comúnmente observados en otros depósitos minerales a nivel global, como son los de ebullición y vaporización pueden ser efectivamente observados, documentados y estudiados en las muestras del distrito.

En este estudio, se revisa la configuración geológica del distrito minero Alhué dando énfasis en las características mineralógicas, texturales y de inclusiones fluidas que proveen mayor evidencia a la presencia de fluidos que efectivamente tuvieron ebullición y/o vaporización en el distrito.

Este trabajo de tesis consta de cinco capítulos principales: una introducción general, seguido de la metodología empleada en cada etapa del trabajo, un artículo científico titulado *Revealing mineralized structures from the Alhué mining district using fluid inclusion and mineral textures*, en donde se integran y discuten los resultados petrográficos de fases y texturas minerales en conjunto con la petrografía y microtermometría de inclusiones fluidas, química de los fluidos mediante la utilización de LA-ICP-MS y reconocimiento de fases volátiles y sólidas en los fluidos mediante la utilización de espectroscopía RAMAN, además de la discusión de los resultados obtenidos. El último capítulo de esta tesis muestra las conclusiones del trabajo realizado.

1.2 Objetivos

1.2.1 Objetivos generales

El objetivo general del presente trabajo es entender los mecanismos de precipitación de metales preciosos y base en el distrito minero de Alhué y las características físico-químicas de los fluidos participantes en la génesis del yacimiento.

1.2.2 Objetivos específicos

1. Determinar la mineralogía de alteración, ganga y mena para cada estructura mineralizada en estudio (Maqui, Lorena y Chilco) con el fin de establecer una secuencia paragenética tanto de fases minerales como de FIA.
2. Determinar las T_h y salinidad de FIA propicios para esto mediante el uso de platina Linkam THMSG600 y Linkham TS1400XY.
3. Determinar las concentraciones de elementos relevantes para la mineralización dentro de FIA mediante el uso de LA-ICP-MS.
4. Determinar cualitativamente las fases minerales referentes a cristales hijos dentro de FIA mediante el uso de espectroscopia RAMAN.
5. Determinar cualitativamente fases líquidas y/o gaseosas dentro de FIA y estimar presiones de atrapamiento mediante el uso de espectroscopia RAMAN.

1.3 Hipótesis de trabajo.

En el depósito mineralógico de Alhué existen mecanismos de precipitación de metales preciosos y base que son estudiables mediante el registro de arreglos de inclusiones fluidas y texturas minerales. Estos registros presentan evidencia directa de la naturaleza físico-química de los fluidos que mineralizaron el sistema y por lo tantos de los agentes que participaron en el transporte metálico de los metales. Los mecanismos de precipitación propuestos corresponden principalmente a ebullición, vaporización, enfriamiento y/o mezcla.

1.4 Ubicación y accesos

El distrito minero Alhué está ubicado en la provincia de Melipilla en la Región Metropolitana de Chile, a 145 kilómetros al suroeste de la ciudad de Santiago (Figura 1). Se encuentra entre las coordenadas (UTM-WGS84) 6233280 N - 6237075 N y 315014 E – 317813 E. Su cota altimétrica mínima varía entre los 500 – 2100 msnm. El acceso desde Melipilla se realiza a través de la ruta G-60 en sentido sur-poniente hasta el cruce "Las Arañas", continuando por la ruta G-66 hacia el sur hasta el cruce "Santa Inés" en donde se debe continuar por la ruta G-692 hacia el este en dirección a la Villa Alhué. Una vez alcanzada la Villa Alhué se debe continuar hacia el este por la misma ruta hasta la localidad "El Asiento", desde ahí, continuando por 7 kilómetros se llegará a la quebrada Las Ánimas en donde se encontrará la entrada a la mina. Todas las rutas anteriormente señaladas se encuentran pavimentadas.

Figura 1. Ubicación y vías de acceso al distrito minero Alhué. Modificado de Google Earth – Imagen Landsat.

1.5 Trabajos anteriores

Dentro del área de interés se han realizado diversos estudios, sin embargo, ninguno ha analizado la química de los fluidos mediante las técnicas utilizadas en esta tesis. Los

siguientes trabajos fueron utilizados como material base de apoyo para la realización de este estudio y se consideraron los más influyentes de los trabajos históricos:

Cotton (1998) estudia la geología y mineralización de la veta Maqui. Concluye que los niveles más profundos del sistema hidrotermal corresponden a estructuras de rumbo norte-sur como Maqui. Este tipo de estructura presenta minerales calco-silicatados, magnetita, esfalerita rica en hierro que fueron depositados en una etapa intermedia de alta temperatura y en donde vetas como Pedro Valencia, Cantillana, Circular representan etapas previas de mineralización que ocurrieron a temperaturas levemente menores pero dentro del rango de temperaturas asociadas a depósitos epitermales. Maqui según el autor se habría formado dentro de un amplio rango de temperaturas desde epitermal a condiciones de formación de skarn. Los depósitos de Pedro Valencia y Maqui según Cotton (1998) presentan una temperatura de homogenización promedio de entre 300 y 320°C y la mayor frecuencia de T_h se encuentra entre los 240 y los 400°C. Cotton (1998) concluye que la variación en las T_h y en las asociaciones observadas para cada veta reflejan la diversidad de las condiciones formadoras de mena debido a la larga vida magmática y tectónica en la cordillera de la costa.

Araya (2001) presenta un informe geológico y una evaluación de recursos del distrito minero Alhué donde destaca que la mineralización de las vetas, además de Au y Ag, corresponde a pirita, magnetita, menor blenda, galena, óxidos de manganeso y escasa calcopirita. La mineralización de oro según Araya (2001) ocurre como electrum atrapado en cuarzo, libre y asociado a sulfuros. También comenta que los minerales de alteración consisten en cuarzo-adularia-epidota-clorita-actinolita a los que se sobreimponen esmectitas-calcita-caolinita-granate. Araya (2001) efectuó un estudio de inclusiones fluidas en dos vetas del distrito. Para la primera veta obtuvo un rango de T_h entre 218 – 322°C con un promedio de 259°C, y para la segunda obtuvo un promedio de 257°C. Para ambas vetas obtuvo salinidades promedio de 4% en peso de NaCl equivalente.

Sepúlveda (2004) realizó en su memoria de título una caracterización geológica y microtermométrica de la veta Lorena del distrito minero de Alhué. En este trabajo el autor divide la estructura en 3 grandes cuerpos: brecha hidrotermal norte, veta de cuarzo central y brecha hidrotermal sur. Concluye que tanto esfalerita como calcopirita precipitaron de manera contemporánea en el sistema. En términos de inclusiones fluidas, el autor describe

como abundante la presencia de inclusiones fluidas trifásicas y polifasicas y comenta que incluso en algunas muestras conforman el único tipo encontrado. Las salinidades para esta veta muestran un patrón cercano al 45% en peso de NaCl equivalente y 328.7°C de T_h promedio. Las altas salinidades y T_h reportados son atribudas a un sistema epitermal a mesotermal con la posible participación de fluidos de origen magmático. Sepulveda (2004) al igual que otros autores reporta que la amplia distribución de temperaturas de homogenización encontradas en su estudio indican que se está en presencia de un sistema que habría involucrado más de un evento hidrotermal, lo que implica una amplia gama de variaciones químicas de los fluidos hidrotermales.

Poblete (2008) presenta una evaluación de prospectos en donde incluye a los yacimientos mesotermales de Alhué y el Distrito minero Las Palmas y define una franja en transición epitermal-mesotermal vetiforme polimetálica en oro y plata del Cretácico Superior en Chile Central. En su tesis calcula la profundidad bajo la paleotabla de agua a la cual ocurrió ebullición durante condiciones de presión hidrostática y menciona que, infiriendo ebullición para Alhué, la profundidad bajo la paleotabla estimada de ebullición sería de alrededor de 620 metros.

Herreros (2009) realiza una caracterización geológica y microtermométrica de la veta Peumo dentro del distrito. Herreros recalca la dificultad de crear una relación temporal de los diferentes sucesos hidrotermales en la veta debido a la amplia distribución de temperaturas de homogenzación que evidencian una clara sobreimposición de eventos. Sin embargo, Herreros (2009) deduce a partir de sus resultados, tres fluidos de composiciones variables entre 140 a 410°C, con salinidades entre 0.9 a 39% NaCl equivalente y en donde el último fluido podría corresponder a la mezcla de los primeros dos. También destaca que estos fluidos serían introducidos a la roca y canalizados a estructuras de fallamiento de dirección NW y concluye que el origen de la mineralización es hidrotermal con una zonación vertical desde una asociación mineral indicativa de alta temperatura, mesotermal, a un ambiente epitermal.

CAPÍTULO 2

METODOLOGÍA

2.1 Investigación bibliográfica y recopilación geológica.

La etapa inicial de este estudio consistió en una compilación de la información disponible sobre la geología distrital del yacimiento, el estudio detallado de inclusiones fluidas realizado a lo largo de la historia del distrito y la documentación existente en cuanto a la caracterización de otros sistemas estructurales mineralizados que fueron estudiados por autores previos a este estudio.

2.2 Trabajo en terreno.

En colaboración con el equipo de Yamana Gold, 192 muestras fueron recolectadas desde afloramientos en superficie, interior mina y sondajes. La colección de muestras recolectadas se focalizó en especímenes mineralizados (con abundante esfalerita, galena, calcopirita y pirita) y sin mineralización. Las muestras que contenían fases minerales translúcidas como cuarzo y calcita en asociación con mineralización fueron también de especial interés debido a la factibilidad de realizar estudios de inclusiones fluidas en ellas. Fue posible recolectar muestras de superficie de la estructura Maqui, que se encontraba aflorando a una altura de 1150 msnm. En interior mina, las muestras fueron tomadas de los frentes y murallas laterales de las zonas de explotación en donde fue posible. Estas áreas incluyeron los siguientes niveles: 740 msnm para Lorena, 740 and 771 msnm para Maqui. Las muestras de sondajes colectadas corresponden a programas de sondajes perforados desde interior mina y desde superficie en donde se pudo tomar muestras correspondientes a la estructura Chilco.

2.3 Trabajo en Laboratorio

El trabajo en laboratorio se dividió en cinco etapas principales. En primer lugar, se realizó una inspección visual y descripción de cada una de las muestras de mano tomadas en terreno en donde se realizó una selección para la confección de *quickplates* en el laboratorio de cortes de la Universidad de Chile. Se cortaron las muestras en “calugas” de 30x30x20 mm que representaban de buena manera la mineralización de las estructuras mineralizadas y en donde existían fases propicias para el estudio de inclusiones fluidas (principalmente cuarzo y calcita). Luego se realizaron inspecciones visuales de las quickplates construidas para la definición petrográfica de fases minerales, texturas minerales y arreglos de inclusiones fluidas dentro de un contexto paragenético. Aquellas muestras que presentaban FIAs propicios para la realización de estudios microtermométricos fueron seleccionadas

para la realización de cortes doble-pulidos o cortes para inclusiones fluidas. Estos cortes fueron realizados en el laboratorio de cortes de la Universidad de Chile. La microtermometría desarrollada en esta investigación se realizó en el laboratorio de inclusiones fluidas y vítreas (FONDEQUIP N. EQM140009) de la Universidad de Chile mediante el uso de *Linkam THMSG 600 heating/cooling stage y Linkham TS1400XY* montados sobre un microscopio óptico estándar y calibrado en el mismo lugar. Finalmente, análisis LA-ICP-MS y de espectroscopía RAMAN en inclusiones dentro de FIA propicios fueron desarrollados en el laboratorio de investigación de fluidos del departamento de Geo-ciencias en Virginia Tech.

CAPÍTULO 3

REVEALING MINERALIZED STRUCTURES FROM THE ALHUÉ MINING DISTRICT USING FLUID INCLUSION AND MINERAL TEXTURES.

Andrés GÓMEZ-GAJARDO[1,2], Daniel MONCADA[1], Gregory De PASCALE[1], Stephen MATTHEWS[2].

[1] Department of Geology, Facultad de Ciencias Físicas y Matemáticas, Universidad de Chile, Plaza Ercilla 803, Santiago, Chile.

[2] Yamana Gold Inc.

Correspoding author:
Andrés Gómez-Gajardo
Departamento de Geología, Universidad de Chile, Chile
andres.gomezg@yamana.com

ABSTRACT

The surge in precious-metals exploration worldwide has resulted in a greater interest in the study of hydrothermal gold deposits. Fluid inclusions studies have provided much information about the physical and chemical environment of ore deposition, nature of mineralizing fluids and the processes by which mineral deposits formed. The gold, silver and base metal veins found at the Alhué mining district in Chile are a classic example of hydrothermal ore deposits, providing a natural laboratory in terms of fluid inclusions, textures and mineral paragenesis.

In order to characterize the ore-forming fluids and understand the ore precipitation mechanisms that occurred in Alhué, detailed petrographic and textural paragenesis combined with: (i) FIA petrography (ii) microthermometry of FIA (iii) single inclusion microanalysis by laser ablation ICP-MS and (iv) single inclusion microanalysis by RAMAN microspectrometry was performed.

At room temperature and based on their present phases and hosts (calcite, quartz or sphalerite), we identified six types of FIA in relation to the ore stages of Maqui, Lorena and Chilco veins. Petrographic features of mineral textures and fluid inclusions and the relationship between their homogenization temperature and salinity shows that: (i) boiling and flashing mechanisms are a common feature in the three systems but may not be the only ones responsible for precious mineral precipitation (ii) there is wide internal variation in homogenization temperatures (183 to 533°C) and salinities (0.2 to 63 wt% NaCl equiv.) due to the diversity of ore-forming fluids that participated in a relatively long period of time. The fluid chemical data obtained by LA-ICP-MS in liquid-rich and vapor-rich FIA demonstrate that Au (up to 3.8 ppm in fluid inclusions) is being transported as chloride and/or sulfide complexes depending on the system and different fluids can transport it. Pressure estimations ranging from 3 – 61 bars in vapor-rich FIA also confirm the importance of rapid fluid depressurization (or flashing) in the precipitation of precious metals in the veins.

The textural and fluid inclusion data obtained in this study documents the existence of sufficient evidence of features related to boiling and flashing processes that participated in the Au mineralization of the mesothermal polymetallic veins from the Alhué mining district.

3.1 Introduction

During the past half-century, numerous fluid inclusion studies of ore deposits were conducted, and much of our understanding of the physical and chemical environment of metal transport and deposition in hydrothermal environments evolved from these studies. The study of geological environments related to ore deposition developed to aid to mineral exploration in the last few decades in part because the better we know how deposits form, the better we know where to look for them (Roedder, 1984). Understanding the nature of the ore fluids from a study of fluid inclusions, textures and mineral paragenesis present in ore bodies may provide a powerful tool to test new needed targets and thus save time and money to exploration companies related to this activity.

Important ligands for aqueous transport of gold (HS^- and Cl^-) set important facts to the hydrothermal transport of the precious metal in crustal fluids and thus the formation of hydrothermal deposits. Dominant gold species in solution are dependent on temperature and fluid composition so boiling and or cooling became important mechanisms in terms of gold precipitation. In this paper we use the term "boiling" to indicate the presence of two immiscible fluids even when is known that the term "effervescing" is more appropriate for multicomponent systems as natural fluids (Roedder, 1984).

The presence or absence of boiling determines the fluid inclusion types that can be observed at room temperatures using an optical microscope. Boiling or fluid immiscibility is commonly associated with precious metal deposition and may control ore metal distribution in the system (Buchanan, 1981; Vikre, 1985; Brown, 1986; Clark and Williams-Jones, 1990; Hedenquist et al, 2000; Simmons et al., 2005). Beneath the boiling horizon many systems are characterized by higher base metal and lower (or absent) precious metal grades, whereas above the boiling horizon precious metals are more common. The highest gold grades are often found immediately above the boiling horizon (Buchanan 1981, Cline et al. 1992, Hedenquist et al. 2000, Moncada et al., 2012). When a system undergoes an extreme pressure reduction to less than hydrostatic pressure, boiling may occur instantaneously, converting 100% of the original liquid into a low density vapor phase. This type of boiling is referred to as "flashing" (Brown, 1986; Moncada et al., 2012).

In systems where flashing occurs, a high grade (bonanza) zone is more likely at the base of the boiling zone (Moncada et al., 2017). Whereas in systems characterized by more gentle boiling precious metal grades may be lower and distributed over a greater vertical distance above the bottom of the boiling zone, and the highest grades may occur at some distance above the bottom of the boiling zone (Simmons and Browne 2000).

Because boiling and flashing events are highly important in terms of gold precipitation and can be observed easily using an optical microscope, our objectives were to study the active mechanisms that influence the hydrothermal fluids present in the Alhué mining district. Additionally we explore the samples for boiling and flashing fluid inclusion assemblages in terms of temperature, composition, time and occurrence.

In this study, we review the geological setting of the Alhué mining district and summarize the available data that documents the close association between boiling and mineralization. Then, we describe mineralogical, textural and fluid inclusion characteristics that provide evidence for the former presence of boiling fluids in the mineralized structures in the Alhué mining district, Chile, and their variation between each mineralized structure.

3.2 Location and geological setting

3.2.1 Regional Geology

The Alhué mining district is located in the *Región Metropolitana*, 94 km. to the Southeast of the Melipilla and 9 km to the East of Villa Alhué (meaning “Place of spirits” in Mapuche). Mining activity in Alhué started in 1739 with the first gold structures discovered in the zone near the district (Iglesias Patrimoniales, 2014).

The Alhué mining district is located southwest of Chile´s capital city of Santiago within the Coastal Range of Central Chile where Jurassic and Lower Cretaceous stratified sequences form a north-trending belt that can be followed along the entire length of central Chile (SERNAGEOMIN, 1982; Aguirre 1985). Composed mostly (>90%) of volcanic and volcanoclastic rocks, this Coast Range belt have a thickness of 10 to 20 km and is located in the western part of the Andes (Vergara et al, 1995). The stratified deposits overlie Paleozoic-

Triassic basement rocks of predominantly magmatic and/or metamorphic origin (Hervé et al, 1987) and dip 10°-70° to the east forming an homoclinal that becomes younger toward the east reaching the central Valley graben and which is infilled with Quaternary deposits. The rocks are intruded by Mesozoic epizonal granitoids, which also decrease in age toward the east (López-Escobar et al, 1979; Vergara et al, 1995). In the region of 33°S to 34°S three main batholiths found are elongated in a north-south direction. The oldest batholith (Paleozoic) outcrops primarily along the western side of the Coast Range (Muñoz-Cristi, 1964; Corvalán 1974) with ages ca. 290-305 Ma (Hervé et al, 1988), the Central Batholith (Cretaceous) occupies mainly the eastern side of the Coast Range and the Longitudinal Depression, and the youngest Batholith (Tertiary) outcrops in the Andean Cordillera. Therefore, the Coast Range is bordered by the Coastal Batholith on the west and by the Central Valley on the east (Vergara et al., 1995).

3.2.1.1 Stratified Units

Composed mostly of Jurassic to later Cretaceous sedimentary and volcanic stratified sequences which unconformably overlie the Paleozoic basement, the stratified rocks represent the transition from a marine environment (Jurassic) to a continental one (late Cretaceous). Sequences ranges from marine clastic sedimentary rocks with limestone intercalations (early Jurassic), through submarine lavas and tuffs (middle Jurassic) to subaerial lavas and ignimbrites from late Cretaceous (Cotton, 1998). Rocks are affected by regional burial metamorphism of the predominantly prehnite-pumpellyite facies. However, this metamorphism is weak in many places that correspond to the lower sequences (Levi, 1969, Levi et al., 1989). Figure 1 shows the regional geological map of the area. Table 1 summarizes the generalized Jurassic to late Cretaceous lithostratigraphic column for the Coast Range of Central Chile.

From oldest to youngest stratified formations shown in Table 1: The Cerro Calera Formation (Middle Jurassic: Aalenian – Bajocian) was defined by Piracés (1976) as a group of marine sedimentary rocks. This unit corresponds to polymictic conglomerates, well-bedded and well sorted volcaniclastic sandstones and siltstones, with minor intercalations of limestone. Local interlayered tuff and basic lavas flows can be found in the central part of the formation. In the cental part of the formation interlayered tuff and autoclastic basic lava

flows are present. The top of the unit is marked by well-sorted, cross-laminated sandstone, which is overlain by the Horqueta Formation. The thickness of the sequence is approximately 760 m south of the Maipo River (Nasi and Thiele, 1982). The unit dips between 30 and 50° to the east and outcrops as an oval body from the locality of Cholqui to Cajón del Rey with a NNE-SSW to N-S strike.

The Aalenian to early Bajocian age (187-180 Ma) of the Cerro Calera Formation was determined by the presence of ammonoid fossils that indicate a late Aalenian age (Nasi and Thiele, 1982).

The Horqueta Formation (Middle to Upper Jurassic: post Bajocian – pre Berriasian) as first interpreted by Thomas (1958) and later modified by Piracés (1976). It corresponds to a group of greenish gray volcanic and volcanoclastic rocks. It is composed principally of basic to intermediate lavas and brecciated andesites. It has intercalations of sedimentary rocks including polymictic conglomerates, well-bedded and well-sorted volcanoclastic sandstones and siltstones, with minor limestone and shales. It conformably overlies the Cerro Calera Formation and underlies Lo Prado Formation in the same way. It is dominated by acid lavas and minor ignimbrites in its lower part and red continental volcanic rocks (breccias, sandsotnes, and subordinate siltstones with mud cracks) in its upper part. Total thickness of the Horqueta Formation in the Cordón de Culiprán area is 4300 m. The sequence dips to the east between 22° to 60° (Nasi and Thiele, 1982).

The Lo Prado Formation (Lower Cretaceous: Berriasian - Hauterivian) interpreted by Thomas (1958) the Lo Prado Formation is separated from the Jurassic units by an unconformity (Carter, 1963). It is divided into a lower marine sedimentary member and an upper, alternately marine and terrestrial member. The lower member is composed of conglomerates, greenish gray graywackes, siltstones and limestones. The upper member consists of alternately marine and continental sedimentary rocks with voluminous volcanic intercalations of bimodal chemistry: acid ignimbrites and subordinate basic lavas (Nasi and Thiele, 1982). The Lo Prado Formation outcrops as a NNW-SSE to N-S belt in the Estero Cholqui till 15 km north of Villa Alhué (Figure 1) It conformably overlies Horqueta Formation and underlies Veta Negra Formation in the same way. Thickness is in the range of 2500 to 6300 m. The age of the Lo Prado formation is considered to be Neocomian due to

the presence of certain ammonites and some pelecypods The lower part of the formation is assigned a Valanginian age (138-131 Ma) and the upper part is assigned a Hauterivian age (131-124 Ma) (Vergara et al., 1995).

Originally defined by Thomas (1958), Veta Negra Formation (Lower Cretaceous: Barremian - Aptian) is composed of a thick sequence of basic to intermediate and acidic lava flows erupted in a continental environment. The lavas typically have very large phenocrysts of plagioclase (up to 3 cm) and pyroxene (up to 1 cm) (Cotton, 1998). Andesites with this kind of phenocrysts (ocoites) intercalated with skarnificated limestones can be observed to the northwest of the Alhué mine. Intercalations of sandstones occur between lava flows. Strongly autobrecciated lavas with a sandstone matrix, hyaloclastitic breccias, and peperites occur in the lowermost part of this formation, suggesting deposition under water or on wet sediments (Vergara et al., 1995). The sequence form a homoclinal ridge with a dip of 20 to 40° to the east and NE-SW strike. The thickness of this unit ranges from 5000 to 15000 m. No fossil records have been found to constrain the age of this unit. However, plagioclase separated from a flow in the middle part of the formation gives K-Ar age of 105 Ma (Vergara and Drake, 1979a). The age is bracketed by the age of the underlying Lo Prado Formation (~124 Ma) , and the minimum age is given by the position in the stratigraphic column under Las Chilcas Formation meaning that the minimum age cannot be less than Aptian (Cotton, 1998).

The Alhué mineralization is located in Las Chilcas Formation (Lower Cretaceous Aptian – Albian) composed of volcanic sequences interlayered with scarce continental sediments. The tuffs are intercalated by andesitic and basaltic lava flows. Rhyolitic tuff is mainly composed of pyroxene, biotite, sanidine, quartz and it is associated with pyroxene andesites and fluvial and lacustrine sediments that make up the formation at this latitude. Magma/wet sediment interaction forming peperite complexes are also common. Crystal Tuff represent the filling of a caldera, with a probable graben geometry. While mega-breccias (with up to 3 meters clasts) may be related to the collapse of the caldera (Matthews, S. 2018). No formal stratigraphy has been reported due to its lateral variation, lack of geochronological data and a complex structural architecture. However, four clear units have been described locally in the Alhué mining district. This sequence is about 1000-1.500 m thick and is

concordantly overlying Veta Negra Formation. Traditionally, this sequence was attributed to the Lo Valle Formation (Thomas, 1958). However, new ages from by U-Pb (zircons) in tuffs indicate 110.5±0.9 Ma (Alhué) and 110.3±1.0 Ma (Cuesta Rancagua). Ar/Ar dating in amphibole from a dacitic clast of a conglomerate in "La Culebra" indicates an age of 106.3±1.0 Ma (Matthews S., 2018). These results show a relation with an Aptian to Albian age for the sequence. Near the district, Selles and Gana (2001) and Selles (2000) obteined U-Pb ages of 110.5 ± 0.5 Ma and 116.1 ± 0.4 Ma in extrusive rocks and they attributed the results to the Las Chilcas Formation. Other ages were reported to the south (Malbrán, 1986; Emparán and Furukawa, 1985) confirming a regional character of the sequence. To the North, Lo Valle Formation overlies the Las Chilcas Formation with an angular discontinuity. In conclusion, the Las Chilcas Formation is related to the Alhué mining district and it is not correct to associate the mineralization with rocks from the Lo Valle Formation (Matthews S., 2018).

Thomas (1958) reported the Lo Valle Formation (Upper Cretaceous) as a sequence principally composed of tuffs and dacitic lavas. The Lo Valle Formation contains up to 300 m of conglomerates and sandstones and 3000 m of acid to intermediate tuffs and intermediate to basic lavas. The Lo Valle Formation represents the beginning of a pure continental environment (formations that underlie the Lo Valle Formation, even though they are dominated by volcanic successions, contain significant intercalations of marine sedimentary rocks). The stratigraphic sequence outcrops as a NW-SE belt with a 20 to 26° dip to the east (Thomas, 1958). The thickness range between 750 to 3500 m. It unconformably overlie the Las Chilcas Formation to the north of the area.

The minimum age of the volcanic rocks of this formation was thought to be Late Cretaceous, due to the K-Ar date of 82 ± Ma in granodiorite that intrudes the formation south of Laguna Aculeo (Vergara and Drake, 1979b). To the east of Central Valley, the base of the Lo Valle Formation, which lies unconformable above the Las Chilcas Formation, has an $^{40}Ar/^{39}Ar$ age of 72.4 ± 1.4, 71.9 ± 1.4, 71.4 ± 1.4 (Gana and Wall, 1997). The previous ages are supported by an K-Ar (plagioclase) age of 70.5 ±2.5 Ma for this unit (Vergara and Drake, 1978).

3.2.1.2 Intrusive igneous rocks

The Central Batholith occupies mainly the eastern side of the Coast Range and the Longitudinal Depression. It generally decreases in age to the east although this is an oversimplification due to the multiple magmatic episodes that formed the batholith during the Cretaceous. Here, two major plutonic complexes from the Jurassic and Cretaceous intrude the stratigraphic sequences of the Coast Range. Cretaceous granitoids, which are more relevant to this study, have ages between 107 and 82 Ma, and host several Au and Cu deposits, including numerous structures in the Alhué district. Both the Jurassic and Cretaceous granitoids are of calc-alkaline affinities and range in composition from granite to gabbro, with granodiorite and monzogranite being the most dominant lithologies (Cotton, 1998). Two intrusive bodies are present in the Alhué mining district: the Tantehue and the Alhué granitoids.

Nasi (1981) reports the Tantehue granitoid which outcrops can be found in the locality of Tantehue to the west, in the locality of the Los Guindos to the south and near the Cerro Talhuén to the north (Figure 1). This unit is composed of coarse grain pink granite, it is strongly weathered and shows granular, hipidiomorphic holocrystalline textures. Following Streckeisen (1976), the Tantehue granitoid corresponds to a hololeucocratic monzogranite, characterized by an intense silicification and chloritization and is commonly in contact with volcanic rocks of the Horqueta Formation. According to Nasi (1981) this unit is older than granites and granodiorites of the Alhué granitoid, having a middle Jurassic to upper Jurassic age. K/Ar dating in biotite from intrusives close to the Tantehue locality suggest ages of 163 ± 3 (Wall et al., 1996).

The Alhué granitoid is present in the southwestern portion of the regional area (Figure 1). It outcrops between the locality of the Chancón to the east and the locality of the El Asiento to the west. It corresponds to monzogranites and diorites. Microscopically shows a porfiric to equigranular texture with a fine to medium gran size and greenish to pale gray color. It is in contact with Cerro Calera, Horqueta, Lo Prado, Veta Negra and Lo Valle formations. The oldest intrusive rocks in the batholith are monzogranites from the Agua Frias ravine. $^{40}Ar/^{39}Ar$ dating of biotite gives an age of 107.24 ± 0.62 Ma (Cotton, 1998) (Figure 1). Intermediate K-Ar ages of 95-92 Ma were obtained in granodiorites and tonalities near

Pichi valley further west (Wall et al, 1996). Discrepancy of ages shown in Figure 1 for this unit may be due to the alteration of biotite to chlorite and the replacement of hornblende for biotite. The younger $^{40}Ar/^{39}Ar$ age in horblende may also be due to either resseting by the 82 Ma dikes in the area and/or by later uplift. In addition, actinolite alteration of hornblende would produce a younger age (Cotton, 1998).

Despite the differences in apparent ages, the mineralogy of the batholith is relatively consistent, ranging from quartz monzodiorite to monzogranite. Fine-grained equigranular textures dominate, suggesting that the intrusions cooled quickly in an epizonal environment. The Early-Mid Cretaceous magmatic episodes, which are generally of felsic to intermediate composition, were followed by widespread intrusion of andesitic to basaltic dikes around 82 Ma. These dikes range in size from diminutive fingers to large subvolcanic bodies that reach sizes of 1 km wide by 8 km long (Figure 1). These are the youngest igneous rocks in the district intruding all other geological units. These dikes possibly are feeder dikes for the relatively mafic basaltic andesites at the top of the stratigraphic sequence.

3.2.2 Local Geology

The oldest rocks in the district are the lower Cretaceous marine and continental volcanic and sedimentary rocks of Lo Prado Formation. This formation is located in the western margin of the district and is unconformably overlain by the younger tuffs, andesites and volcanic-derived sandstones and conglomerates of the Las Chilcas Formation (Matthews, S. 2017). The volcanic rocks in the district are intruded by, and form roof pendants above Cretaceous granitoids (monzogranite to quartz monzodiorite in composition, generally granodiorites) of the Alhué batholith. All rocks and structures in the district are cut by younger andesitic to basaltic subvolcanic dikes of upper Cretaceous age (83 ± 4 Ma). The age of the mineralization is bracketed by the age of the youngest mineralized granitoids (92 ± 2 Ma) and by the post-mineral subvolcanic dikes (83 ± 4 Ma). The majority of mineralization occurs in quartz-filled structures within andesitic lavas and trachytic tuffs and breccias (Cotton, 1998).

3.2.2.1 Stratified Sequences

The Las Chilcas Formation consist of tuffs with andesitic and basaltic lavas and continental sediments intercalations. It has important lateral variations and no complete geochronological data together with a complex structural architecture make it hard to understand. However, five basic lithologic units can be identified in the Alhué district for this unit (Figure 3). In general, the sequences are in an homoclinal ridge with variable strikes in the range of N30ºE and N30ºW and dips of 20 to 30º E. From oldest to younger ones:

1) The basal lithic-crystal tuff forms the base of the stratigraphic sequence in the Alhué district (Figure 3). Exposed outcrops are present in the southern and western margins of the district. The base of this suite is intruded by granitoids of the Alhué batholith, and has a minimum thickness of 230 m. it is presented as a N-S strike stripe. The groundmass is greenish and glassy with fragments of plagioclase, quartz and k-feldspar indicating an andesitic to dacitic composition. Clasts are composed of andesite and crystalline tuff fragments, and generally 0.3 to 10 cm in diameter. Lenticular outcrops of brecciated tuffs are described in the northwestern part of the Quebrada Las Ánimas as part of this unit (Romero and Mundaca, 1997). It is <10 m wide and present <100 m lateral extension. The gray-greenish groundmass is composed of orthoclase, plagioclase, tuff and andesitic fragments. Porphiric and aphanitic andesites and tuffs form clasts that reach up to 30 cm long.

2) The lower Andesite is described as andesitic to basaltic lavas lies conformably above the lithic-crystal tuff and in the same way below the tuff unit (Figure 3). It is present throughout the district with a relatively constant thickness of approximately 390 m, and can be described as a massive flow of porphyritic andesite (Romero and Mundaca, 1997). Neither individual flows, nor small-scale differences in texture or grain size are distinguishable in the field (Cotton, 1998). Lavas show a dark gray with a greenish tint due to regional propylitic alteration. Phenocrysts of plagioclase (10-20%) are between 0.5 to 4 mm in diameter and are locally altered to epidote, chlorite and montmorillonite. Phenocrysts of pyroxenes (2-5%) are highly altered to chlorite. Aphanitic groundmass (80-90%) is composed of plagioclase and ferromagnesian minerals containing disseminated pyrite and magnetite also. Moderate to strong propylitic alteration and silicification affect groundmass.

3) The main Tuff and sedimentary unit consist in a few rhyolitic tuffaceous lithological series next to some sedimentary sequences belong to this unit (Figure 3). It has a

variable thickness of 400 to 600 m in the Alhué district and is composed of several different grain sizes with different degrees of welding, including ash tuff, lapilli tuff, and breccia tuff. The more strongly welded tuffs are generally more felsic than the other rock types (Cotton, 1998). Outcropping as a belt of 4.5 km long it overlies conformably above the lower andesites and its below a sedimentary sequence showing intercalations in both roof and base (Herreros, 2009). In general, tuffs show pinkish gray color with moderate to strong propylitic alteration and silicification defined by chlorite, epidote and silica. Argilization is weak. Diseminated pyrite can be found in this part of the sequence.

4) Sedimentary levels with variable thickness between 3 to 20 m are described for the upper part of this unit (Figure 3). Intercalations exists with both, tuffs from the lower part of the unit and andesites with the upper andesites younger sequence. Showing red dun to purple colors the sedimentary level is composed of sandstones and conglomerates of volcanic origin. The thickness of the unit vary between 3 and 20 m. Shales are also present reaching thicknesses of 10 m.

5) The Upper Andesites unit is located in the northeastern part of the district. Basaltic and andesitic lavas with N-S strike belt shape. It lies conformably above the main tuff and sedimentary unit. its roof is the current erosion surface and its thickness is at least 500 m. it is composed of two lithological types. The basal one is a 10 to 50 m thick sequence of porphyritic andesite with amphibole fenocrysts. Groundmass (94%) is micro-phaneritic with gray greenish color. Diseminated magnetite and scarce epidote-quartz veins are described (Herreros, 2009). The upper part is a porphyritic andesite that lies conformably above the previous sequence. It has a black color and its plagioclase and amphibole phenocrysts represent 30% of total volume. Groundmass (70%) is micro-phaneritic and black. Diseminated magnetite can also be found. At its base, several peperites can be observed due to the interaction of wet sediments (underlying sandstones, Figure 3) and lava flows of this unit.

The Quaternary deposits found here is composed of colluvium and alluvium. It has variable thickness with a 10 to 25 m maximum value. Colluvium is present at higher altitudes and on steep slopes. The grain size is large. Whereas alluvium is found in all ravines and

valleys, with rounded pebbles and boulders composed of all stratigraphic units found in the area.

3.2.2.2 Intrusives

The stratified rocks are intruded by the already mentioned Central Batholith which was divided into two major intrusive bodies, Tantahue (Middle to Upper Jurassic) and Alhué (Upper Cretaceous) granitoids (Nasi, 1981). Five important intrusive bodies were recognizes locally in the area (Matthews, S. 2017):

To the west of the Alhué mine the Agua fría pluton body in fault contact with Las Chilcas Formation (i.e. Boundary Fault, Figure 2). It is made up monzodiorite, quartz monzonite and pyroxene and biotite monzogranites. Mixing and pegmatitic textures can be observed in outcrops. It has a 108.2 ± 1.0 Ma U-Pb age in zircons (Matthews, S. 2018). Ar-Ar age of 107.2 ± 0.6 Ma and a K/Ar age of 104 ± 3 Ma (Cotton, W.B. 1999) are also reported and may be related to late alteration events of the pluton. It is cut by rhyolitic and andesitic dykes corresponding to Upper Cretaceous (early), key feature to recognize this unit. Agua Fría intrusive body may represent the magmatic chamber of the sequence related to Las Chilcas Formation (Matthews, S., 2018).

Several minor intrusives can be recognized in the width whole area after the Las Chilcas Formation and Agua Fría Pluton. Sills and dykes between 50 cm and 5 m width and hundreds of meters long are also present. There are two types of rhyolites in the area; porphyritic and aphanitic. A big rhyolitic dyke intruding the Las Chilcas Formation in “La Culebra” sector has been dated obtaining an age of 108.9 ± 0.8 Ma while another dyke intruding Agua Fria Puton shows an age of 102.6 ± 1.0 Ma. (Matthews, S., 2017).

Andesitic and dacitic flats: Numerous sills and dykes with basaltic, andesitic and dacitic compositions also intrude the Lower Cretaceous units. Sills can reach up to 30 m width and can be found typically along low angle extensional faults. An Ar/Ar analysis (sericite) in a ductil deformation zone corresponding to an andesitic sill in the El Membrillo showed an age of 88.2 ± 0.3 Ma (Matthews, S. 2017). This result is considered the best age estimation to these bodies.

Talamí Pluton is a tabular body from the upper part of the upper Cretaceous. It has variable width ranging from 100 to 700 m. It is composed by pyroxene and biotite monzodiorites with scarce hornblendes after pyroxenes. The second, Antena intrusive complex is composed by pyroxene, horblende and biotite quartz diorites and horblende and biotite granodiorite. Monzonites, monzodiorites, gabbros and tonalites are also observed. Ar/Ar ages (in biotite, hornblende and k-feldspar) and U/Pb ages report ages ranging between 82-85 Ma. Ages for these intrusives are analogous to mineralization ages describe for the Alhué mining district (85-83 Ma) but they do not necessarily correspond to the origin of the fluids due to the nature of the granites: using zircon saturation temperatures, these granitoids where classified as "hot granites" between 800-860°C with probable low water contents. (Matthews, S. 2017).

There are also sills and dykes related to aphanitic basalts spacially related to mineralized zones and temporally after minerlization events. The second andesites and hornblende porphyritic basalts (lamprophyres) with hornblende-gabbro xenoliths interpreted as restites. Ar/Ar in amphiboles shows 86.3 ± 0.9 Ma, 83.3 ± 0.6 Ma and 80.6 ± 0.9 Ma in these rocks. (Matthews, S. 2017).

Minor intrusive bodies (dikes) with dacitic composition are located in the southeastern part of the district. There are two major dikes in the area, named Casino and Cadena, they are typically 3-8 meters in width, with a north-trending strikes and dip gently to the east. An Ar/Ar age of 83.3 ± 0,6 Ma is reported for Casino intrusive body (Matthews, S. 2018). In addition, very small dikes (1cm-1m width) intrude the Maqui vein parallel to the structure (Cotton, W.B. 1998; Matthews, S. 2017). All dikes, except for one that is found along the footwall of the Pedro Valencia vein (Dique Sur), intruded after mineralization. Radiometric dating of Casino dike, which intrude the Pedro Valencia – Maqui vein system, gives a whole rock K-Ar age of 83 ± 4 Ma (Cotton, W.B. 1998; Matthews, S. 2017). This can be considered the minimum age of mineralization in the district, since the dike cuts all veins, dikes and rocks in the district. Chilled margins indicate that the country rock was cool when dikes intruded. This give further evidence that subvolcanic dikes are a separate, later magmatic event, probably intruded during a period of waning volcanism in the Coast Range (Cotton,

1998). Hornblende and clinopyroxene-rich Casino dyke has been interpreted as a product of lamprophy-crystal fractionation.

Basalts with no geochronological data are also reported. They show inter-mineral relations and correspond to vesicular olivine sills and dykes of basaltic composition. Geochemistry of these basalts shows higher contents of Co and Cr than cretaceous plutons and no plagioclase fractionation. La/Sm vs SiO_2 relations for these basalts show a lower crustal evolution and show no Eu anomalies (not shown in this study). Some basalts (as the ones related to Arrayan location) contain high concentrations of Ti and do not show negative anomalies of Nb. These basalts were interpreted as within plate basalts and/or island arc tholeiite basalts following ternary diagrams of Ti, Zr and Y from Pearce et al., 1973 (Matthews, S. 2018).

3.2.2.4 Local Alteration

Main alteration styles in the district correspond to strong silicic after an intense propylitic. Also local potasic alteration is present and supergene related to argillic is reported (Romero and Mundaca, 1997). Propylitic alteration spreads in vast zones due to its regional behavior. Gradational contacts can be seen with the no-altered rocks. Chlorite-epidote-calcite-±pyrite is the main association. Andesites and brecciated tuffs are the most common rocks altered by this process. Silicic alteration is the most common alteration. It corresponds to an intense alteration which provoke the replacement of micro-crystalline quartz for crypto-crystalline quartz in lithic fragments and/or matrix of tuffs. Locally is associated with fine euhedral pyrite. It can be observed affecting lithic and crystalline tuffs mainly. Both alterations (propylitic and silicic) increase their degree while approaching to mineralized veins and/or structures (Figure 4).

Very local potassic alteration is found in the upper andesites units. K-feldspar or Adularia is observed in some of the mineralized veins and hydrothermal breccias. Supergene shows a regional behavior (as propylitic) by generating a superficial argilization. Iron and manganese oxides and hydroxides are also present. This argilization can be found down to 30 m where faults, fractures and veins are. In summary, nine types of metasomatic processes has been identify in the district: (1) Potassic: in andesitic rocks, the mineral assemblage of magnetite-

flogopite-plagioclase can be found. Sometimes, flogopite veins are present. This alteration is responsible for the high magnetic susceptibility related to some andesites (Matthews, S. 2017b). (2) Potassic-calcic: Most tuffs, especially crystal tuffs are affected by this kind of alteration related to k-feldspar-quartz-epidote. Replacement of primary magnetite cause decreasing in magnetic susceptibility of the rocks. This kind of alteration is particularly intense around important structures like Agua Fria which has a notorious k-feldspar halo. (3) Sodic to Sodic-Calcic: Intermediate to acidic rocks show strong albitization with minor epidote, actinolite, k-feldspar, calcite, chlorite, hematite. Sodic-Calcic metasomatism is considered as halo of mineralized structures. (4) Propilitic: This alteration forms important halo zones around mineralized structures. Mineral assemblage corresponds to chlorite-epidote-albite-calcite-hematite. There is a continuum between propilitic and sodic-calcic alteration with more or less chlorite and/or albite. This alteration was dated in a breccia (Milenio) using Rb-Sr in chlorite-epidote resulting in 83.7 ± 4.6 Ma (Matthews, S. 2017b). (5) Late calcic: With a mineral assemblage of quartz-calcite-garnet-amphibole (hornblende-actinolite-tremolite) with epidote halos, this event is related to veinlets and expressed around major mineralized structures. Variable ages have been obtained for this event, between 83 and 71 Ma using Ar/Ar method in amphiboles (Matthews, S. 2017b). (6) Phyllic: above mineralized sectors, illite-sericite replacement of tuff`s k-feldspar can be observed. This alteration is more prominent in areas which have been under potassic-calcic processes previously, removing almost all k-feldspar. This alteration is related to the mineralization principal core with a supergene kaolinite-limonite-hematite after quartz-sericite-pyrite assemblages. Sericite Ar-Ar ages in surroundings areas of the Alhué mining district show similarity with principal age of mineralization which is about 83-85 Ma. (Matthews, S. 2017b) (7) Zeolites: Laumontite in veins and fractures together with albite and calcite is very common in the district. This event is considered the latest and the one related with the lowest temperatures. (8) Argillic: smectite and clays related to fault zones with post-mineral movements. No further studies have been conducted in clays due to their irrelevance respect mineralization. (9) advanced argillic: Interpreted as such by the presence of pyrophyllite close to major fault zones (Matthews, S. 2017b). No further studies have been conducted in clays due to their irrelevance respect mineralization.

Minerals formed by metamorphism and hydrothermal alteration shows gradual temperature decreasing reaching epithermal conditions in general. Metamorphism and alteration zones have plumes shapes which are centered in principal fault systems and close to groups of mineralized structures. This idea is sustented in aeromagnetic footages and in reseted geochronological data (Matthews, S. 2018)

3.3 Tectonic history and structural setting

Active tectonics has persisted throughout the history of the Andean margin. Consequently, veins in the Alhué mining district have a fundamental structural control. This tectonic is represented by strong ductile and fragile deformations that affected the district and prepare it for the coming mineralizing fluids creating the resulting gold-rich veins. Thus, the majority of the ore deposits in Alhué are open fillings faults that were formed prior to mineralization. Total displacements of faults associated with larger deposits in the area (e.g. syn-mineral sinistral Maqui´s movement) exceed 200 m. Post-mineral movement along faults is ubiquitous in the district, but the greatest displacement after mineralization occurred along north-trending faults (e.g. post-mineral normal-dextral Maqui´s movement), and along northeast-trending strike-slip and normal faults that are not mineralized (Cotton, 1998).

Romero (1997) identified two main structural systems for the district. The first one corresponds to pre-mineral and syn-mineral faults and the second one is related to post-mineral ones, detailed structural analysis is beyond the scope of this study, but the results of the before mentioned work are summarized below.

The pre-mineral and syn-mineral faults were generated previous and during the hydrothermal system development. They were used as conduits by the mineralizing fluids and thus, nowadays, they are the mineralized structures. Several gold and silver-rich quartz veins have been found in the district (more than 76). These veins have different lengths, widths and metal (Au, Ag, Zn an Pb) contents but all of them are directly linked to faults. The structures used as conduits may have a Lower Cretaceous age (Herreros, 2009). Four systems represent these structures, the first correspond to N 10º - 20º W / 70º - 75º E strike-slip faults. Romero 1997 described this system as the principal one because it controls the majority of the veins in the area and it corresponds to the direction of major veins (e.g. Maqui structure). This direction represent only the 8% of the total number of structures measured,

but it is of great importance for the generation of all faults in the district (Cotton, 1998). They represent first order structures (R Riedel shear) and are synthetic sinistral-normal faults. In terms of length, the up to 1400 m in some cases (e.g. Pedro Valencia Occidental) (Herreros, 2009). The second group is described as N 80º - 90º W / 60º - 85º N-S strike-slip faults with first order Riedel Conjugate (R`), antithetic, dextral-normal slip structures which are related to east-west veins that are shorter than the ones described above reaching lengths of 350 to 400 m (Herreros, 2009). They represent the 43.4% of total structures present. The Predro Valencia, Los Patos and Lorena structures are examples of mineralized systems related to this type of structures. The third type of structures related to N 30º - 40º E / 70º - 75º NW – SE strike-slip faults correspond to 3.7% of the total number of measured structures make up this set (Cotton, 1998). These secondary structures probably are related to rotation of the structural system during a period of compression (Romero, 1997).

Finally, the strike-slip faults with direction N 50º - 60º W / 55º - 75º NE – SW correspond to tensional systems that make up 45% of the structural measurements. Romero (1997) mentioned that veins and/or structures that show this geometry present textural and structural characteristics that are related to tensional stresses. In general, these structures have limited lengths and thicknesses. Examples of this style are veins such as Loreto, Circular, and other small veins along the footwall of the Maqui structure.

The post-mineral faults are distinguishable by their ENE strike and 65º-90º N dips. They have dextral displacements reaching tens of meters. This structural system is considered the last stage in the evolution of the geography of the district. Thus, this system is one that cut, displace and intercept the mineralized structures moving them in a brittle regime (Romero, 1997).

There is an ENE strtike of faults here that is quite important in the development of the district's structural evolution. The Maqui fault is displaced by several faults in this direction. The normal slip direction of major faults such as the Las Animas fault cause the Maqui fault to be displaced in an apparent sinistral direction. In addition, dextral strike-slip faults displace (maximum of 3 meters) the Maqui fault. (Cotton, 1998).

From cross-cutting relationships it is apparent that the north-trending and east trending structures were the first faults to form in the district. Their formation was coeval,

but later slip along the north-striking faults caused significant brecciation and displacement. In the northerly-trending structures, small subvolcanic dikes are abundant but demonstrate no quartz veining. Later movement along NE-trending dextral strike-slip and ENE-trending normal faults displaced all structures, and permitted the intrusion of many dikes along these structures. (Cotton, 1998).

Mineralized systems in the Alhué district have a definite structural control demonstrated by the fact that the veins fill normal and strike-slip faults with significant displacements. Pre-mineral oblique slip (left-lateral and normal) along the Maqui vein is estimated at hundreds of meters. This basic structural regime is present throughout the district, with the most productive structures having an E-trending direction (e.g. Pedro Valencia, Flor de Alhué, Megías, Quesería, El Membrillo, etc.). These structures are genetically related to large regional N-trending faults such as the Maqui fault (Cotton, 1995; Cotton, 1998) in where intersections with E-trending systems become richer.

Post –mineral faulting in the Alhué district is exhibited by significant displacement of all geologic units by normal- and strike-slip faults that have NE-trending strikes. In addition, normal slip in the N-trending and E-trending veins on the order of 4-6 meters us common in the area (Cotton, 1995).

Finally it is uncertain if tilting of the volcanic sequence occurred before or after mineralization but the large pre-mineralization displacements along faults indicate that the greatest period of tectonic activity in the Coast Range occurred before the veins were formed. These data indicate that tilting probably occurred before mineralization. (Cotton, 1998).

3.4 Methodology

3.4.1 Sample Collection and Preparation

In collaboration with staff of Yamana Gold, 192 samples were collected from surface outcrops and underground locations, including drill cores. Collection of samples focused on mineralized (with abundant sphalerite, galena, chalcopyrite and pyrite) and unmineralized specimens. Samples that contained transparent minerals that could be examined for fluid inclusions, especially quartz and calcite, were also collected.

Surface samples were collected for the Maqui structure, which was the one encountered outcropping on the surface (at 1150 meters above mean sea level). In the underground mines, samples were collected in mineralization fronts and walls of productive pits where access is permitted. Underground areas sampled included the following mines levels: Lorena vein (740 level) and Maqui Vein (740 and 771 levels, levels indicate meters above mean sea level). Drill core samples were obtained from the underground and surface drilling program. At each location, we collected one representative sample of the dominant style of mineralization and/or vein texture. In some cases, two or more samples were collected at a given location to better capture the diversity of mineralization styles. Drill cores belonged to deeper levels than 740 for the Lorena Vein and others were related to an exploration campaign in the north-east part of the district related to Tribuna Este zone. Specifically the Chilco vein was studied for this zone.

All hand-samples were cut for mineral and textural observations. When possible, the cut was perpendicular to the vein in order to produce a section that extended from the vein wall towards the center of the vein keeping in consideration that the material closest to the vein wall is the oldest material in the vein. Once cut, off-cuts were made by cutting the sample in prismatic shapes of about 30 x 30 x 20 mm in particular zones (defined for example by the presence of the wall-rock and/or for better representation of the vein as mentioned above). This off-cuts were used to make “quick plates” of approximately 70 to 100 µm thick. Quick plates sections preparation was done at Universidad de Chile´s laboratories and after observing under an optical microscope, some off-cuts were supplied to Universidad de Chile´s laboratories for doubly polished sections preparation. Quick plates were prepared following the procedure in Goldstein and Reynolds (1994) by cleaning off-cuts with an

ultrasonic cleaner (Branson 2510E-MTH) to eliminate silicon carbide contamination due to off-cut polishing (step done to eliminate the macroscopic imperfections produced by cutting the sample). Next, the sample was mounted to a polished (320 silicon carbide powder) glass slide with epoxy adhesive. The final process consisted of cutting and grinding the sections to 75–100 micron thickness (Goldstein and Reynolds, 1994) in order to study the fluid inclusions and mineral textures. Geochemistry of drill cores samples was available and geochemical analysis were asked to Yamana Gold staff for the samples.

The mineralization and gangue phases, including textures (of quartz an calcite mainly) and FIAs (hosted by quartz, calcite and sphalerite) of the Alhué mining district´s samples were described and summarize in three paragenetic sequences which represent the evolution of three vein systems in the district: Maqui, Lorena and Chilco structures. These paragenetic sequences were completed by macroscopic and microscopic observations using both optical (Olympus BX53) and scanning electronic microscopes (FEI, Quanta 250) at the Department of Geology, University of Chile and supported also with Raman spectroscopy analysis at Virginia Tech's Department of Geosciences (JY Horiba Lab HR – 800 mm).

Raman spectroscopy is a non-destructive technique for fluid inclusion analysis, with a wide field of applications ranging from qualitative detection solid, liquid and gaseous components to identification of polyatomic ions in solution. The main advantages of this technique are the minimal sample preparation and the high versatility (Frezzotti et al., 2012). Raman analyses were performed at Virginia Tech´s Department of Geosciences, by using a JY Horiba Lab HR (800 mm) spectrometer, with 1800 grooves/mm gratings. The slit width was set to 150 µm, and the confocal aperture at 400 µm. Excitation was provided by a 514 nm (green) Laser Physics 100S-514 Ar^+ laser. The laser output was 42 mW at the source and 6.3 mW at the sample. The laser was focused through a 100X objective. Primary and secondary FIA from all investigated structures: Maqui, Lorena and Chilco were analyzed by Raman spectroscopy. Solid, liquid and gaseous qualitative detection inside the inclusions was conducted in different FIAs. In addition, in order to complete and understand mineral paragenesis from Lorena and Chilco veins some measurements were performed in samples 240912Q2 (Lorena) and 241117Q1ZA1 (Chilco).

The elemental concentrations of individual fluid inclusions were measured using LA-ICP-MS at the Department of Geosciences Fluids Research Laboratory at Virginia Tech. The system features a GeolasPro Excimer 193-nm ArF laser ablation system coupled with an Agilent 7500ce quadrupole mass spectrometer. Samples were ablated in a 1.5-cm^3 ablation cell, using a laser output energy of 150 mJ and adjusting beam diameter to ensure ablation of the entire fluid inclusion. The energy density (fluence) was between 7 and 10 J/cm^2. For all inclusions, we analyzed for B, Na, Mg, Al, Si, K, Ca, Ti, Mn, Fe, Cu, Zn, Ge, As, Se, Mo, Ag, Cd, In, Sb, Te, Ba, Au, Pb. In some analysis Sr, Cs and Tl were added. A dwell time of 10 milliseconds (ms) was used for all elements, except for Au and Ag, where dwell time of 50 (ms) was used to improve detection limits. Microanalyses by LA-ICP-MS were carried out on 102 individual inclusions. Due to sharding of the quartz (most common host), surficial damage sometimes extended over 100 µm, but inclusion separation was such that individual inclusions could generally be opened separately. Using this approach, inclusions, including any daughter mineral present, were completely destroyed in the ablation process, leaving a cylindrical hole in the sample.

3.5 Gold transportation and precipitation mechanisms.

Ogryzlo (1935) identified that HS^- and Cl^- are important ligands for aqueous transport of Au, setting important facts to the hydrothermal transport of the precious metal in crustal fluids. According to the hard-soft classification, Au occurs in nature dominantly as Au^+ or Au(I) so it is considered a soft metal and will tend to bond preferentially with soft ligands (William-Jones et al., 2009). The dominant Au(I) species in solution are dependent on temperature and fluid composition. The most important ligands at temperatures responsible for the formation of hydrothermal deposits are HS^- and Cl^-. At temperatures lower than 350°C, HS^- becomes the main responsible for Au transportation (Seward, 1973) with $AuHS^0$ predominating at lower pH and $Au(HS)_2^-$ at higher pH (considering acidic to neutral environments, Stefánsson and Seward 2004). At the higher temperatures of magmatic-hydrothermal systems, $AuCl_2^-$ will predominate. In terms of the pH of the fluid $AuCl_2^-$ will tend to dominate under acidic (and oxidizing) conditions, $Au(HS)^0$ at acidic to intermediate

pH and $Au(HS)_2^-$ at higher pH. (Stefánsson and Seward 2004). According to the following equations:

$$Au_S + HS^- + H^+ + \frac{1}{4}O_2 \rightarrow Au(HS)^0 + \frac{1}{2}H_2O \qquad (1)$$

$$Au_S + 2HS^- + H^+ + \frac{1}{4}O_2 \rightarrow Au(HS)_2^- + \frac{1}{2}H_2O \qquad (2).$$

Deposition of Au can be achieved by a decrease in the activity of HS^- and fO2 and increase in pH. Four paths are described to Au deposition: (i) boiling, in where H_2S is strongly fractionated into the vapor phase lowering the activity of HS^- (causing Au deposition) via the following equation:

$$HS^- + H^+ \rightarrow H_2S \qquad (3)$$

Boiling increases pH by partitioning acidic components into the vapour supporting Au deposition. fO_2 increases in a boiling system as hydrogen partitions strongly into the vapour promoting dissolution of Au. (ii) Cooling. At temperatures above 350°C, $AuCl_2^-$ controls the solubility of Au in chloride-rich systems. The solubility will follow the equation:

$$Au_S + 2Cl^- + H^+ + \frac{1}{4}O2 \rightarrow AuCl_2^- + \frac{1}{2}H_2O \qquad (4)$$

Gold deposition can be favoured by a decrease in ligand activity and fO_2 or an increase of pH. Cooling can be an effective mechanism in systems where Au is transported as a chloride complex and the total concentration of S is buffered to much lower values with decreasing temperature (avoiding an increasing solubility of gold due to the increased stability of bisulphide species at lower temperatures, Gammons and Williams-Jones 1997). (iii) Sulphidation of iron-bearing minerals in the wall rocks to form pyrite is another effective means of reducing HS concentration. Indeed, this is a frequently proposed explanation for the genesis of mesothermal Au deposits, where hydrothermal alteration commonly involves pyritization and where commonly there is a close spatial association between gold and pyrite (William-Jones et al., 2009). (iv) Solubility of gold is highly sensitive to fO_2 changes as can be observed in Figure 5 (Jhonson et al., 1992). A relatively small increase in fO_2 leads to a precipitous drop in HS^- concentration and consequently in Au solubility. Deposition of Au at

the conditions imposed by the diagram in Figure 5 is strongly favored by oxidation as a result of mixing with oxygenated meteoric waters for example.

3.6 Results

3.6.1 General Concerns

One hundred samples were selected for "quick-plate" confection and were examined using a petrographic microscope. Goldstein and Reynolds (1994) describe the technique for observing "quick-sections" which implies the use of a specific inmersion oil that improves the optical properties of the sample in order to check for fluid inclusions. Because the samples consisted mostly in quartz we use an oil with 1.515 index of refraction. The first step was to identify and classify minerals textures. Then we identify FIAs with their petrographic characteristics at room temperature. Fluid inclusions represent a special type of inclusion composed of a fluid phase coexisting with the host mineral during crystallization or recrystallization. Lemmlein (1929) introduced genetic aspects to the classification of fluid inclusions, and distinguished primary and secondary inclusions considering these crystallization and recrystallization processes. FIAs represent a group of fluid inclusions that are all trapped at the same time (Goldstein and Reynolds, 1994; Bodnar, 2003a) and thus represent the physical and chemical conditions in the system at the time of trapping.

3.6.2 Silica and calcite Textures

In hydrothermal veins (such as Maqui, Lorena and Chilco veins in the Alhué mining district), quartz is a dominant gangue mineral and is typically the only phase deposited throughout the life of the hydrothermal system. Therefore, the characteristics of quartz (morphology, crystal structure, chemical composition, and physicochemical properties) might reflect differing hydrothermal conditions during vein growth, including those which favor Au mineralization (Dong et al., 1995). Although the Alhué mining district does not represent an epithermal deposit *sensu stricto*, quartz and calcite´s textures defined in these kind of systems can be used to describe the textures observed in the samples collected and to interpret processes due to the analogous processes occurring in both kind of systems: phase separation in mesothermal environments and boiling in epithermal ones (Herrington and

Wilkinson, 1993). Silica and carbonate phases can have highly variable and sometimes diagnostic textures that identify the physical conditions associated with mineralization (Adams, 1920; Bodnar et al., 1985; Sander and Black, 1988; Dong et al., 1995, Moncada et al., 2012). Three major classes of textures from a genetic point of view are mainly accepted and can be divided into those that represent primary growth textures, those that are in association with recrystallization processes, and those that represent replacement of originally precipitated material (Dong et al, 1995). Some of these textures may contain usable fluid inclusions that can be analyzed to infer conditions of the paleo-hydrothermal system, whereas others rarely contain useful fluid inclusions (*e.g.* As noted by Bodnar et al. 1985 and by Moncada et al. 2012). The silica phase that is deposited with Au and/or Ag in epithermal deposits is rarely appropriate for trapping and preserving fluid inclusions. Here, we characterized the mineralogy and mineral textures observable in hand samples and under microscope of one hundred samples from the Lorena, Chilco and Maqui veins in the Alhué mining district.

Ten different textures were observed under quick-plates and thin section examination using and optical microscope (jigsaw, euhedral 1, euhedral 2, feathery, anhedral, crustiform-colloform, comb, rhombic calcite, bladed calcite). According to its relative abundance they are presented below.

The most common mineral texture observed in the samples correspond to an anhedral mosaic texture or anhedral jigsaw. This texture is present in 65 out of 100 samples representing a 47.8% of relative abundance of textures. (Figure 6). Anhedral jigsaw-textured quartz correspond to a recrystallization texture that is characterized by aggregates of microcrystalline to crystalline quartz crystals with interpenetrating gran boundaries that is only recognizable when observed under crossed polars (Dong et al., 1995; Moncada et al., 2012). The texture is interpreted to result from recrystallization of massive chalcedony or amorphous silica (Dong et al.,1995). No primary fluid inclusions were found in this texture.

Next most abundant texture is mosaic texture in which the quartz grains consist in subhedral to euhedral crystals. 22 out of 100 samples present this texture representing 16.2% of the total amount (in Figure 6 as euhedral 1). Abundant and very small (<5μm) primary

fluid inclusions can be observed in quartz grains of this texture. Secondary fluid inclusions are present in this texture evidencing fluid conditions after crystallization.

Prismatic subhedral quartz correspond to subhedral to euhedral crystals that grow perpendicular to the vein´s walls. It is simply the same texture presented before with the difference that the c-axis of quartz is oriented different in relation to the vein wall. This kind of texture is the third most common of the samples present in 21 out of 100 samples representing 15.4% of texture abundance (in Figure 6 as euhedral 2).

Crustiform and colloform textures are present in 12 out of 100 samples indicating 8.8% of relative texture abundance (Figure 6). Crustiform texture is a primary depositional texture described primarily by Adams (1920) who used the term crustification banding. Lindgren (1933) and Shaub (1934) also described this texture saying that involves successive, narrow (up to a few centimeters), and subparallel bands which are distinguished by differences in texture, mineral proportion and/or color. Commonly, banding is symmetrically developed from both walls of a fissure (Dong et al., 1995) and is formed as a result of rapid, episodic fluctuations in temperature, pressure or fluid conditions during boiling or flashing (Dong et al., 1995; Moncada et al., 2012). In the samples, this kind of texture is defined by the variations of textures and grain size showed by the different bands. A central band with opaque minerals (usually galena, sphalerite, pyrite, chalcopyrite and/or magnetite) is common in crustiform veins of the district. Fluid inclusions trapped in this kind of texture refer to the sub-textures that composed the crustiform banding. That is to say, fluid inclusions trapped in anhedral jigsaw, prismatic subhedral grains and feathery texture. The cockade texture, which is a subtype of crustiform banding described in Adams (1920), is included in the crustiform families in this study. It refers to concentric bands surrounding isolated fragments of wall rocks or early vein materials.

Colloform texture silica, first proposed by Rogers (1917), is present where the external surface of the mineral or mineral aggregate shows combined spherical or botryoidal forms (Dong et al., 1995) creating continuous bands of silica. Colloform texture silica sometimes shows a jigsaw texture characterized by banding of fine grained silica near the wallrock contact, with the size of grains increasing towards the vein center, and is most easily recognized when the sample is viewed under crossed polars and in hand samples.

Colloform texture silica is a primary depositional texture that has been interpreted to indicate rapid deposition of chalcedonic silica in open space in shallow epithermal systems to produce the rhythmic banding (Roedder, 1984; Bodnar et al., 1985; Fournier, 1985). This type of silica contains no useful fluid inclusions (Bodnar et al., 1985).

Feathery texture is present in very few samples (4 out of 100 with a 2.9% of relative texture abundance observed, Figure 6). Sander and Black (1998) described this texture that shows variable extinction positions when observed under crossed polars. It corresponds to a recrystallization texture developed from aggregates of fibrous chalcedony with rounded external surfaces which originate as silica gel (Dong et al., 1995). The silica gel is originally precipitated when silica supersaturation occurs in response to rapid cooling and concomitant pressure decrease followed by precipitation of amorphous silica (Henley and Hughes, 2000). Primary fluid inclusions in this type of quartz do not record the original depositional conditions, but secondary inclusions provide information concerning later conditions.

Very uncommon textures in the samples are big anhedral grains (3 out 100) pseudo-acicular (2 out of 100) and comb (2 out of 100) textures representing 2.2%, 1.5% and 1.5% of relative texture abundance respectively (Figure 6). The latter two do not have primary and/or secondary fluid inclusions. Pseudoacicular texture was first described by Lindgren and Bancroft (1914) and later reported by Adams (1920) and Schrader (1923). This texture refer to a replacement texture in which silica minerals display a radial acicular appearance (Dong et al., 1995). No useful fluid inclusions were found in this kind of texture.

Comb texture quartz is a primary depositional texture that was observed in a few samples. This texture is characterized by coarse, imperfect, euhedral crystals growing into open space perpendicular to the vein walls (Adams, 1920). This type of quartz often contains numerous microfractures that contain secondary fluid inclusions (Bodnar et al., 1985) but no fluid inclusions related to this texture were found in the samples of the Alhué mining district.

Finally, calcite (when present) showed both bladed (2 out of 100) and rhombic (3 out of 100) habits with 1.5% and 2.2% of relative abundance respectively. While bladed calcite is thought to be characteristic of deposition from a boiling solution, and association between rhombic calcite and boiling is less clear (Bodnar, 2003a). Boling-calcite is confirmed by the presence of vapor rich fluid inclusions coexisting with liquid rich fluid inclusions in the same FIA.

3.6.3 Fluid Inclusions

A rock may contain millions of fluid inclusions per cubic centimeter and consequently, an intelligent selection of the fluid inclusions for detailed analysis is indispensable (van den Kerkhof and Hein, 2001). Initial information about the presence and phase composition of fluid inclusions can be obtained by the inspection of "quick-plates" under an optical microscope with lenses with proper magnification (40x and more). One hundred samples (quick plates) were inspected to determine mineral paragenesis, quartz and calcite textures, fluid inclusions and Fluid Inclusion Assemblages (FIAs). A FIA represents a group of fluid inclusions that were all trapped at the same time (Goldstein and Reynolds, 1994; Bodnar, 2003a) and thus represent the physical and chemical conditions in the system at the time of trapping. FIAs might be composed of primary inclusions trapped during precipitation of the host, or might contain secondary inclusions that are trapped along fractures in the host at some time after the mineral has formed. After isolating the inclusion in the growing (or healing) crystal, further phase changes in the fluid inclusion are isochoric and isoplethal. In other words, volume and composition of the inclusion are fixed.

Trapping of a homogeneous fluid at one particular episode of the rock evolution results in fluid inclusions which are essentially identical in appearance, composition, and density. Therefore, the inclusions will show the same phase behavior when observed under the microscope at room temperature (van den Kerkhof and Hein, 2001). However, heterogeneous trapping can occur if the inclusions are trapped in a boiling or immiscible fluid system (Bodnar et al., 1985). Trapping of immiscible liquids or during boiling may result in fluid inclusions of variable composition and density and therefore the inclusions may not have identical appearance. During petrographic examination, FIAs that contained inclusions with variable liquid to vapor ratios in consistent primary or secondary trails at room temperature were classify as FIAs with boiling features and thus, direct evidence of boiling.

Boiling FIAs were found during petrographic examination of the samples of Lorena and Maqui structures and also in the system linked to the exploration campaign called Chilco. These FIAS were composed by halite ans solids bearing inclusions coexisting with vapor-rich inclusions or liquid rich inclusions coexisting with vapor rich inclusions.

Optical examination showed six major groups of fluid inclusions assemblages in the samples from Chilco, Maqui and Lorena structures. The classification process was based on their appearance at room temperature, mechanism of formation involved (e.g. boiling or flashing), coexistence and phase ratios.

Type I FIAs refer to primary and secondary boiling assemblages in where liquid-rich fluid inclusions coexist with consistent vapor-rich fluid inclusions related to phase separation stages hosted in quartz. Halite crystals and/or some subordinate solids can be found inside liquid-rich fluid inclusions present in these FIAs as shown in Figure 8 and Figure 9 (A and B). This group is present in the three analyzed systems (Maqui, Lorena and Chilco) implying that boiling is a common process in the three systems. Type II FIAs refer to primary and secondary boiling assemblages consisting in liquid-rich FI coexisting with consistent vapor-rich FI hosted in calcite grains (primary assemblages in bladed calcite and secondary in rhombohedral (Figure 8 and Figure 9G). These assemblages were described for Lorena and Chilco structures. Figure 9G shows a no useful FIA hosted in bladed calcite in a sample related to Chilco structure.

Type III FIAs consist in secondary vapor-rich only FI in quartz grains referring to flashing events (Figure 8). This kind of FI can be found in all three systems and are very common. Type IV FIAs consist in primary and secondary liquid-rich FI with consistent liquid to vapor ratios hosted in quartz grains Figure 9F. Type V FIAs are primary and secondary liquid-rich fluid inclusions in sphalerite grains sometimes related to disseminated pyrite and chalcopyrite mineralization as shown in Figure 9D. This type of FIAs were observed in Maqui and Chilco structures. Type VI FIAs consist in halite bearing inclusions and/or other chlorides together with subordinate solids (opaques) inside the inclusions as shown in Figure 9 (C,H,I and J). This type of FIA is mostly found in samples from Lorena vein but can be found in Maqui and Tribuna Este (Chilco) zones too. Figure 8 shows all the FIAs found in the samples of the Alhué mining district, considering samples of Maqui, Lorena and Chilco structures. Rounded chlorides are related to Chilco and Lorena structures only.

3.6.4 Mineral assemblages and paragenetic sequences.

Main sulfide-mineralization in the Alhué mining district corresponds to sphalerite, galena, chalcopyrite and pyrite. Magnetite is present related to the formation of host rock (e.g. andesite in Maqui vein) and also represents hydrothermal alteration after host rock consolidation (e.g. Lorena vein). In this study, gold was found mainly as electrum in Maqui and Lorena veins. Native gold (inclusions in quartz) or in cumulates with sulphides is also reported (Araya, 2001). Silver appears as native silver, electrum, argentite, pyrargirite, and associated with quartz and sulfides also (Araya, 2001). Silver was found also inside sphalerite grains in tellurides (hessite) as solid inclusions in a sample from Chilco structure (Figure 10)

Based on the different vein types, the presence of brecciation processes and the textural relationships between them, three mineralization stages (pre, main, and post-ore stages) have been established for Maqui structure. Whereas, two mineralization (pre and main-ore) stages were defined for Lorena and Chilco veins. Paragenetic sequences were constructed including FIAs petrography and textural characteristics related to quartz and calcite.

3.6.4.1 Maqui Structure

Stage 1 Pre-ore stage

The stage 1, or pre-ore stage, is characterized by the formation of the protolith which refers to an andesite with plagioclase phenocrysts (<2mm) and it´s later potassic (secondary biotite) and propylitic (epidote-chlorite) hydrothermal alterations (wallrock alteration). Nor sulfide neither precious mineralization is present at this stage and only disseminated magnetite can be recognized as the main opaque. No fluid inclusions assemblages were described in this stage (Figure 11).

Stage 2 Base metal-Au-Ag stage

The stage 2, or base-metal Au and Ag stage, represents the highest volume of mineralization in the Maqui system ore deposit. During this stage, base metals sulfides and Au/Ag-bearing minerals precipitated in symmetric and asymmetric veins sometimes forming crustiform (or colloform) veins associated with mineralization. This stage can be divided into two substages: substage 2A is characterized by stockwork veinlets principally filled with jigsaw-textured quartz and minor euhedral quartz (kind 1, see Figure 11). The main base metal sulfide is disseminated sphalerite inside this veins but also pyrite and galena can be found in minor proportions. Propylitic alteration (epidote-chlorite-actinolite) is dominant and a red silicate (jasper?) appears for the first time. Gold and silver are related to electrum which is associated with the precipitation of jigsaw quartz. Secondary FIAs can be found in euhedral quartz. FIAs in this kind of quartz are composed of vapor-rich only inclusions (type III flashing type inclusions), vapor-rich inclusions coexisting with liquid-rich inclusions (type I boiling type inclusions) and liquid-rich inclusions bearing up to three solids where one corresponds to sodium chloride (type VI halite bearing inclusions and subordinate solids). Substage 2b is characterized by symmetric veins where major contents of base metal sulfides can be found together with precious metal mineralization referring to electrum and hessite phases. Alteration silicate minerals present in this substage are late chlorite and jasper only. Primary FIAs are present in this substage hosted in quartz. Secondary FIAs are present in quartz, calcite and sphalerite. Anhedral jigsaw-textured quartz host only secondary FIAs consisting in only vapor-rich fluid inclusions (type III flashing), only liquid-rich fluid inclusions sometimes bearing subordinate solids (type IV inclusions) and vapor-rich fluid inclusions coexisting with liquid-rich bearing halite inclusions (type I boiling assemblages fluids). Euhedral quartz type 1 host in this substage both, primary and secondary liquid-rich FIAs (type V), boiling assemblages (type I) and hypersaline fluids (type VI). Euhedral quartz type 2 host tiny (< 5μm) primary liquid-rich inclusions coexisting with vapor-rich inclusions (indicating boiling processes, Type I) and secondary vapor-rich inclusions (indicating flashing processes, Type III). Rhombohedral calcite host no useful vapor-rich only inclusions and late bladed calcite is hosting secondary liquid-rich inclusions (also negligible in size). Fluid inclusions hosted in calcite in this structure were not useful due to the limited number of them and reduced size presented. These calcite hosted FI were not classified therefore.

Secondary FIAs consisting in liquid-rich fluid inclusions hosted in sphalerite grains (type V inclusions) are found in this substage (Figure 11).

Stage 3 Post-ore stage

The stage 3, or post-ore stage, is characterized by the presence of very thin veins filled with very fine grain jigsaw-textured quartz. Disseminated pyrite and minor contents of chlorite and epidote are present. No precious metal are present and no FIAs were found (Figure 11).

Fluid Evolution in Maqui system.

Fluid evolution was constructed by using previous information. Propitious FIA´s for doing microthermometry studies allowed the construction of fluid evolution paragenesis (Figure 12). Base on petrography, stages 2A and 2B were the only ones with useful FIA´s for microthermometry revisions in Maqui structure. Figure 12 shows the temporary sequence of primary and secondary FIA´s by taking in consideration the T_h and calculated salinities (wt% NaCl eq.). A trend from relatively high (~520°C) to relatively low (~320°C) T_h and from relatively high to relatively low salinities (wt% NaCl eq.) can be observed independently of the type and genesis of the FIA (hosted in quartz and or sphalerite, primary or secondary).

3.6.4.2 Lorena Structure

Hydrothermal quartz breccias collected in Lorena vein show two clear mineralization stages. The first one correspond to a pre-ore stage where clasts of the protolith were highly altered. The second stage or base metal-Au-Ag stage can be divided in two substages: substage 2A reflects the brecciation processes and its mineralization and the substage 2B refers to crustiform mineralized veins cutting the breccia. One last stage defined by the oxidation of magnetite to hematite can be observed (Figure 13).

Stage 1 Pre-ore stage

The stage 1, or pre-ore stage, is characterized by the pervasive alteration of protolith clasts. Massive magnetite associated with biotite, chlorite, epidote and rhodonite can be found in cumulates after protolith clasts. Pyrite is disseminated inside some clasts. No FIA were described for this stage (Figure 13).

Stage 2 Base metal-Au-Ag stage.

The stage 2, or base-metal Au and Ag stage, represents the highest volume of mineralization in the Lorena system ore deposit. During this stage, base metals sulfides and Au/Ag-bearing minerals precipitated in the breccia´s matrix (substage 2A, Figure 13) and in later symmetric crustiform veins (substage 2B, Figure 13). Substage 2A is characterized by the presence of chalcopyrite, pyrite and magnetite as base metal mineralization. Electrum is disseminated in association with jigsaw-textured quartz in substages 2A and 2B. Epidote is the main alteration mineral being in the two stages (1 and 2). FIAs described in this substage are only secondary FIAs composed of coexisting liquid-rich and vapor-rich fluid inclusions in rombohedral calcite (type II fluid inclusions), liquid and vapor-rich fluid inclusions (not coexisting) bearing salt crystals (type VI), only vapor-rich fluid inclusions (type III), only liquid-rich fluid inclusions (type IV). Arzakite and anhydrite phases were also recognized in this substage as alteration minerals by using Raman-spectrum. Substage 2B is the highest volume of mineralization of the paragenetic sequence where major contents of sphalerite, chalcopyrite, pyrite and magnetite are present. Hydrothermal alteration is related to epidote-chlorite-actinolite and many textures of quartz are present (e.g. jigsaw, type 1 euhedral, type 2 euhedral, feathery, crustiform and colloform). Numerous FIAs have been describe in this substage. Rhombohedral calcite contains secondary FIAs consisting of coexisting liquid-rich and vapor-rich inclusions (type II). Jigsaw-textured quartz has secondary FIAs defined by vapor-rich only (type III), liquid-rich (type IV) and halite bearing (type VI) inclusions. In type 1 euhedral quartz FIAs consist in secondary liquid-rich (type IV), liquid rich FI bearing rounded chlorides and solids (type VI), vapor-rich only inclusions (type III) and halite bearing inclusions coexisting with consistent vapor rich inclusions (type I). Type 2 euhedral quartz has primary vapor-rich only inclusions (type III) and secondary liquid rich FI bearing rounded chlorides and solids (type VI) inclusions. Finally, secondary vapor-rich only (type

III) and liquid-rich bearing halite crystals (type VI) FIAs were described in association with feathery-textured quartz (Figure 13).

Stage 3 Base metal-Au-Ag stage.

Abundant hematite crystals were recognized in the samples by using Raman spectroscopy. We suggest that hematite is a response to late oxidation states that affect magnetite crystals in this system. (Figure 13). Laser Raman microprobe analysis indicates that this mineral has a Raman spectrum with distinct bands at about 226, 247, 293, 410, 500, 613 and 1310 cm-1.

Fluid Evolution in Lorena system.

Fluid evolution was constructed by using previous information. Useful FIAs were selected for microthermometry and to construct paragenesis sequences (Figure 14). Base metal Au-Ag mineralization stage (2A and 2B) showed useful FIAs for microthermometry studies in Lorena vein. Figure 14 shows the temporary sequence of primary and secondary FIAs by taking in consideration T_h and calculated salinities (). T_h range from ~280 to ~540°C. Calculated salinities range from ~10 to ~60 wt% NaCl eq implying that significant salty fluids participate in this system. No Th neither calculated salinity trends are observed.

3.6.4.3 Chilco Structure

Samples collected in Chilco vein show two clear mineralization stages. The first one correspond to a pre-ore stage where jigsaw textured quartz dominance is accompanied with the association magnetite+chlorite+epidote+actinolite. The second stage or base metal-Au-Ag stage can be divided in two substages: substage 2A reflects the main event of mineralization (massive sphalerite) and substage 2B which implies late boiling events reflected by the presence of bladed calcite.

Stage 1 Pre-ore stage

The stage 1, or pre-ore stage, is characterized by the presence of scarce magnetite+chlorite+epidote+actinolite in jigsaw-textured quartz. Only secondary FIAs were

described in this type of quartz. Fluid inclusion assemblages from types III, IV and VI were observed in secondary trails.

Stage 2 Base metal-Au-Ag stage.

The stage 2, or base-metal Au and Ag stage, represents the highest volume of mineralization in Chilco system ore deposit. During this stage, base metals sulfides and Au/Ag-bearing minerals precipitated. In substage 2A, Massive sphalerite (Figure 15 and Figure 9D) and precipitation of chalchopyrite, pyrite, galena, gold, silver and hessite are observed. No calcite is present and quartz can be found in as jigsaw-textured quartz, euhedral type 1, euhedral type 2, colloform and crustiform. Primary FIAs were found associated to Type III (vapor-rich-only) inclusions hosted in euhedral quartz (types 1 and 2) and Type V liquid-rich FI hosted in sphalerite (see Figure 9D and Figure 15). Secondary FIAs related to Type I (boiling assemblages), Type III (flashing assemblages) and Type VI (halite bearing fluids) were also described in euhedral quartz. Secondary FI associated to Type V (liquid-rich hosted in sphalerite) are also present. In substage 2B, minor proportions of gold and silver were inferred due to the presence of clear bladed calcite (see Figure 7J). Bladed after rombohedral calcite is observed containing scarce and tiny vapor-rich fluid inclusions and Type II assemblages (see Figure 15 and Figure 9J) respectively.

Fluid Evolution in Chilco system.

Useful FIAs for microthermometry allowed the construction of fluid evolution in Chilco system (Figure 16). Useful fluid inclusions were found only in substage 2A that represents the ore stage 2 in Chilco mineralized structure. The Figure 16 shows the temporary sequence of secondary FIA´s by taking in consideration Th and calculated salinities (wt% NaCl eq.). Boiling and or flashing FIAs show the highest Th.

3.6.5 Vertical Zonation of Maqui, Lorena and Chilco structures.

Vertical zonations of fluid inclusions and quartz and calcite textures for Maqui (Figure 17), Lorena (Figure 18) and Chilco (Figure 19) systems were constructed. Also,

whole rock average values of gold (ppm), silver (ppm) and copper (ppm) for the samples collected in each level are indicated. In Maqui, just three levels were completed: 740, 771 and 1150 representig meters above mean sea level (m.a.m.s.l.). Just Type III (vapor-rich-only) inclusions were found in the deepest level related to jigsaw quartz. Most relevant level for this vein is 771 in where a broad range of FIA and calcite and quartz textures are found. Highest values for gold and copper can be observed here too. At 1150 m.a.m.s.l. types I, III, IV and VI FIA are present with lower abundance of textures and metal content.

Zonation in Lorena (Figure 18) is poor due to the proximity of both levels, FIA related to types I, II, III, IV and VI were observed and quartz shows jigsaw, feathery, crustiform and euhedral textures. Finally, 6 levels were considered for the zonation in the Chilco system (Figure 19). All FIAs types were observed in different levels. Most common FIA types are halite-bearing and vapor-rich-only fluids which are present in the whole column. Type V (liquid-rich FI hosted in sphalerite) and II (boiling assemblages in calcite) FIA are present in levels 780 and 810 respectively. Type I (boiling assemblage in quartz) FIA are common but not ubiquitous. Level 780 is the most relevant level with the presence of abundant fluid inclusions assemblages related to halite-bearing fluids and the highest Au (2.8 ppm) contents.

3.6.5 Microthermometry

Several fluid inclusion studies have been conducted (Díaz, 1986.; Piñana, 1993.; Cotton, 1998.; Fuentealba, 2002.; Poblete, 2008.; Alcázar, 2001.; Sepúlveda, 2004.; Harris et al., 2013.; Herreros, 2009) in veins of the Alhué mining district such as El Membrillo, Piscina, Garza, Maqui, Pedro Valencia, Cantillana, El Roble, Valeria, Peumo, Lorena and Marisol. Summary of these studies is presented in Table 1. Vapor-rich (V-rich) and liquid-rich (L-rich) inclusions are most common features in the veins. Liquid-rich bearing halite crystals (L-rich+H) and liquid-rich bearing halite crystals and some solids (L-rich+H, solids) are also described. Less common are liquid-rich bearing halite and sylvite (L-rich+NaCl, KCl) and liquid-rich containing two vapor phases in which one is CO_2 (L-rich+CO_2), both of them described in Peumo vein (Herreros, 2009). In general, inclusions in the system are not bigger than 40 µm. Reported homogenization temperatures (T_h) range between 115-500°C

melting temperature of halite (T_m) range between 149-543°C. No systematic increase or decrease of T_h with depth is present. The lowest T_h and salinities values in the area are reported by Piñana (1993) in El Membrillo vein. In contrast, values for these parameters in other veins of the system are significantly greater than those reported for El Membrillo. Indeed, since the T_h in other veins such as Pedro Valencia, El Maqui, Cantillana, El Roble deposits have averages between 300°C to 320°C, data reported by Piñana (1993) may be interpreted as distant fluids from their causative plutons and/or major interaction degrees with meteoric fluids (Cotton, 1998). The internal variation in homogenization temperatures and salinities in the veins (e.g. Maqui vein) may reflect the diversity of ore-forming conditions of the mining district but may also reflect the study of FIA´s that are not involved in mineralizing processes also. Data is usually grouped in mine levels (meters above mean sea level) or grouped by T_h obtained instead taking petrographic features for this purpose. In general (with the exception of the newest study of Harris et al., 2013), workers do not comment whether the samples contained boiling assemblages with liquid-rich FI coexisting with consistent vapor-rich FI. In fact, boiling and even flashing events are barely mentioned in this studies linked to petrographic evidences (textural and FIAs) and even though Harris et al., 2013 propose boiling horizons (between levels 731 and 488) for Piscina and Garza veins with fluid inclusions evidences no relationship between the boiling FIAs and mineral texture and/or paragenesis is mentioned. Authors agree that broad distribution of T_h found in different veins but also within a unique one indicate the presence of different multi-stage hydrothermal events for each vein and therefore every vein may be studied separately considering substantial chemical variations in the fluids (Pincheira et al., 1994; Rodriguez et al., 2000; Sepulveda 2004, Harris et al., 2013). Finally, all microthermometric studies were done in quartz as host mineral, fluid inclusions in sphalerite are reported in Peumo vein without further studies (Herreros, 2009).

In this study, data were collected only from well-defined Fluid Inclusion Assemblages (FIAs) (Goldstein and Reynolds, 1994), representing groups of fluid inclusions that were trapped at the same time. Most FIAs studied here represent secondary fluid inclusions occurring along well-developed and clearly definable trails (healed microfractures; Figure 9E). Fewer FIAs composed of primary inclusions (occurring along growth zones; Figure 9D) were analyzed. FIAs in samples were classified first at room temperature as follows: (i) Type

I: liquid-rich inclusions coexisting with vapor-rich inclusions in quartz, (ii) Type II: liquid-rich inclusions coexisting with vapor-rich inclusions in calcite, (iii) Type III: vapor-rich inclusions in quartz, (iv) Type IV: liquid-rich inclusions hosted in quartz, (v) Type V: liquid-rich inclusions hosted in sphalerite and (vi) Type VI: halite (and/or other solids) bearing inclusions together hosted in quartz.

Following detailed petrographic examination of the samples, 32 FIAs (representing 223 total fluid inclusions) were selected for microthermometric analysis. Inclusions were measured using a Linkam THMSG 600 heating/cooling stage mounted on a standard petrographic microscope. The stage was calibrated using synthetic fluid inclusion standards (Sterner and Bodnar, 1984). The precision and accuracy of measured homogenization temperatures are estimated to be ±1.0 °C and the precision and accuracy of ice-melting temperatures are estimated to be ±0.1 °C. The ice-melting temperatures were measured in order to estimate a fluid salinity to calculate boiling point with depth curves, but are not discussed further below. The measured fluid inclusions are hosted by subhedral sphalerite, jigsaw quartz, euhedral quartz (types 1 and 2), feathery quartz and rhombohedral calcite as secondary fluid inclusion assemblages; primary fluid inclusions are present in subhedral sphalerite and euhedral quartz (types 1 and 2). The homogenization temperatures of fluid inclusions from the Alhué Mining District are described for each individual mineralized structure, from north to south. We emphasize that our goal in studying the fluid inclusions is only to determine if boiling occurred at the location where the sample was collected and, if so, the temperature at which boiling occurred. As noted above, much of the quartz in the veins was originally precipitated as amorphous silica and contains no fluid inclusions representative of the original depositional conditions.

During heating experiments, FIAs in samples from Chilco mineralized structure were classified as: In quartz, (1) Secondary liquid-rich inclusions with consistent liquid to vapor ratios that homogenize by vapor disappearance with a $Th_{L\rightarrow V}$ ranging from 183 to 212 °C. Tm ranges from -13 to -12.1°C. (2) Secondary vapor-rich FI bearing halite crystals where halite disappearance (Tm_{halite}) is equal to liquid disappearance ($Th_{V\rightarrow L}$). $Th_{V\rightarrow L}$ and Tm_{halite} range from 404 to 418°C. (3) Secondary liquid-rich inclusions coexisting with vapor-rich inclusions where $Th_{L\rightarrow V}$ ranges from 400 to 416°C and Tm ranges from -3.5 to -3.3ºC. In

Sphalerite, (1) Primary liquid-rich with consistent liquid to vapor ratios FI with homogenization temperatures ($Th_{L\rightarrow V}$) ranging from 289 to 294°C and final ice melting temperature (Tm) ranges from -20.7 to -17.6 ºC. (2) Secondary liquid-rich with consistent liquid to vapor ratios FI with homogenization temperatures ($Th_{L\rightarrow V}$) ranging from 191 to 240°C and final ice melting temperature (Tm) ranges from -11.9 to -9.5 ºC.

FIAs in samples from Maqui mineralized structure were classified as: In quartz, (1) Secondary liquid-rich inclusions with consistent liquid to vapor ratios that homogenize by vapor disappearance with a $Th_{L\rightarrow V}$ ranging from 400 to 405 °C. Tm ranges from -1.8 to -1.2°C. (2) Primary liquid-rich inclusions with consistent liquid to vapor ratios that homogenize by vapor disappearance with a $Th_{L\rightarrow V}$ ranging from 345 to 350 °C. Tm ranges from -18.6 to -15.9 °C. (3) Secondary liquid-rich inclusions coexisting with vapor-rich inclusions where $Th_{L\rightarrow V}$ ranges from 384 to 387°C and Tm ranges from -0.3 to -0.1ºC. (4) Primary liquid-rich inclusions coexisting with vapor-rich inclusions where $Th_{L\rightarrow V}$ ranges from 318 to 326°C and Tm ranges from -4.6 to -3.1ºC. (4) Secondary vapor-rich FI that homogenize by liquid disappearance. $Th_{V\rightarrow L}$ ranges from 445 to 455°C and Tm from -5.3 to -0.6. (5) Secondary liquid rich inclusions bearing halite crystals coexisting with vapor rich inclusions. $Th_{L\rightarrow V}$ ranges from 381 to 386°C and Tm_{halite} ranges from 500 to 502°C. (6) Primary liquid rich inclusions bearing halite crystals coexisting with vapor rich inclusions. $Th_{L\rightarrow V}$ ranges from 405 to 424°C and Tm_{halite} ranges from 511 to 520°C. In sphalerite, (1) Secondary liquid-rich with consistent liquid to vapor ratios FI with homogenization temperatures ($Th_{L\rightarrow V}$) ranging from 326 to 336°C and final ice melting temperature (Tm) ranges from -2.4 to -2.1 ºC.

FIAs in samples from Lorena mineralized structure were classified as: In quartz, (1) Primary liquid-rich inclusions coexisting with vapor-rich inclusions where $Th_{L\rightarrow V}$ ranges from 480 to 484°C and Tm ranges from -17.6 to -12.6ºC. (2) Secondary vapor-rich inclusions where $Th_{V\rightarrow L}$ ranges from 521 to 525 and Tm ranges from -18.1 to -16.9. (4) Secondary liquid-rich with consistent liquid to vapor ratios FI with homogenization temperatures ($Th_{L\rightarrow V}$) ranging from 334 to 407°C and final ice melting temperature (Tm) ranges from -12.9 to -3.9 ºC. (4) Secondary liquid-rich FI bearing halite crystals and solids where $Th_{L\rightarrow V} < Tm_{halite}$. $Th_{L\rightarrow V}$ ranges from 213 to 295°C and Tm_{halite} between 271 and 359°C. (5)

Secondary liquid-rich FI bearing halite crystals and solids where $Th_{L\rightarrow V}$ > Tmhalite. $Th_{L\rightarrow V}$ ranges from 373 to 377°C and Tm_{halite} between 227 and 232°C (6) Secondary liquid-rich FI bearing rounded chlorides and solids. $Th_{L\rightarrow V}$ ranging from 264 to 289 °C and $Tm_{chloride}$ ranging between 329 to 352°C. (7) Secondary vapor-rich bearing halite crystals FI where $Th_{V\rightarrow L}$ ranges from 359 to 384°C and Tm ranges from 521 to 529°C. In rhombohedral calcite, (1) Secondary liquid-rich inclusions coexisting with consistent vapor-rich inclusions where $Th_{L\rightarrow V}$ ranges from 383 to 533°C and Tm ranges from -19.5 to -4.5ºC. T_h (°C) versus salinity (wt% NaCl) corresponding to each group of fluid inclusions defined previously at room temperature and considering petrographic features is presented in Figure 21. Same arrangements classified this time by the system in which each FIA was found are presented in Figure 20. Whole microthermometric data for fluid inclusions from Maqui, Lorena and Chilco veins is shown in Table 3.

3.6.6 LA-ICP-MS

The elemental concentrations of individual fluid inclusions were measured using LA-ICP-MS at the Department of Geosciences Fluids Research Laboratory at Virginia Tech. Transient signals of fluid inclusion were observed for the six kinds of inclusions presented in Figure 22 and Figure 23 show transient signals examples of fluid inclusions hosted in quartz grains. Fluid inclusion in Figure 22 is represented by a transient and notorious signals in Na, K, Mn, Ca, Fe, Ag, Pb, Zn, As, Cd. Au and Cu do not belong to the FI and thus no transient increment in the signal is observed for this fluid inclusions in particular (not shown in Figure 22) . In Figure 23, vapor-rich (Type III) fluid inclusions transient signals are related to Na, K, Mn, As, Pb, Sb and Au.

Fluid inclusions from all three localities contain measurable concentrations of Na, K, Ca, Mn, Fe, As, Ag, Cd, Ba, Pb, B, Al. Concentrations of other elements (Cu, Zn, Mo, Sb, Tl, Mg, Ge, Sr, In, Cs, Au) in fluid inclusion are less common and appear in certain FIAs and in no more than two systems.

Our compilation of mean concentrations of metals (Mn, Fe, Cu, Zn, As, Mo, Ag, Cd, Sb, Ba, Pb) and major alkalis (Na, K, Ca) in the six fluid types in the Alhué system defined in this study is summarized in Table 4 and presented in Figure 24. Figure 25 presents the same mean concentrations of metals (Mn, Fe, Cu, Zn, As, Mo, Ag, Cd, Sb, Ba, Pb) and major alkalis (Na, K, Ca) classified by the mineralized structure in which a certain fluid is participating.

For each fluid inclusion type, variations up to four orders of magnitude in alkali content have been observed (100s to 100000s ppm). Based on the mean concentrations calculated for alkalis (Na, Ca, K), the following relative abundance trends for the six fluid inclusion types can be established: (1) in type I and II boiling assemblages hosted in quartz and calcite: Na>K>Ca. (2) Type III flashing assemblages hosted in quartz: Na~K (3) Type IV liquid-rich FI hosted in quartz Ca>Na>K. (4) Type V liquid-rich FI hosted in sphalerite grains show Na~Ca>K. (5) Type VI hypersaline fluids shows Na>K>Ca. Na shows a positive correlation with Ba and microthermometric-calculated salinity in Maqui fluids and with K in Chilco fluids. K shows a positive correlation with Ba and T_h for Maqui fluids, with Mn, Cs,

Tl and salinity for Lorena fluids and with Na for Chilco fluids. Ca shows a positive correlation with Cu for both Maqui and Lorena fluids, and with salinity for Chilco fluids.

Mn shows concentration variations up to 3 orders of magnitude (~100s to~10000s ppm). Types VI and IV inclusions have the greatest concentrations of Mn (1000s~10000s ppm) followed by type III and I (~100s ppm). Lorena system is the richest in Mn concentrations followed by Chilco and Maqui systems. Mn shows positive correlations with K, Sr, Tl, Ba, Cs and salinity in Lorena vein.

Fe shows concentration variations up to 4 orders of magnitude (~10s to ~10000s ppm). Types VI inclusions have the greatest concentrations of iron (~1000s to ~10000s ppm) followed by types IV and III (~100s to ~1000s ppm). Type I inclusions shows the lowest concentrations of this metal (~10s to ~100s ppm). Lorena is the Fe-richest system of all three and Fe shows positive correlations with Ag and salinity in this system.

Cu shows concentration variations up to 3 orders of magnitude (~10s to ~1000s ppm). Type V inclusions have the highest concentrations of this metal reaching ~1000s ppm. Type VI has greater values than type II inclusions having ~100s ppm in comparison with ~10s ppm. Maqui vein is richer in this metal than Lorena vein reaching up to two orders of magnitude greater than the latter (~1000s ppm). Chilco fluids do not have Cu concentrations above the limit of detection. Cu has positive correlation with Ca, Ag and salinity in Lorena vein and positive correlations with Ca and T_h in the Maqui system.

Zn shows concentration variations up to 2 orders of magnitude (~1000s to ~10000s ppm). Types VI and I inclusions have the greatest values followed by type II and IV inclusions. Only Lorena vein fluids contain measureable quantities of Zn in the fluids and this element shows positive correlations with Sr and salinity in the system.

As shows concentrations variations up to 3 orders of magnitude (~10s to ~1000s ppm). Type IV and V inclusions shows in average the lowest contents of As with widest range in concentration. Type I and III inclusions instead shows the highest average values of As concentration. Types II and VI have similar values. The As-richest system is Maqui vein containing 100s to 1000s ppm. Lorena vein and Chilco zone have lower values. As shows positive correlations with Pb ang Ge in Lorena vein and with T_h in Chilco.

Mo is present just in type VI fluid inclusions containing just a few ppm (~10s). Lorena vein is the only one system reporting this metal. Mo shows positive correlations with Ba in this system.

Ag shows concentrations variations up to 4 orders of magnitude (~1s to ~1000s ppm) in the fluids. Type V inclusions show the highest average content with a wide variation (1s to 1000s ppm). Type VI and II fluids have medium average contents (~10 ppm) and types III, IV and I have the lowest values (~1 to ~10 ppm). Chilco fluids are richer (in average) in Ag than Lorena and Maqui systems. Ag shows positive correlations with Cu and Fe in Lorena and with T_h in Tribuna Este. A general positive correlation between Ag and salinity for all the system is observed also.

Au is observed in just three FIAs present in Maqui and Chilco veins corresponding to type V (2.1 ppm average, Chilco) and type III (1.6 ppm average, Maqui) inclusions.

Pb shows concentration variations up to 4 orders of magnitude (~10s to ~10000s ppm) in the fluids. Type VI and II fluids have higher average values (~1000 ppm) of Pb. Type I, III, IV and V fluids have similar lower contents in average (~100 ppm). Lorena vein has a higher average value of Pb (~1000s ppm) in comparison to Maqui and Chilco systems (~100s ppm). Pb shows positive correlations with K, Cd, Cs, Ba and Tl in Lorena vein and with As and Th in Maqui vein.

3.6.6.1 Maqui Structure

Our compilation of mean concentrations of metals (Mn, Fe, Cu, Zn, As, Mo, Ag, Cd, Sb, Ba, Pb) and major alkalis (Na, K, Ca) for the Maqui mineralized structure is shown in Figure 25. For each fluid inclusion type recognized in Maqui, variations no greater than one orther of magnitude in alkali (Na, K, Ca) contents have been observed (100s to 1000s ppm). Elemental content in secondary vapor-rich inclusions hosted in quartz (type III), secondary liquid-rich inclusions with consistent liquid to vapor ratios hosted in quartz (type IV) and secondary liquid-rich inclusions with consistent liquid to vapor ratios hosted in sphalerite (type V) were measured using LA-ICP-MS analysis. Na contents (expressed as wt% Na_2O) are similar in type IV and V inclusions ranging from 0.7 - 1 wt%. Na contents in vapor-rich only inclusions are lower with an average of 0.4 wt%. K (expressed as wt% K_2O) shows greater values in

vapor rich (type III) inclusions ranging from 0.2 – 0.5 wt% and a positive correlation with Ba and T_h. Ca contents (expressed as wt% CaO) were only detectable in liquid rich inclusions hosted in sphalerite ranging from 0.06 to 0.2 wt% and a positive correlation with Cu contents. Mn and Fe were detectable in vapor rich only inclusions with values contents around ~100s ppm. Cu content was detectable in liquid-rich inclusions hosted in sphalerite ranging from 8493 to 9535 ppm and shows a positive correlation with Ma values in the same FIA. Pb was detectable in the three types of inclusions measured in Maqui structure (types III, IV and V) with variations in one order of magnitude (100s to 1000s ppm). Vapor-rich only inclusions showed the greater values reaching up to 1241 ppm. As was detectable in the three types of inclusions measured in Maqui structure (types III, IV and V) with variations in one order of magnitude (100s to 1000s ppm). Vapor-rich inclusions showed the greater values reaching up to 2441 ppm. Ag was measured in the three types of FIA. Vapor-rich FI showed values ranging from 7 to 9 ppm of Ag, liquid-rich hosted in quartz showed 6 to 9 ppm and liquid-rich hosted in sphalerite have 21 to 30 ppm. Gold was detectable in vapor-rich only inclusions with values ranging from 1.5 to 1.6 ppm.

3.6.6.2 Lorena Structure

Our compilation of mean concentrations of metals (Mn, Fe, Cu, Zn, As, Mo, Ag, Cd, Sb, Ba, Pb) and major alkalis (Na, K, Ca) for the Lorena mineralized structure is shown in Figure 25. For each fluid inclusion type recognized in Lorena, variations up to one orther of magnitude in alkali (Na, K, Ca) contents have been observed (1000s to 10000s ppm). K shows positive correlations with Mn, Cs, Tl and microthermometric-calculated salinity. Ca shows a positive correlation with Cu contents. Elemental content measured using LA-ICP-MS analysis was completed in primary liquid-rich FI coexisting with vapor-rich FI hosted in quartz (type I), secondary liquid-rich FI coexisting with vapor-rich FI hosted in calcite (type II), secondary vapor-rich FI hosted in quartz (type III), secondary liquid-rich FI hosted in quartz (type IV), secondary liquid rich bearing halite and one solid FI (type VI), secondary liquid-rich bearing halite and two solids FI (type VI), secondary liquid-rich bearing a rounded chloride and a solid FI (type VI) and secondary vapor-rich bearing halite FI (type VI). Primary liquid-rich FI coexisting with vapor-rich FI hosted in quartz (type I) shows comparable values of alkali

contents (1000s ppm). Pb, Mn and Fe contents in these inclusions range from 55 to 156 ppm. Ag was detectable in one FI containing 2.9 ppm. Secondary liquid rich FI coexisting with vapor-rich FI hosted in calcite (Type II) report greater values of Na in comparison with K. Na (expressed as wt% Na_2O) range from 3.0 – 6.6 wt% and K (expressed as wt% K_2O) from 1.6 to 2.8 wt%. Zn an Pb shows comparable values reaching from 2315 to 5077 ppm. Inclusions in these group contains between 6 and 23 ppm of Ag. Vapor-rich inclusions hosted in quartz (Type III) shows comparable amounts of Na and K ranging from 1.0 to 2.4 wt% and minor Ca and Mn contents ranging from 0.3 to 1.1 wt%. Base metals as Zn, Fe and Pb report values between 1224 and 2953 ppm. Some inclusions contain Ag reporting 3.1 and 2.2 ppm. Secondary liquid-rich fluid inclusions assemblages hosted in quartz (type IV) show greater contents of Na (between 4.6 – 4.8 wt% Na_2O) than K and Ca (between 1.3 – 1.9 wt%). Mn range from 0.2 – 0.3 wt% MnO and base metals Fe, Zn and Pb from 169 to 294 ppm. As range from 265 to 292 ppm. Secondary Liquid-rich inclusions bearing a rounded chloride and a solid (Type VI) show similar contents of Na, K, Ca and Mn ranging from 3.5 to 6.2 wt%. Fe is the most abundant base metal ranging from 24134 to 25938 ppm (3.1 – 3.3 wt% FeO). Zn and Pb contents are between 7001 and 9940 ppm. Silver contents may reach up to 63 ppm. Secondary liquid-rich inclusions bearing a halite crystal and one solid (Type VI) contain variable Na contents ranging between 0.5 – 7.3 wt% Na_2O with relatively high contents of K, Ca, Mn and Fe ranging from 2.1 to 9.5 wt%. Base metals Pb, Fe and Zn contents shows values between 3658 to 22571 ppm. As and Ba contents range from 70 to 1036 ppm. Ag and Cd show similar contents between each other reaching up to 106 ppm. Secondary liquid-rich inclusions bearing halite crystal and two solids (Type VI) show high contents of Na ranging between 2.1 and 9.5 wt% Na_2O with lower K, Ca and Mn contents ranging between 1.8 and 5.1 wt%. Fe is the most abundant base metal reaching up to 27882 ppm (3.6 wt% FeO). Zn and Pb are less abundant ranging from 1505 to 23746 ppm. As and Ba contents range from 118 to 809 ppm. Ag is found ranging from 12 and 44 ppm. Mo contents reach up to 14 ppm. Cd contents range between 30 and 212 ppm.

3.6.6.3 Chilco Structure

Our compilation of mean concentrations of metals (Mn, Fe, Cu, Zn, As, Mo, Ag, Cd, Sb, Ba, Pb) and major alkalis (Na, K, Ca) for the Chilco mineralized structure is shown in Figure 25.

For each fluid inclusion type recognized in Chilco, variations up to three orthers of magnitude in alkali (Na, K, Ca) contents were observed (100s to 10000s ppm). Na shows a positive correlation with K in Chilco Fluids. Ca shows a positive correlation with calculated salinity for Chilco fluids. Elemental content in secondary liquid-rich coexisting with vapor-rich FI hosted in quartz (type I), secondary liquid-rich FI hosted in quartz (type IV), primary and secondary liquid rich FI hosted in sphalerite (Type V) and secondary vapor-rich FI bearing halite crystals (Type VI) were measured using LA-ICP-MS analysis. Secondary liquid rich FI coexisting with vapor-rich FI hosted in quartz (type I) show Na contents ranging from 1.6 to 1.9 wt% Na_2O. Lower contents of K and Ca are observed ranging between 0.2 and 0.5 wt%. Ba is barely present with 20 to 87 ppm. Liquid-rich FI hosted in quartz (Type IV) have higher Na and Ca contents than K ranging between 1.6 to 4.9 wt% for the two first ones and from 0.3 to 0.5 wt% K_2O to the latter. Ba is barely present reaching up to 43 ppm. One inclusion in this group report 15 ppm of Ag. Primary liquid-rich inclusions hosted in sphalerite (Type V) contain relatively high contents of Na and Ca. Na contents range from 2.8 to 5.7 wt% Na_2O. Ca contents range from 4.9 to 8.0 wt% CaO. K is less abundant with contents ranging between 0.07 to 1.2 wt% K_2O. B and As contents are similar and range from 42 to 1047 ppm. Pb contents range from 39 to 754 ppm. Ag is in the range of 5 to 1193 ppm. Au is present in one inclusion of this group with 3.8 ppm. Ba is the less abundant element reaching up to 35 ppm. Secondary liquid-rich inclusions hosted in sphalerite (Type V) have similar contents of Na and Ca ranging from 1.4 to 4.8 wt% and lower contents of K ranging between 0.4 to 0.8 wt% K_2O. Mn and Cu are present in one FIAs of this class ranging between 1.7 to 2.0 wt% MnO and from 311 to 10796 ppm respectively. Pb contents are lower than other base metals ranging between 660 to 1060 ppm. Ag is present in one FIA of this group (Type V) with contents ranging from 12 to 364 ppm. Au appears in type V FI ranging between 0.3-3.9 ppm. As and Ba contents range from 117 to 299 ppm.

3.6.7 Raman Spectroscopy

Solid, liquid and gaseous qualitative detection inside the inclusions was conducted in different FIAs. In addition, in order to complete and understand mineral paragenesis from Lorena and Chilco veins some measurements were performed in samples 240912Q2 (Lorena) and 241117Q1ZA1 (Chilco). Raman spectroscopy shows that sample 240912Q2 contains hematite, arzakite, sphalerite and anhydrite related to early stages of mineralizations of Lorena structure. Diseminated Opaques in the same trend of a FIA (Type III Vapor-rich+H FIA in sample 241117Q1ZA1) from Chilco was analyzed obtaining good correlations and peak matching with kipushite [$Cu_6(PO_4)_2(OH)_6\ H_2O$] although Cu contents were not detected in the same FIA with LA-ICP-MS analysis.

Fluid inclusions type VI (L-rich+IC,S1) in sample 240910VQ1ZA contained pyrosmalite-Fe [$Fe^{2+}{}_8Si_6O_{15}(OH)_{10}$], an iron-rich member of the pyrosmalite series (Figure 26). Relative proportions of this solid phase vary from sample to sample, but are similar within individual fluid inclusion assemblages. This suggests that ferropyrosmalite is a daughter mineral rather than captive phase. Optical properties show that this daughter mineral in the fluid inclusions is colourless to pale green, stubby or prismatic with high relief and moderate birefringence.

Carbon dioxide (CO_2)-bearing fluids are common in many geological environments including various ore-forming systems (Roedder, 1984; Bodnar, 1995; Bodnar et al., 2014; Hedenquist and Henley, 1985; Roedder and Bodnar 1997). Raman spectroscopy is used to confirm the presence and abundance of CO_2 in fluid inclusions (Lamadrid et al., 2017). During petrographic and/or microthermometric analysis we do not observed any CO_2, so we check by Raman Spectroscopy our samples to test the presence of CO_2 (and other volatiles) in fluid inclusions. The detection limit for CO_2 in fluid inclusions by Raman Spectrocopy is less than 1 bar and because CO_2 preferentially partitions into the vapor phase, the vapor bubble was targeted within two phase liquid-rich inclusions (Simpson et al., 2015). Vapor-rich and vapor-rich bearing halite (vapor-rich+H) fluid inclusions were also tested in this case. CO_2 was detected in three types of fluids: vapor-rich (Type III), vapor-rich+H (Type VI) and two phase liquid-rich hosted in quartz (Type IV) fluid inclusions. Except for water and CO_2, all other volatiles were less than their detection limit in all types of inclusions.

Early Raman studies of carbon dioxide showed that the distance between the two characteristics peaks of this molecule (1285 and 1388 cm^{-1}) is density (pressure) dependent (Wright and Wang, 1973, 1975). After that, several studies (Rosso and Bodnar, 1995; Kawakami et al., 2003; Yamamoto and Kagi, 2006; Song et al., 2009; Fall et al., 2011; Wang et al., 2011; Lamadrid et al., 2017) have proposed equations that relate the splitting of the Raman Fermi diad (Δ, cm^{-1}) with the density of CO_2. Thus, pressure estimations can be done by using these equations. We checked several vapor-rich fluid inclusions from the three systems and calculated pressures estimations by using the densimeter proposed by Lamadrid et al. (2017), in which ΔCO2 is corrected by using ΔNe (Neon light) as a standard for calibration (Figure 27). Results are shown in Table 5. Equations were used after data treatment procedure done by Labspec Software at Virginia Tech. It is important to highlight that no statistic data treatment has been performed. Only one measure per inclusion was realized in order to obtain CO_2 and Ne peaks. The inclusion was discarded if the peaks were not obtained at the second attempt.

3.7 Discussion

Historically, the hydrothermal systems inside the Alhué mining district were categorized as low, intermediate and high sulfidation epithermal deposits (e.g. Piñana, 1993; Cotton, 1998; Herreros, 2009) but also as intrusion related gold systems with mesothermal affinities (Herreros, 2009; Harris et al 2013), copper mantos mineralized bodies (Cotton, 1998), Zn-Pb-Ag rich skarn systems (Cotton, 1998) and others (e.g. transition epithermal-mesothermal deposit with adularia-sericite alteration. Poblete, 2008). There are a few examples in literature of similar deposits with so many origins. The closest analogs (in terms of mineralization) are the Groundhog Mine in New Mexico (Meinert, 1987; Hawksworth and Meinert, 1990), and mines near San Francisco del Oro-Santa Barbara district Mexico (Grant and Ruiz, 1988) in which skarns deposits related to porphyry copper ore bodies are described (Cotton, 1998). The mineralized structures present in the Alhué mining district show a transition from high temperatures calc-silicate bearing veins to those related to low temperature with epithermal features over a compressed vertical interval of only about 300 meters (Sillitoe, H.R., 2007).

It is clear that the Alhué mining district shows a transition from a dominant high temperature (sometimes containing calc-silicate minerals. e.g. Maqui vein) environment (mesothermal) to a weak low temperature system (epithermal). This can be observed not only in paragenetic sequences where bladed calcite appears at the end of the mineralization stages (Figure 11 and Figure 15) but also in the wide variety of T_h that can be obtain for a single system (Figure 12, Figure 14, Figure 16, and Figure 28). Some interesting characteristics of the deposit are: the presence of peripheral mushketovite, sodic (albite), calcic (epidote) and potassic (k-feldspar-biotite-magnetite) alterations (especially in the southeastern part of the district), massive magnetite veins and the presence of apatite and escapolite phases in some of the veins. Quartz may be considered as a later vein component that brecciated and cemented early calc-silicate and iron oxides veins (Figure 4). The main mineralization control present in Las Chilcas Formation corresponds to a structural one (Figure 2). Mineralized strike-slip, normal and inverse faults are the principal targets of the Alhué mining district. Mineralized structures are in the four principal volcanic units: basal lithic-crystal tuff, lower andesites, main tuff unit and upper andesites (Figure 3). At a distrital scale, Las Chilcas Formations corresponds to a damage zone between two competent rocks (Cretaceous intrusives) making possible the mineralization of larger structures like Maqui. Permeability of this fault is relatively high so fluids are more susceptible to migrate and mineralize through this area. Rapid coseismic dilation induced at specific structural sites such as dilational fault jogs and bends may induce localized transient reductions in fluid pressure (Sibson, 2000). In support of this, very low pressures were calculated in vapor-rich fluid inclusions (associated to flashing processes) reaching values ranging between 3.1–61.4 [bars] (Figure 27, Table 5).

Abundant theoretical, experimental and observational evidence in fossil and current geothermal systems suggests that boiling and/or flashing processes are an effective depositional mechanism for gold and silver in the hydrothermal (epithermal) environments (Brown, 1986; Seward et al., 2014). Various mineralogical, textural and fluid inclusion features have been genetically linked with boiling in hydrothermal systems. For example, coexisting liquid-rich and vapor-rich fluid inclusions contained in a FIA (Figure 9A, B and G) provide unarguable proof of the presence of boiling fluids (Bodnar et al., 1985; Goldstein and Reynolds, 1994). Similarly, if intense boiling or flashing occurs such that little or no liquid remains in the system, FIAs composed of only vapor-rich inclusions may result (Figure

9E) and may be considered direct evidence that extreme-boiling (flashing) occurred in the fluids. FIAs with boiling features were found during petrographic examination in the samples from Lorena and Maqui veins and in the system linked to the exploration campaign called Chilco vein. Heterogeneous trapping related to boiling or immiscible fluid systems was observed in the three systems and documented in paragenetic sequences (Figure 11, Figure 13, Figure 15). When boiling occurs, the phases that are precipitated may be amorphous or so fine-grained that trapping of fluid inclusions is not possible. However, the boiling fluids that are precipitating the amorphous/fine-grained phases may be trapped as secondary inclusions in earlier precipitated phases that have crystallized (or re-crystallized) to produce coarser grained phases that are amenable to hosting fluid inclusions. Thus, secondary fluid inclusions become important tools for recognizing that boiling occurred, even though the boiling event that is being recorded by the inclusions occurred after the material hosting the inclusions was originally precipitated. (Moncada et al,. 2017).

Boiling also leads to distinct mineralogy and mineral textures in the hydrothermal environment owing to the physical and chemical changes that take place as a result of boiling including rapid temperature decrease, decrease in the amount of liquid available to accommodate the dissolved components, loss of gases that lead to changes in fluid chemistry and increase pH of the fluid associated with the boiling (Moncada et al., 2017).

Textures described in this study are thought to be produced by (re)-crystallization of amorphous silica or chalcedony that may have precipitated from boiling solutions which is usually linked to metal deposition in precious metal systems (Buchanan, 1979; Roedder, 1984; Bodnar et al., 1985; Brown, 1986; Simmons and Christenson, 1994; Etoh et al., 2002; Moncada et al., 2012). Several textures that may be related to boiling were found in samples (e.g. jigsaw, feathery, crustiform, colloform, pseudo acicular and bladed calcite, Figure 7) with jigsaw textured quartz being the most common texture in relation to precipitation under probable boiling environments (47.8% of the samples contain this texture, Figures 6 and 7A). Anhedral jigsaw-textured quartz correspond to a recrystallization texture that is characterized by aggregates of microcrystalline to crystalline quartz crystals with interpenetrating gran boundaries that is only recognizable when observed under crossed polars (Dong et al., 1995; Moncada et al., 2012). The texture is interpreted to result from recrystallization of massive chalcedony or amorphous silica (Dong et al.,1995). No primary fluid inclusions were found

in this type of texture although many trails of secondary fluid inclusions were present implying fluid conditions after recrystallization of the original chalcedony or amorphous silica.

In pure water systems, the solubility of quartz increases systematically with temperature up to ~370 °C, but at higher temperature, it´s solubility is retrograde. The presence of alkali salts, such as NaCl and KCl, reduces the solubility of quartz at low temperature but increases it at temperatures above 250 °C (Williams-Jones, A.E. and Migdisov, A.A., 2013). As a result, the originally silica-undersaturated fluid may achieve high degrees of silica supersaturation, leading to the precipitation of amorphous silica. With time, the amorphous silica may recrystallize to chalcedonic silica and/or quartz (Fournier, 1985) to produce many of the textures observed in this study. For example, jigsaw-textured quartz, characterized by equant, anhedral interlocking grains, may indicate crystallization from amorphous silica that precipitated from a solution very supersaturated in silica (Fournier, 1985).

Those textures observed here that are thought to be produced directly by precipitation from supersaturated solutions, or by crystallization of chalcedony or quartz from original amorphous silica, include mosaic (jigsaw), prismatic subhedral, feathery, crustiform, colloform, pseudo-acicular. In each sample, the presence of these textures has been noted and used to infer whether boiling occurred at the sample location at some time during or after deposition of the original material.

The presence of adularia (observed in Lorena paragenetic sequence, Figure 13) or colloform banded quartz (Figure 7G), are all also considered to be evidence of boiling. Other quartz textures that suggest original precipitation of silica gel (amorphous silica) or chalcedony, such as jigsaw/mosaic, feathery, plumose, flamboyant and ghost sphere quartz are consistent with deposition from boiling solutions but could form from other processes that result in rapid silica precipitation (Moncada et al., 2017).

One important aspect is that electrum was found in jigsaw-textured quartz implying not only that boiling is recognizable at a textural level but also that is an efficient mechanism to precipitate gold and silver mineralization in the structures. Textures indicative of boiling as this one can be observed in the three paragenetic sequences: Lorena, Maqui and Chilco structures (Figure 11, 13 and 15) and are always in relation to the ore stages independently

of the structure. Also, a clear late texture suggested epithermal substage can be observed in the sequences of Chilco and Maqui (Figure 11 and 15) by taking in consideration the presence of late bladed calcite precipitation (Figure 7J, 11 and 15).

The loss of CO2 due to boiling results in the rapid precipitation of calcite, which favors the formation of bladed crystals rather than rhombohedral crystals that would form during slower growth. Thus, the presence of bladed calcite is another strong evidence for boiling (Moncada et al., 2017). The occurrence of platy calcite, crustiform-colloform silica and K-feldspar (adularia) in the structures indicates the existence of boiling conditions to precious-metal deposition (Simmons and Browne, 2000).

Besides the evidence of FI indicating boiling (Type I and II FIAs in Figure 8) and flashing (Type III FIAs in Figure 8) processes, a wide variety of FI were observed in the samples from the three systems. L-rich FI hosted by quartz and sphalerite crystals (type IV and V in Figure 8 respectively) and FI related to hypersaline fluids containing chlorides and opaques solids (up to 3) inside the inclusions (type VI in Figure 8) were also found and described in Lorena, Maqui and Chilco structures. These types of inclusions (IV, V and VI) are also a common feature in quickplates and thin sections and may contain evidence of non-boiling (or flashing) processes that mineralized the systems. Important facts related with the above mentioned are: (1) Type V inclusions were found (in some cases) related to disseminated mineralization of chalcopyrite and pyrite (sulfides following the trend of FIA, Figure 9D) implying that precipitation of sulphides was directly related to non-boiling fluids (boiling neither flashing are the mechanisms to precipitate chalcopyrite, pyrite, sphalerite, gold and silver). (2) Type VI inclusions presented daughter minerals related mainly to halite crystals (although the presence of some other chlorides as potassium chlorides was observed) and opaques inside (Figure 9C,H,I and J). In this in multiphase fluid inclusions (containing liquid, vapour, and sometimes more than two solid phases at room temperature) ferropyrosmalite, an iron-rich member of the pyrosmalite series [$(Fe,Mn)_8Si_6O_{15}(OH,Cl)_{10}$] has been determined. Using Raman spectrums, two distinct bands at 615 cm^{-1} and 1022 cm^{-1} were identify and related to this mineral (Figure 26). Type VI FIA (L-rich+IC,S1) containing ferropyrosmalite occur in hydrothermal infill and alteration quartz, which is closely associated with sulphide mineralization. During heating experiments, ferropyrosmalite behave stable and no detectable decrease in size up to 570°C (maximum

temperature used in this study) was observed. These higher homogenization temperatures may represent temperatures of the mineralizing fluids prior to ore deposition (e.g. Adshead, 1996). An important fact detected by using LA-ICP-MS microanalyses in singular FI belonging to FIAs show Types VI inclusions have the greatest concentrations of iron (~1000s to ~10000s ppm) consistent with the presence of ferropyrosmalite. Besides, Lorena structure, in where these type of inclusions were more abundant, is the iron-richest system of all three and iron shows positive correlations with Ag and salinity in this system. The above mentioned idea is consistent also with the transient signals observed on Type VI fluid inclusions where notorious signals in Na, K, Mn, Ca, Fe, Ag, Pb, Zn, As, Cd are observed (Figure 22). Type VI fluid inclusions (FI) that homogenize by halite disappearance are common in the structures of the Alhué mining district (Lorena, Maqui and Chilco) as it happens in many hydrothermal ore deposits, including porphyry copper (e.g., Bodnar and Beane, 1980), skarn (e.g., Baker and Lang, 2003) and iron-oxide copper gold (IOCG) (e.g., Niiranen et al., 2007) systems, as well as in medium to high grade metamorphic environments (e.g., Scambelluri et al., 1997). Microthermometric measurements were made on all six types of fluid inclusions assemblages defined previously (see Figure 8). In terms of microthermometry, fluid inclusions were classified during heating from room temperature and considering their host phase and their genetic origin (primary or secondary FIAs). Due to the variety of FIAs present in the samples from the Alhué mining district (Figure 8) there is a wide internal variation in Th and salinities observed at all scales: district, structural, and hand sample scale (Figure 20 and 21). Figure 28 shows typical ranges of ore-precipitating fluids projected in temperature-salinity fluids from Wilkinson (2001) and the T_h and salinities of the fluids from the Alhué mining district. No univocal setting is observed. The data is dispersed consistently with the above mentioned.

The internal variation in homogenization temperatures and salinities in the structures (e.g. Maqui vein) may reflect the diversity of ore-forming conditions of the mining district but may also reflect the study of FIAs that are not involved in mineralizing processes also.
In historical FI studies (Cotton, 1998., Araya, 2001., Sepúlveda, 2004., Herreros, 2009., Harris et al., 2013) authors agreed that broad distribution of T_h found in different structures but also within a unique one indicate the presence of different multi-stage hydrothermal events for each structure and therefore every structure may be studied separately considering

substantial chemical variations in the fluids. Gold concentration determined by LA-ICP-MS in fluid inclusion is observed in just three FIAs from two samples (*241108* from Chilco structure and *2508163* from Maqui mineralized structure) corresponding to primary and secondary type V FI and secondary type III FI. In sample 241108 from Chilco, primary liquid-rich FIA hosted in sphalerite (Type V) contain 3.8 ppm of Au. Secondary liquid-rich FIA hosted in sphalerite (Type V) contain 0.13 ppm of Au. In sample 2508163 a type III FIA contain 1.5 ppm average of Au. Salinities related to type V inclusions containing gold range from 14.1 to 22.1 wt% NaCl. Due to the nature of this type of inclusions, gold chloride complexes are active components transporting the gold in Chilco vein and precipitating it under mechanism besides boiling and/or flashing (cooling and/or mixing). Type I and II (boiling) and type III (flashing) FIAs are very common in Chilco vein so this mechanism may be participating more or less in the precipitation of Gold (Figure 19). Vapor-rich inclusions (type III) transporting gold were observed in a FIA from a surface Maqui vein sample (sample 2508163). This low density fluid (2.8 to 3.9 wt% NaCl) is related to minor gold concentrations consistently with the upward loss of this precious metal in a boiling-fluid column. In fluids of this nature H_2S is strongly fractionated into the vapor phase lowering the activity of HS^- (causing gold deposition) implying that HS^- is an important ligand also in the Alhué mining district. The Alhué mining district has, as said before, a first order structural control. “Falla de Borde” or “Agua Fría” transtensive fault is highly important in the upward migration of the deep fluids that mineralized the district. This fault was interpreted from aeromagnetic data as a boundary fault between the Lower Cretaceous Agua Fría pluton to the west and a basin filled with a volcanic succession called Las Chilcas Formation to the east (Matthews, S. 2018). This fault may have a regional character due to its lenght (see Figure 2) and nature and may have undergone an inversion during its history. Figure 29 shows a general model in which high temperature fluids probably as products of a devolatilization from mafic magma fluids emplaced deep in the crust reach subsurface conditions by using the fault systems present in the Alhué mining district. Here, boiling and flashing processes may occur connected to continuous seismicity that triggers progressive precipitation of gold and silver during time. Boiling and flashing processes are effectively precipitating precious metals in the district but others processes should not be discarded due to the evidence presented in this study.

3.8 Conclusions

The main mineralization control in the district corresponds to a structural one. The presence of peripheral mushketovite, sodic (albite), calcic (epidote) and potassic (k-feldspar-biotite-magnetite) alterations (especially in the southeastern part of the district), massive magnetite veins and the presence of apatite and scapolite phases in some of the veins are other important characteristics of the district. As the main mineralization control in the district corresponds to a structural one, rapid coseismic dilation induced at specific structural sites such as dilational fault jogs and bends may induce localize transient reductions in fluid pressure and thus the trigger for precipitating mechanisms such as boiling and/or flashing events (Huizenga and Parker, 2017). Textural and FIA evidence of these two mechanisms have been found in the three localities studied: Maqui, Lorena and Chilco but they may not be the only ones participating in the precious mineral precipitation. The presence of gold and silver in both vapor-rich only FIA hosted in quartz (type III) and liquid-rich FIA hosted in sphalerite (type V) implies that gold is being transported as chloride and/or sulfide complexes depending of the system. Although the paragenetic sequence for Chilco system show late boiling textures such as bladed calcite, current data suggest that gold is being transported in chlorides complexes and precipitating by cooling and or mixing of fluids. Cooling can be an effective mechanism in systems where gold is transported as a chloride complex but boiling and/or flashing participation can not be discarded due to the presence of textural and FI evidence of these two mechanisms in Chilco structure. Gold in Maqui FIA was found in vapor-rich only FI with values that range between 1.48 to 1.56 ppm. Sulfide complexes transporting the gold are more probable for this system due to the nature of the fluids found. Boiling and/or flashing events may be more important in the precipitation of gold in certain structural sites (dilatational jogs) for Maqui mineralized structure. Lorena structure represents the deepest zone studied and contain fluids with higher salinity than the fluids studied from Maqui and Chilco. These fluids have clear halite crystals as daughter minerals and, in some cases, other rounded chlorides and solids. Also, the highest homogenization temperatures were found in this system reaching up to 533°C supporting the idea of the proximity of Lorena fluids to the source. Daugther minerals as pyrosmalite inside FIA in Lorena represent that iron-rich high-density fluids mineralized the deeper structures as

Lorena. Quartz textures observed in the Maqui, Lorena and Chilco structures such as mosaic (jigsaw), prismatic subhedral, feathery, crustiform, colloform and pseudo-acicular are thought to be produced directly by precipitation from supersaturated solutions (or by crystallization of chalcedony or quartz from original amorphous silica) which is usually linked to metal deposition in precious metal systems. The presence or absence of these textures were used in this study to infer whether boiling occurred at the sample location at some time during or after deposition of the original material. In the three localities boiling and flashing evidence is observed at a textural level but also in consideration of the nature of the FIA in the samples. Boiling and/or flashing as precipitation mechanisms can not be discarded for any system and are considered important in those who show strong evidence (e.g. Maqui structure). Variability of the presence of more or less FIA suggesting boiling/flashing processes can be observed. Maqui is the structure where the most FIA related to boiling and or flashing mechanisms can be found, followed by the Lorena structure and finally by the Chilco structure. Textures indicative of boiling can be observed in the three paragenetic sequences and are always in relation to the ore stages, electrum in mosaic (jigsaw) quartz from Lorena sample (sample 240909) as a precious metal phase may be an important fact in the demonstration of that boiling is effectively precipitating precious metal mineralization in the Alhué mining district. Liquid-rich FI hosted in quartz or sphalerite (Types IV and V FIA) and liquid-rich FI related to hypersaline fluids containing chlorides and opaques solids (up to 3) inside the inclusions were also found and described in Maqui, Lorena and Chilco structures. These types of FIA (IV, V and VI) are evidence of non-boiling (or flashing) processes that mineralized the system. Important facts related with the above mentioned are: (1) Type V inclusions in Chilco structure were found (in some cases) related to disseminated mineralization of chalcopyrite and pyrite (sulfides following the trend of FIA, Figure 9D) implying that precipitation of sulphides were directly related to non-boiling trapped inclusions (implying that boiling neither flashing are the mechanisms to precipitate chalcopyrite, pyrite, sphalerite, gold and silver). (2) Type VI inclusions presented daughter minerals related mainly to halite crystals (although the presence of some other chlorides as potassium chlorides was observed) and up to three opaques inside (Figure 9C,H,I and J) implying that mineralization of Mn, Fe, Zn, Pb, Cd and Ag (elements present in LA-ICP-MS analysis done in Type VI Lorena FIA) may be due to non-boiling precipitation mechanisms.

Ferro-pyrosmalite was found in this type of FIA consistently with iron (~1000s to ~10000s) contents measured in LA-ICP-MS analysis. Type VI FI that homogenize by halite disappearance are common in the structures of the Alhué mining district (Lorena, Chilco and Maqui) as it happens in many hydrothermal ore deposits, including porphyry copper and iron-oxide (IOCG) systems. In terms of microthermometry, there is wide internal variation in T_h and salinities observed at all scales (distrital, mineralized structures and hand samples) as reported by previous studies (Cotton, 1998., Araya, 2001., Sepúlveda, 2004., Herreros, 2009., Harris et al., 2013). This may reflect the diversity of ore-forming conditions in the mining district, the variability of processes and geochemical components acting in certain location or the study of FIA that are not involved in mineralizing processes. Authors of older studies agreed that broad distribution of T_h found in different mineralized structures but also within a unique one indicate the presence of different multi-stage hydrothermal events that mineralized the structures unevenly. Thus in conclusion, the Alhué mining district has a first order structural control in where important transtensive faults like the "Agua Fría" fault make possible the upward migration of the fluids to reach subsurface conditions and in where boiling and flashing processes may occurred in connection with ancient ongoing seismicity that triggered progressive precipitation of gold and silver during time. Boiling and flashing processes are effectively precipitating precious metals (as outlined by Huizenga and Parker, 2017) in the district but others processes such as cooling and/or mixing of fluids should not be discarded due to the evidence presented in this study.

Acknowledgments

This research was supported by FCFM-UChile granted to Moncada D., CEGA Fondap-Conicyt Project 15090013, FONDEQUIP EQM 140009 and the Núcleo Milenio Trazadores de Metales NC130065.

References

Adams, S. F., 1920. A microscopic study of vein quartz. Economic Geology, v. 15, p. 623-664.

Adshead, N.D., 1996. Extended abstract, MIC'96. Townsille 1-4.

Aguirre, L., 1985. The Southern Andes, In: Nairn, A. E. M., Stehli, F. G., and Uyeda, S., (eds), The Ocean Basins and Margins: The Pacific Ocean, Volume 7A. New York, Plenum Press, p. 265–376.

Alcázar, P., 2001. Geología y estimación de reservas de Sistema de vetas Valeria, distrito minero Alhué región metropolitana. Memoria para optar al título de geólogo. Universidad de Chile. 100 p.

Araya, J., 2001. Informe geológico y evaluación de recursos distrito minero Alhué. Memoria de Título. Universidad de Chile, Santiago, Chile. 160 p.

Becker, S.P., Eichhubl, P., Laubach, S.E., Reed, R.M., Lander, R.H., Bodnar, R.J., 2010. A 48 m.y. history of fracture opening, temperature and fluid pressure: cretaceous Travis Peak Formation, East Texas basin. Bulletin of the Geological Society of America 122 (7/8), 1081–1093.

Bodnar, R. J., 2003a. Introduction to fluid inclusions, *in* Samson, I., Anderson, A., and Marshall, D., eds., Fluid Inclusions: Analysis and interpretation: Mineralogical Association of Canada, Short Course 32, p. 1-8.

Bodnar, R. J., 2003b. Reequilibration of fluid inclusions, *in* Samson, I., Anderson, A., and Marshall, D., eds., Fluid inclusions: Analysis and interpretation: Mineralogical Association of Canada, Short Course 32, p. 213–230.

Bodnar, R. J.; Beane, R. E., 1980. Temporal and Spatial Variations in Hydrothermal Fluid Characteristics during Vein Filling in Preore Cover Overlying Deeplly Buried Porphyry Copper-Type Mineralization at Red Mountain, Arizona. Economic Geology, Vol. 75, pp. 876-893.

Bodnar, R. J., Reynolds, T. J., and Kuehn, C. A., 1985. Fluid- inclusion systematics in epithermal systems. Reviews in Economic Geology, 2, p. 73-97.

Brown, K.L., 1986. Gold deposition from geothermal discharges in New Zealand. Economic Geology 81 (4), 979–983.

Buchanan, L. J., 1979. The Las Torres Mines, Guanajuato, Mexico: Ore controls of a fossil geothermal system. Unpublished Ph. D. dissertation, Colorado School of Mines, Golden, Colorado, 138 pp.

Buchanan, L. J., 1981. Precious metal deposits associated with volcanic enviroments in the Southwest. Arizona Geological Survey Digest, 14: 237-262.

Carter, W.D., 1963. Unconformity marking the Jurassic-Cretaceous boundary in the La Ligua area, Aconcagua Province, Chile. U.S. Geological Survey Proffesional Paper 450-E. p. E61-E63.

Corvalán, J., 1974. Paleozoic crystalline basement complex of central Chile. IAVCEI - International Symposium on Volcanology. Guide book D-6. Santiago-Chile: Departamento de Geología. Universidad de Chile. 1l pp.

Cotton, W. B., 1998. Geology and Ore Deposits of the Maqui Vein, Alhué Mining District, Coast Range of Central Chile. MS, University of Colorado.130 p.

Cotton, W. B. III, Atkinson, W. W. Jr, Sharaky, A. M., 1999. Geology and ore deposits of the Maqui vein, Alhué mining district, Coast Range of Central Chile. Geological Society of America, Annual Meeting, Denver, Colorado, USA, Abstract 52241.

Clark, J.R. and Williams-Jones, A.E., 1990. Analogues of epithermal gold.silver deposition in geothermal well scales. Nature, 346(6285): 644-645.

Diaz, S., 1986. Geología Económica y Prospección Geoquímica del área de la Mina La Leona, distrito minero Chancón, VI Región. Memoria para optar al Título de Geólogo. Universidad de Chile. 196 p.

Dong G, Morrison, G., Jaireth , S., 1995. Quartz textures in epithermal veins, Queensland; classification, origin and implication. Economic Geology. 90(6): 1841-1856.

Etoh, J., Izawa, E., Watanabe, K., Taguchi, S., Sekine, R., 2002. Bladed quartz and its relationship to gold mineralization in the Hishikari low-sulfidation epithermal gold deposit, Japan. Economic Geology 97 (8), 1841–1851.

Fournier, R.O., 1985. The behavior of silica in hydrothermal solutions. Reviews in Economic Geology 2, 45–61.

Frezzotti, M.L., Tecce, F., Casagli, A., 2012 Raman spectroscopy for fluid inclusión analysis. Journal of Geochemical Exploration. 112. 1-20.

Fuentealba C., 2002. Geología y Mineralización de Oro en el Distrito Minero de Alhué, Cordillera de la Costa de Chile Central. Memoria para optar al Título de Geólogo. Universidad de Chile. 96 p.

Gammons CH., Yu Y, Williams-Jones A.E., 1997. The disproportionation of gold chloride complexes at 25 to 200°C. Geochimica et Cosmochimica Acta 61: 1971-1983

Gana, P. and Wall, R., 1997. Evidencias geocronológicas ^{40}Ar-^{39}Ar y K-Ar de un hiatus Cretácico Superior – Eoceno en Chile central (33°-33°30'S). Revista Geológica de Chile. Vol. 24. No. 2. p. 145-163.

Ganerod, G.V.; Braathen, A.; Willemoes-Wissing, B., 2008. Predictive permeability model of extensional faults in crystalline and metamorphic rocks; verification by pre-grouting in two sub-sea tunnels, Norway. Journal of structural Geology. 30. 993 – 1004.

Grant, G. and Ruiz, J., 1988. Pb-Zn-Cu-Ag deposits of the Granadena mine, San Francisco del Oro-Santa Barbara district, Chihuahua, Mexico. Economic Geology. Vol. 83. Pp.1683-1702.

Gropper, J., 2011. Franjas metalogénicas de edad Jurásica y Cretácica en la cordillera de la costa de Chile central, entre los 32° y los 35° 20' de latitud sur. Memoria para optar al título de geólogo. Universidad de Chile.

Goldstein, R.H., Reynolds, T.J., 1994. Systematics of fluid inclusions in diagenetic minerals: SEPM Short Course Notes, 31, p. 213.

Harris, J., Matthews, S., Perez, M., 2013. Informe técnico campaña de exploración 2008-2012. Proyecto Chancón – Membrillo. Región metropolitana y libertador Bernardo O´higgins, Chile. Informe preparado por Yamanca Gold Inc. Inédito. 178 p.

Hawksworth, M. and Meinert, L., 1990. Alteration and Fluid inclusion study of the Groundhog vein system, Central Mining District, New Mexico. Economic Geology. Vol. 85, pp 1825-1839.

Hedenquist, J. W., Arribas, A. and Eliseo, G.-U., 2000. Exploration for epithermal gold deposits. Society of Economic Geologists Reviews, 13: 245-277.

Henley, R. W., and Hughes, G. O., 2000. Underground fumaroles: "Excess heat" effects in vein formation. Economic Geology, 95, 3, p. 453-466.

Herreros, D., 2009. "Caracterización geológica y antecedentes microtermométricos de la veta Peumo Distrito Valencia, Región Metropolitana, Chile. Memoria de título. Universidad de Concepción. Departamento de Geología. 106 p.

Herrington, R.J., Wilkinson, J.J., 1993. Colloidal gold and silica in mesothermal vein systems. Geology, v. 21, p. 539-542.

Hervé, F., Godoy, E., Parada, M. A., Ramos, V., Rapela, C., Mpodozis, C., and Davidson, J., 1987. A general view on the Chilean-Argentinian Andes, with emphasis on their early history, in Monger, J. W. H., and Francheteau, J., eds., Circum-Pacific orogenic belts and the evolution of the Pacific basin: Washington, D. C., American Geophysical Union, Geodynamic Series, v. 18, p. 97–113.

Hervé, F., Munizaga, F., Parada, M.A., Brook, M., Parkhurst, R., Snelling, N., Drake, R., 1988. Granitoids of the Coast Range of Central Chile: Geochronology and geologic setting: Journal of South American Earth Sciences, v.1, p. 185-194.

Iglesias Patrimoniales Chile, 2014. Historia de Iglesias Patrimoniales. http://iglesiaspatrimoniales.cl/iglesia-de-alhue-historia (acceso 13 de Agosto, 2018).

Johnson JW, Oelkers EH, Helgeson HC, 1992. SUPCRT92: A software package for calculating the standard molal thermodynamic properties of minerals, gases, aqueous species, and reactions from 1 to 5000 bar and 0 to 1000°C. Computers & Geosciences 18: 899-947

Lamadrid, H.M., Moore L.R., Moncada, D., Rimstidt J.D., Burrus, R.C., Bodnar, R.J., 2017. Reassessment of the Raman CO_2 densimeter. Chemical Geology. 450. 210-222.

López-Escobar, L., Frey, F., Oyarzún, J., 1979. Geochemical Characteristics of Central Chile (33-34°S) Granitoids. Contributions to mineralogy and petrology, 70, 439-450.

Lemmlein, G.G., 1929. Sekundäre Flüssigkeitseinschlüsse in Mineralen. Z. Kristallogr. 71, 237-256.

Levi, B., 1969. Burial metamorphism of a Cretaceous volcanic sequence west from Santiago, Chile: Contributions to Mineralogy and Petrology, v. 14, p. 39-49

Levi, B., Aguirre, L., Nystrom, J.O., Padilla, H., Vergara, M., 1989. Low-grade regional metamorphism in the Mesozoic-Cenozoic volcanic sequences of the Central Andes: Journal of Metamorphic Geology, v. 7, p. 487-495.

Levi,B., Padilla, H, Nyström, J., Vergara, M., 1988. Facies de Alteración Regional en las secuencias volcánicas Mesozoicas y Cenozoicas de Chile Central. Revista Geológica de Chile, Vol. 15, Nº 1. Servicio Nacional de Geología y Minería.

Lindgren, W., 1933 Mineral deposits, 4th edition, New York, McGraw-Hill, 930 pp.

Lindgren, W. and Bancroft, H., 1914. The ore deposits of the Republic mining district: U.S. Geological Survey Bulletin. 550, 147p.

Matthews, S., 2017a. Geología Distrital Florida. Informe inédito. Yamana Gold Inc.

Matthews, S., 2017b. Metamorfismo y alteración. Informe inédito. Yamana Gold Inc.

Matthews, S., 2018. Geología del Distrito Minero Alhué. Presentación inédita. Yamana Gold Inc.

Moncada, D., Baker, D., Bodnar, R.J., 2017. Mineralogical, petrographic and fluid inclusion evidence for the link between boiling and epithermal Ag-Au mineralization in the La Luz area, Guanajuato Mining District, México, Ore Geology Reviews.

Moncada D., Mutchler, S., Nieto, A., Reynolds, T.J, Rimstidt, J.D., Bodnar, R.J., 2012. Mineral textures and fluid inclusion petrography of the epithermal Au-Ag deposits at Guanajuato, Mexico: Application to exploration. Journal of Geochemical Exploration 114, p 20-35.

Meinert, L., 1997. Application of skarn deposit zonation models to mineral exploration. Explor. Mining Geol. Vol. 6. No 2. Pp. 185-208.

Munizaga, F. and Vicente, J.C., 1982. Acerca de la zonación plutónica y del volcanismo miocénico en los Andes de Aconcagua (lat. 32-33°S): Datos radiométricos K-Ar: Revista Geológica de Chile. Vol. 16. p. 3-21.

Muñoz-Cristi, J, 1964. Estudios petrográficos y petrológicos sobre el Batolito de la Costa de las provincias de Santiago, y Valparaíso. Inst. Geol. Univ. Chile. Publ. No. 25, 93 pp.

Nasi, C., 1981. Estratigrafía del Jurásico y Cretácico de la Cordillera de la Costa al sureste de Melipilla (Chile Central). Memoria de título (Inédito), Departamento de Geología Universidad de Chile,. 246 p.

Nasi, C., 1981. Estratigrafía del Jurásico y Cretácico de la Cordillera de la Costa al sureste de Melipilla (Chile Central). Memoria de título (Inédito), Departamento de Geología Universidad de Chile,. 246 p.

Nasi, C., Thiele, R., 1982. Estratigrafía del Jurásico y Cretácico de la Cordillera de la Costa al sur del río Maipo, entre Melipilla y Laguna de Aculeo (Chile Central). Revista Geológica de Chile Nº 16 p. 81-99.

Niiranen, T.; Poutiainen, M.; Manttari, I. Geology., 2007. Geochemistry, fluid inclusion characteristics, U-Pb age studies on iron oxide-Cu-Au deposits in the Kolari región, northern Finland. Ore Geology reviews. Volume 30. Issue 2, pages 75-105.

Ogryzlo SP., 1935. Hydrothermal experiments with gold. Economic Geology 30: 400-424.

Pincheira, M., Frutos, J., Hernádez, L., Zamarreño, J., 1994. Antecedentes mineralógicos texturales en la mineralización estratoligada del distrito Punta del Cobre, Chile. VII Congreso Geológico Chileno, Concepción, Chile, Vol. 2, p. 873-877.

Piñana, X., 1993. Mineralización epitermal de oro distrito minero "El Membrillo de Alhué". Memoria para optar al título de geólogo. Universidad de Chile. 113 p.

Piracés, R., 1976. Estratigrafía de la Cordillera de la Costa entre la Cuesta El Melón y Limache, Provincia de Valparaíso. Chile. Primer Congreso Geológico chileno, Actas, v.1, p. 65-82.

Poblete, J., 2008. Geología, Alteración y mineralización en los prospectos Au-Ag Las bellas y Don Bernardo, comuna de Alhué, región metropolitana. Memoria para optar al título de geólogo. Universidad de Chile. 104 p.

Rodriguez, M., Campos, E., Barra, F., 2000. Antecedentes mineralógicos y microtermométricos del yacimiento Manto Verde, distrito minero Punta del Cobre, Norte de Chile. 5p. Inédito.

Roedder, E., 1984. Fluid Inclusions. Mineralogical Society of America. Reviews in Mineralogy, vol 12. 644p.

Rogers, A.F., 1917. A review of the amorphous minerals: Journal of Geology. v. 25. p. 515-541

Romero, N., Mundaca, P., 1997. Geología del Distrito Minero Alhué. Informe Inédito S.L.M. LAS CENIZAS. 55 p.

Sander, M. V. and Black, J. E., 1988. Crystallization and recrystallization of growthzoned vein quartz crystals from epithermal systems, implications for fluid inclusion studies. Economic Geology, 83, 5, p. 1052-1060.

Scambelluri, M.; Piccardo, G.; Philippot, P.; Robbiano, A.; Negretti, L., 1997. High-salinity brines from recycled seawater in deeply subducted serpentiinite. Earth Planet. Sci. Lett. 148. 485-499.

Seward, T.M., Williams-Jones, A.E. and Migdisov, A.A., 2014. The Chemistry of Metal Transport and Deposition by Ore-Forming Hydrothermal Fluids. In: 42 H.D.H.K. Turekian (Editor), Treatise on Geochemistry (Second Edition). Elsevier, Oxford, pp. 29-57.

Schrader, F.S., 1923. The Jarbidge mining district, Nevada: U.S. Geological survey Bulletin 741, 86 p.

Sepúlveda, F., 2004. Caracterización geológica y antecedentes microtermométricos de la veta Lorena, distrito minero Alhué, región metropolitana, Chile. Memoria para optar al título de geólogo. Universidad de Chile. 85 p.

SERNAGEOMIN., 2003. Mapa Geológico de Chile: versión digital, publicación geológica digital, No 4, Santiago, Chile, Servicio Nacional de Geología y Minería, escala 1:1000 000.

Seward, T.M., 1973 Thio complexes of gold and the transport of gold in hydrothermal ore solutions. Geochimica et Cosmochimica Acta 37: 379–399

Shaub, B.M., 1934. The cause of banding fissure veins: A:merican Mineralogist, v. 19, p. 393-402.

Sibson, R.H., 2000. Fluid involvement in normal faulting. Journal of Geodynamics 29. 469-499.

Sillitoe, R. H., 2007. Comments on the Alhué, Jerónimo, Esperanza and Encrucijada Gold Properties, Chile. Internal. Internal Meridian Report: Unpublished.

Simmons, S.F. and Browne, P.R.L., 2000. Hydrothermal minerals and precious metals in the Broadlands-Ohaaki geothermal system: Implications for understanding low-sulfidation epithermal environments: Economic Geology, 95: 971−999.

Simmons, S.F., Christenson, B.W., 1994. Origins of calcite in a boiling geothermal system. American Journal of Science 294 (3), 361–400.

Simmons, S.F., White, N.C. and John, D.A., 2005. Geological Characteristics of Epithermal Precious and Base Metal Deposits. Economic Geology 100th Anniversary Volume, Economic Geology; One Hundredth Anniversary Volume, 1905-2005: 485-522.

Stefánsson, A., Seward T.M., 2004. Gold(I) complexing in aqueous sulphide solutions to 500°C at 500 bar. Geochimica et Cosmochimica Acta 68: 4121-4143

Streckeisen, A., 1976. To each plutonic rock its propert name. Earth Science Reviews, 12: p.1-33.

Thomas, H., 1958. Geología de la Cordillera de la costa entre el Valle de la Ligua y la Cuesta Barriga. Instituto de Investigaciones Geológicas, boletín Nº 2, 86 p.

Van den Kerkhof, A.M., Hein, U.F., 2001. Fluid inclusion petrography. In: Andersen, T., Frezzotti, M.-L., Burke, E.A.J. (Eds.), Lithos. Special volume in honour of Jacques Touret: Fluid inclusions: Phase relationships- methods- applications, pp. 27–47.

Vergara, M., Levi, B., Nystrom, J.O., and Cancino, A., 1995. Jurassic and Early Cretaceous island arc volcanism, extension, and subsidence in the Coast Range of central Chile, GSA Bulletin, v. 107, no. 12, p. 1427-1440.

Vergara, M. and Drake, R., 1979a. Edades K/Ar en secuencias volcánicas continentales postneocomianas de Chile Central, su depositación en cuencas intermontañas restringidas: Asociación Geológicas Argentina. Revista XXXIV. Vol. 1. p. 42-52.

Vergara, M. and Drake, R., 1979b. Eventos magmáticos plutónicos en los Andes de Chile Central. II Congreso Geológico Chileno (Arica). Vol. 1. p. F19-F30.

Vikre, P.G., 1985. Precious metal vein systems in the National District, Humboldt County, Nevada. Economic Geology, 80(2): 360 -393.

Wall, R, Gana, P, Gutiérrez, A., 1996. Mapa Geológico del área de San Antonio-Melipilla. Regiones de Valparaíso, Metropolitana y del Libertador Bernardo O'Higgins. Servicio Nacional de Geología y Minería (Chile). Mapa geológico N° 2, escala 1:100.000. 20 p.

Huizenga, J.M., and Parker, A.G., 2017. Hydrothermal Au mineralisation caused by fluid decompression and cooling in dilatational cavities. In: EGRU Contribution (69), p. 57. From: FUTORES II Conference: future understanding of tectonics, resources, environment and sustainability, 4-7 June 2017, Townsville, QLD, Australia.

Wilkinson, J.J., 2001. Fluid inclusions in hydrothermal ore deposits. Lithos 55, 229-272.

Williams-Jones, A., Bowell, R., Migdisov, A., 2009. Gold in solution. Elements 5(5):281-287.

Wright, R.B., Wang, C.H., 1973. Density effect on the Fermi resonance in gaseous CO2 Raman scattering. J. Chem. Phys. 58, 2893–2895.

Wright, R.B., Wang, C.H., 1975. Effect of density on the Raman scattering of molecular fluids. II. Study of intermolecular interactions in CO2. J. Chemical Physics. 61, 2707–2710.

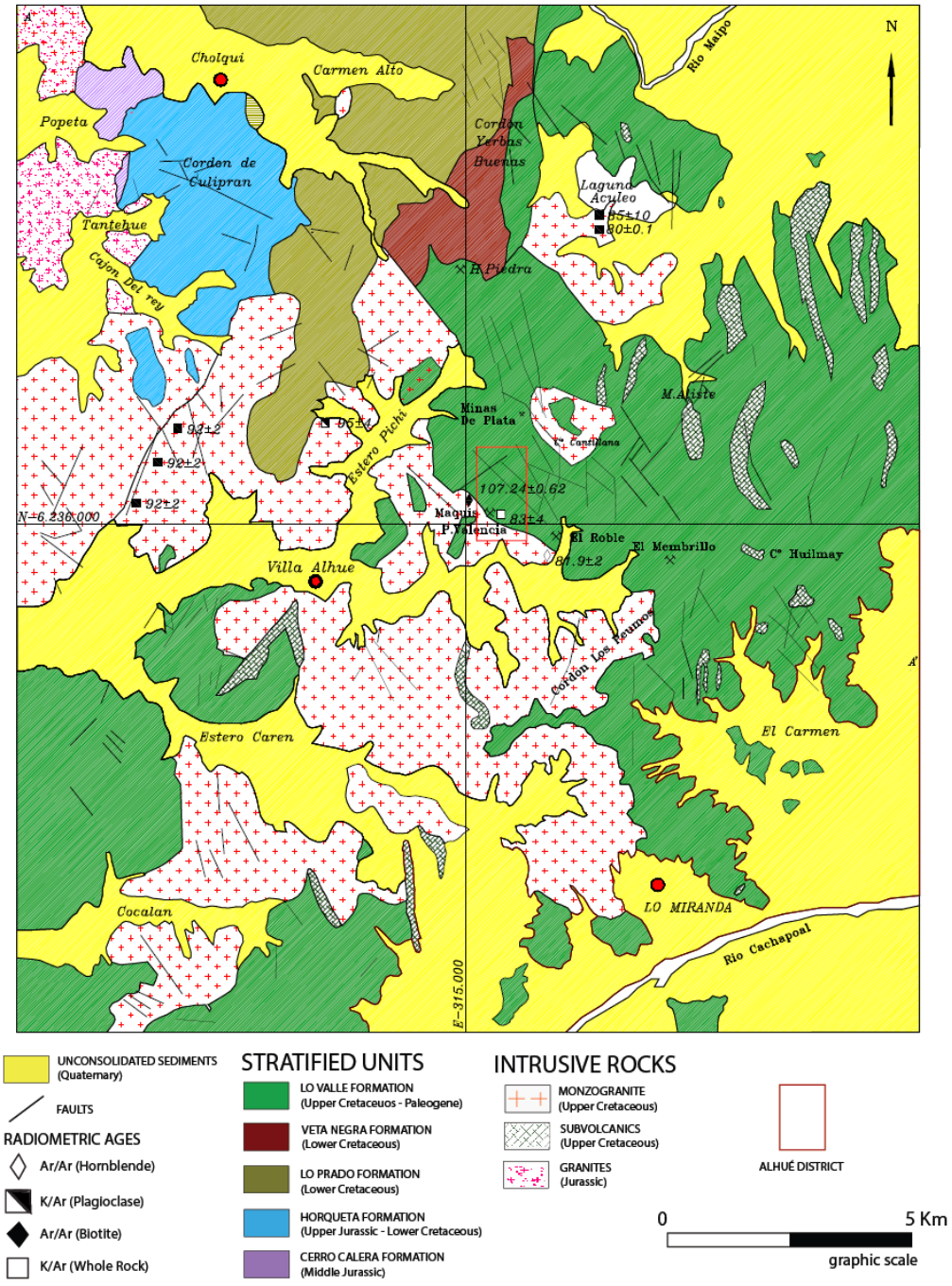

Figure 1. Geologic Map of the Coast Range. Central Chile. Modified after Herreros (2009). Nasi and Thiele (1982) and SERNAGEOMIN (1982).

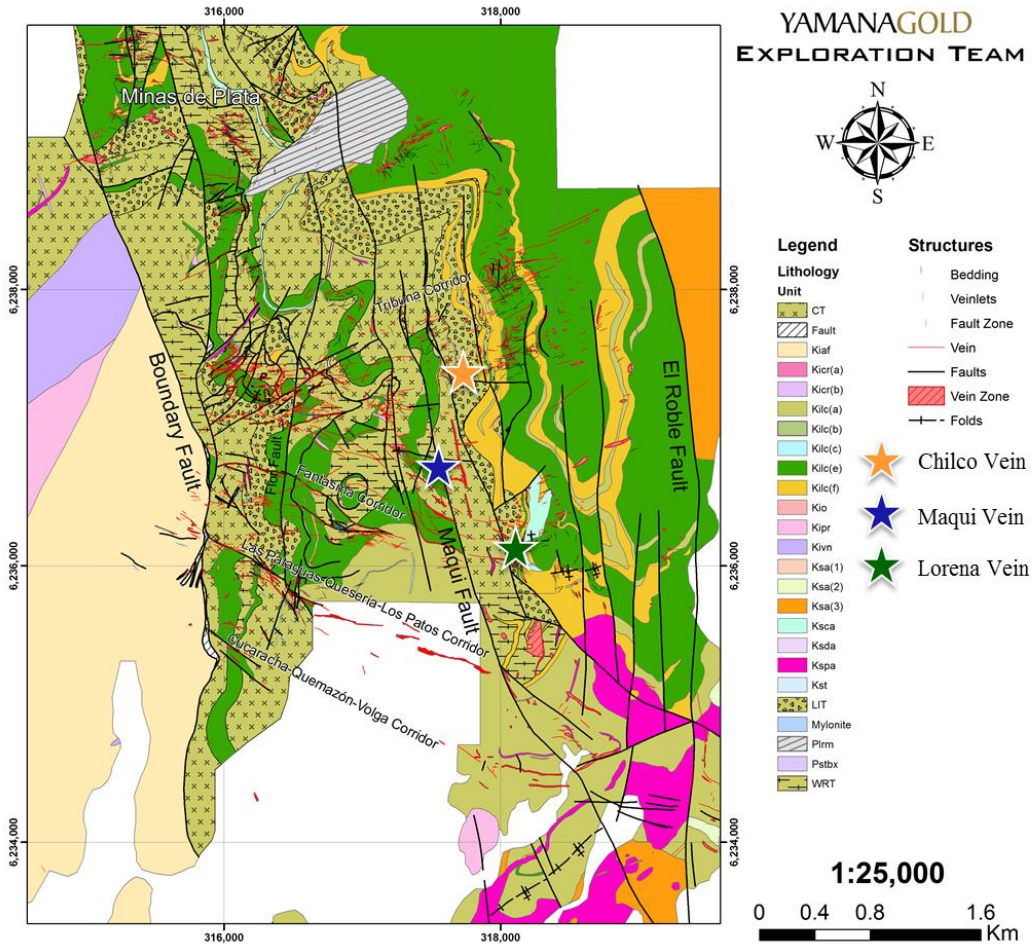

Figure 2. Geologic Map of the Alhué Mining District. 1: 25.000. Yamana Gold (unpublished).

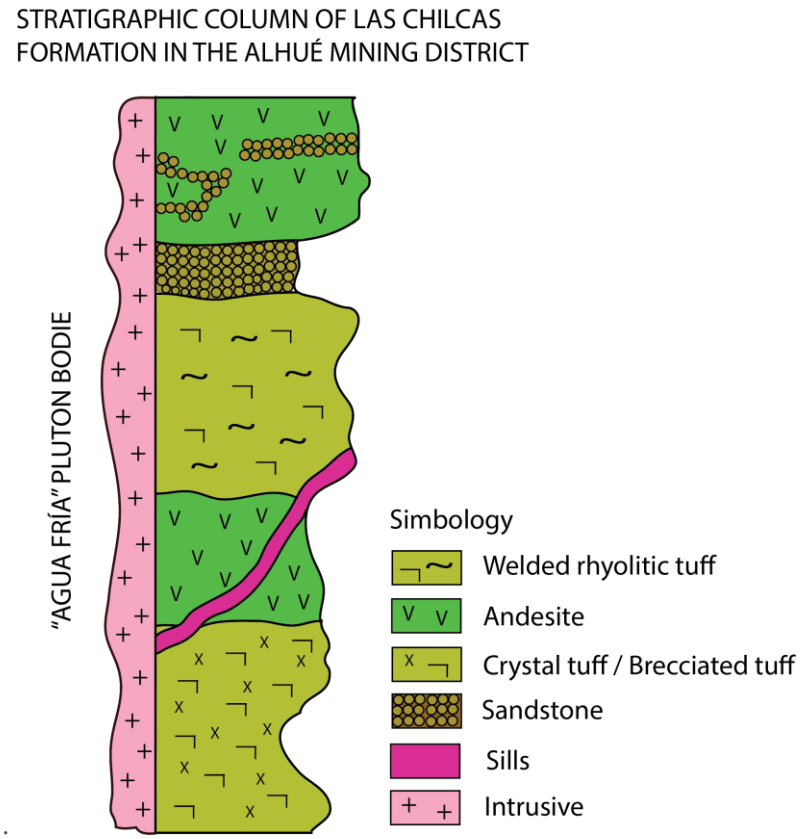

Figure 3. Stratigraphic column of Las Chilcas Formation in the Alhué mining district. Also the fault contact to the W with the Agua Fría pluton body is shown.

Figure 4. Hand-sample of Lorena vein, where massive quartz vein with magnetite-chalcopyrite-pyrite mineralization can be observed. Minor chlorite and epidote.

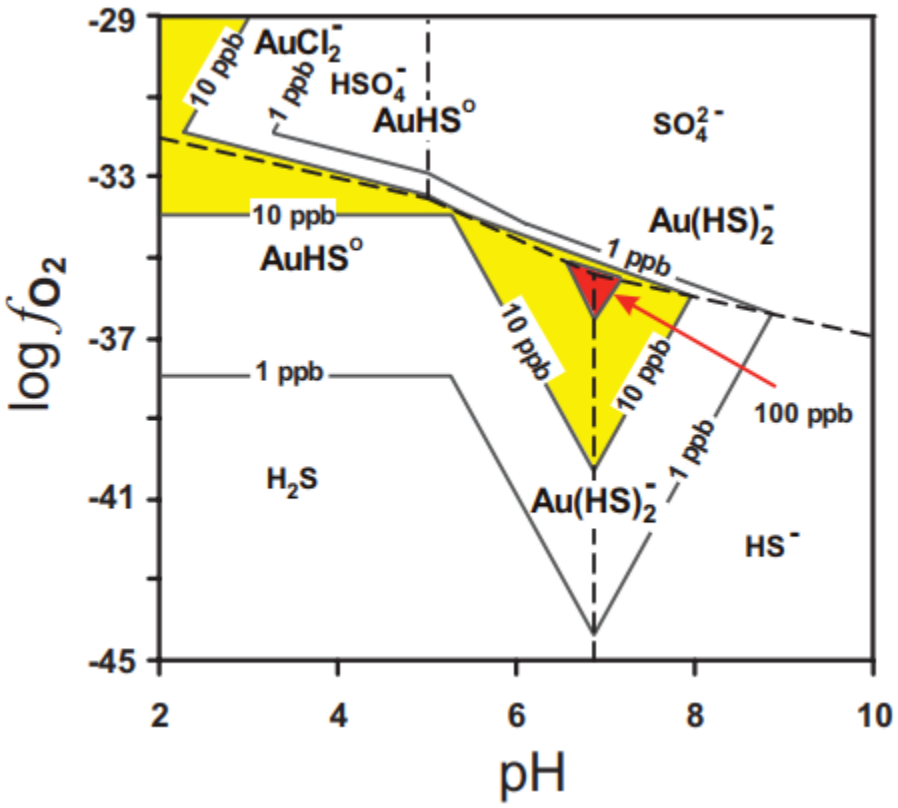

Figure 5. Gold solubility (in parts per billion; solid lines) and speciation at 500 bar and 250°C as a function of log fO2 and pH in a solution containing 1 m NaCl with ΣS = 0.01 m. The dashed lines separate regions of predominance of H2S, HS, SO_4^{-2} and HSO_4^- . Regions of high solubility are highlighted. The stability constants for gold species are from Stefánsson and Seward (2004), and thermodynamic data for other species are from the SUPCRT92 database (Johnson et al. 1992).

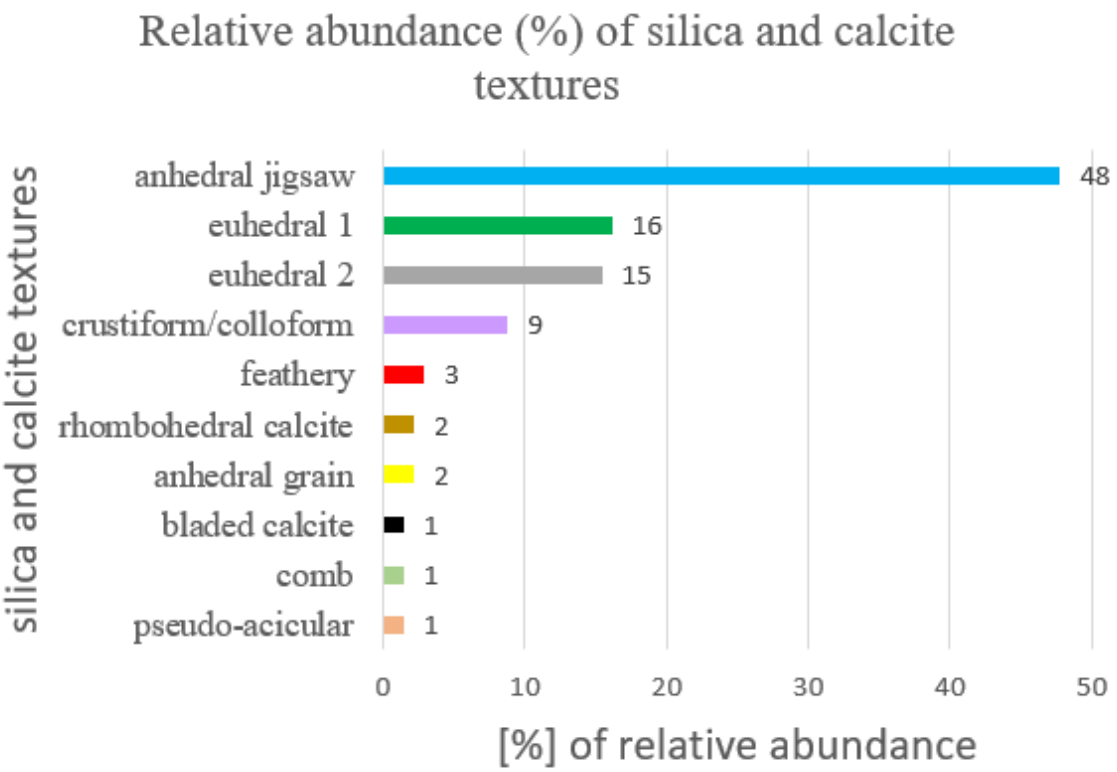

Figure 6. Relative abundance (%) of silica and calcite textures observed in samples from the Alhué mining district.

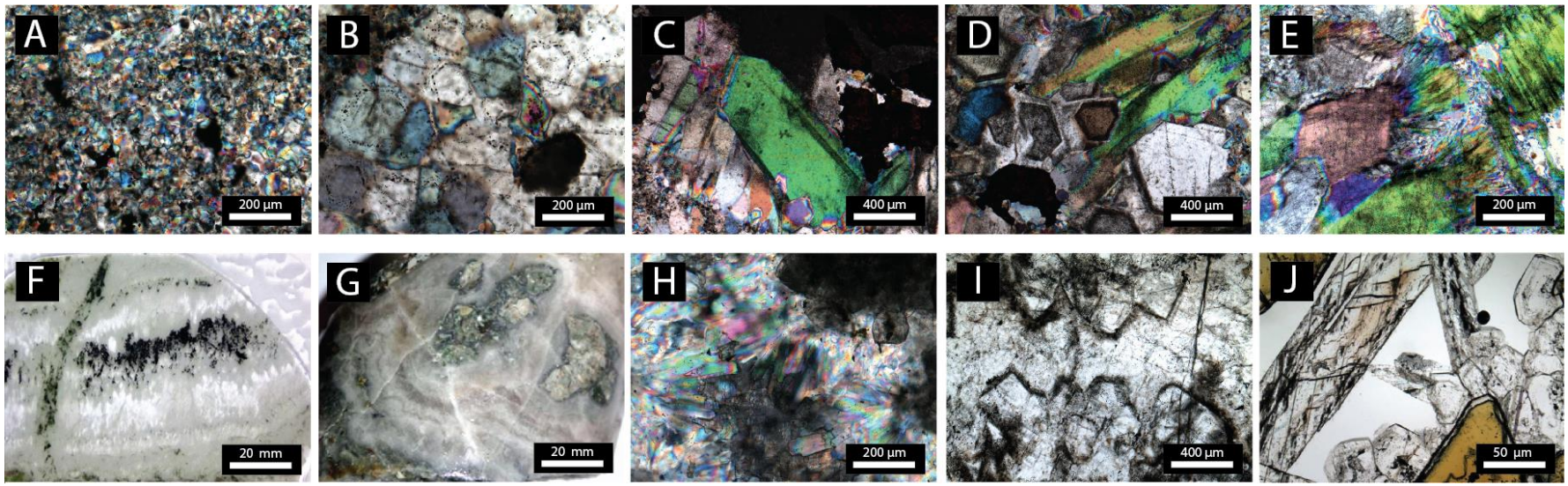

Figure 7. Textures observed in hand samples, quick-plates and thin sections. A. jigsaw-textured quartz under cross polars. (10x). B. euhedral quartz kind 1 under cross polars (10x). C. Euhedral quartz kind 2 under cross polars (4x). D. euhedral quartz kind 1 and 2 under cross polars (4x). E. feathery. F. crustiform in quickplate. G. colloform in hand sample. H. pseudo-acicular quartz. I. Comb-textures quartz. J. Bladed after Rhombohedral calcite in thin section.

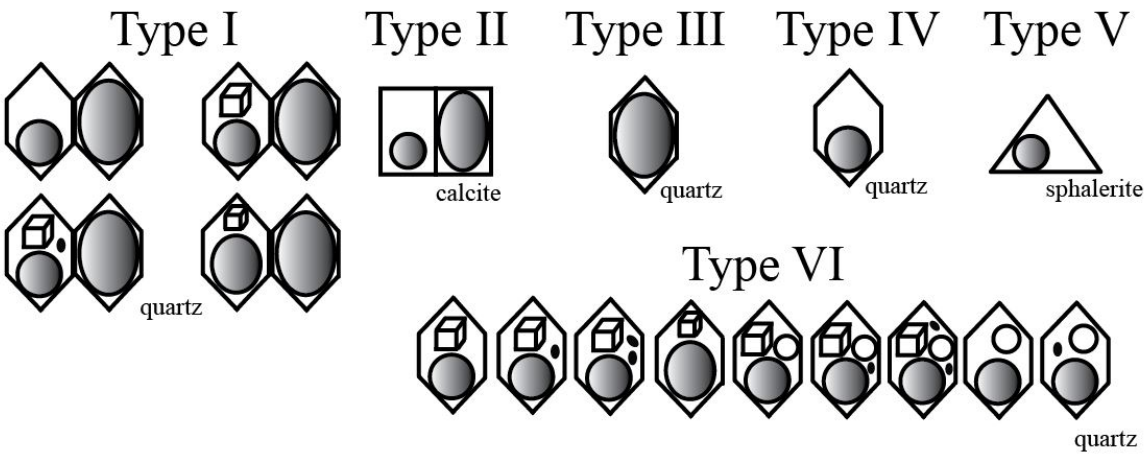

Figure 8. Petrographic classification of FIAs from the Alhué mining district. Type I. Boiling assemblages hosted in quartz. Type II. Boiling assemblages hosted in calcite grains. Type III. Flashing assemblages hosted in quartz. Type IV. Liquid-rich fluid inclusions hosted in quartz. Type V. Liquid-rich FI hosted in sphalerite. Type VI. Hypersaline fluids containing chlorides and solids.

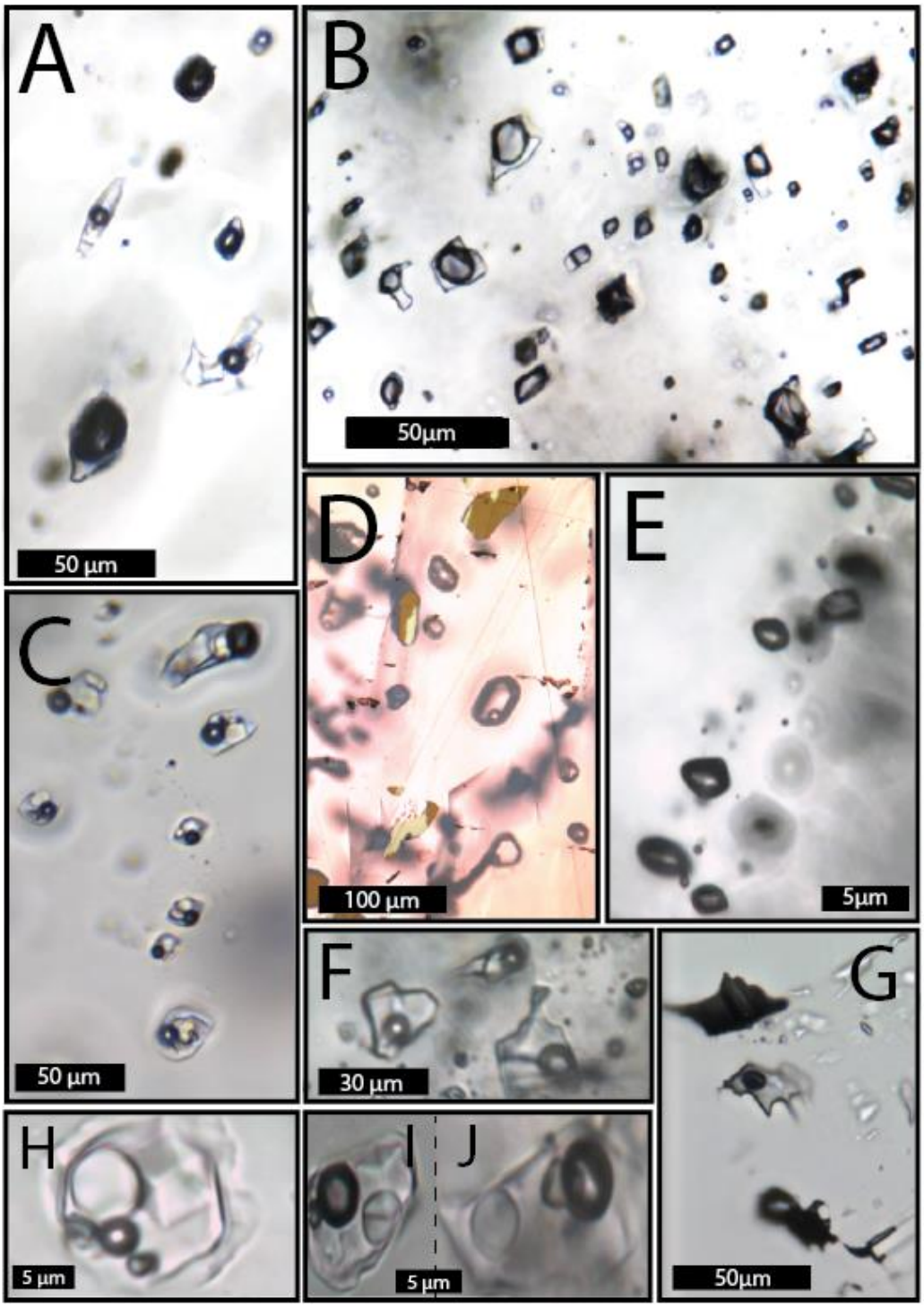

Figure 9. FIAs examples. A. Boiling assemblage: Vapor-rich fluid inclusions coexisting with liquid-rich fluid inclusions containing halite crystals. (Type I FIA). B. Boiling assemblage: Vapor-only FI coexisting with liquid-rich FI (Type I FIA). C. FIA of liquid-rich FI containing halite crystals and opaques (Type VI FIA). D. Type V FIA, L-rich FI hosted in sphalerite with disseminated mineralization of pyrite and chalcopyrite in the same trend. E. Type III FIA, V-rich FI hosted in quartz. F. Type IV FI, L-rich FI hosted in quartz. G. Type II FIA, decrepitated boiling assemblage hosted in bladed calcite. H, I and J. Type VI FI with halite and/or rounded chloride and solids (opaques).

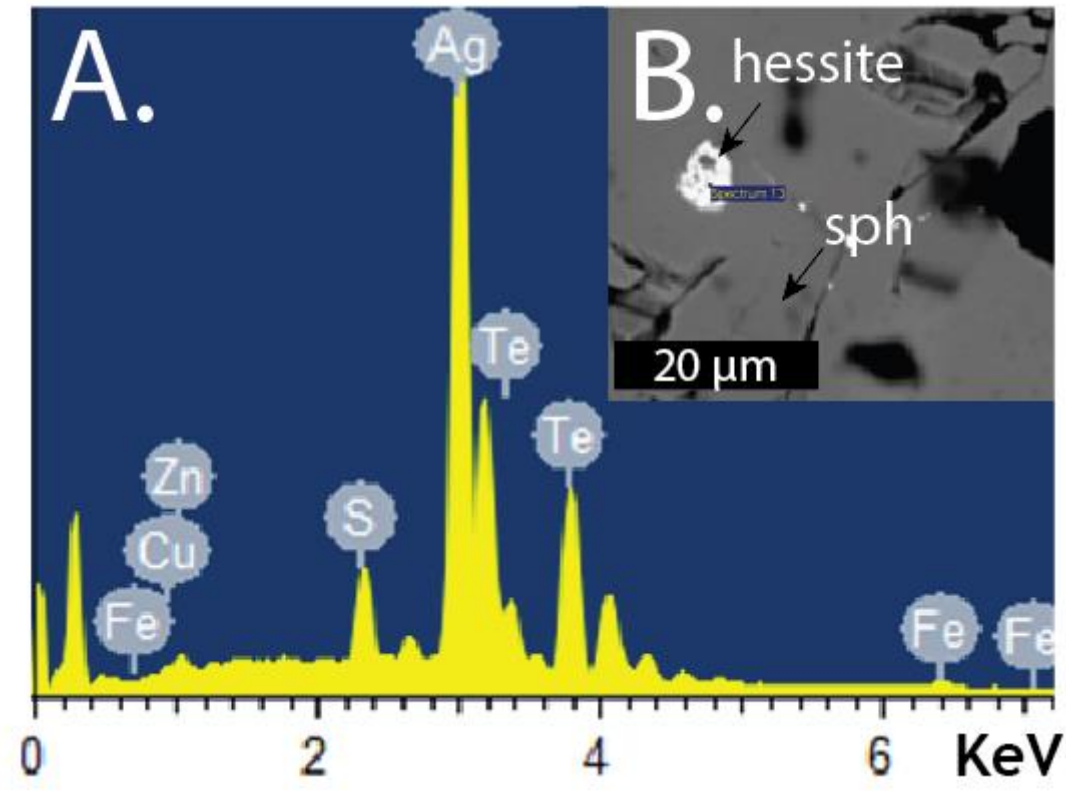

Figure 10. A. SEM spectrum. Hessite (Ag_2Te). Atomic% (Ag) = 59.08 ; Atomic% (Te) = 25.81. B. Backscattered image showing reflective mineral analized by SEM. Hessite inclusion in sphalerite.

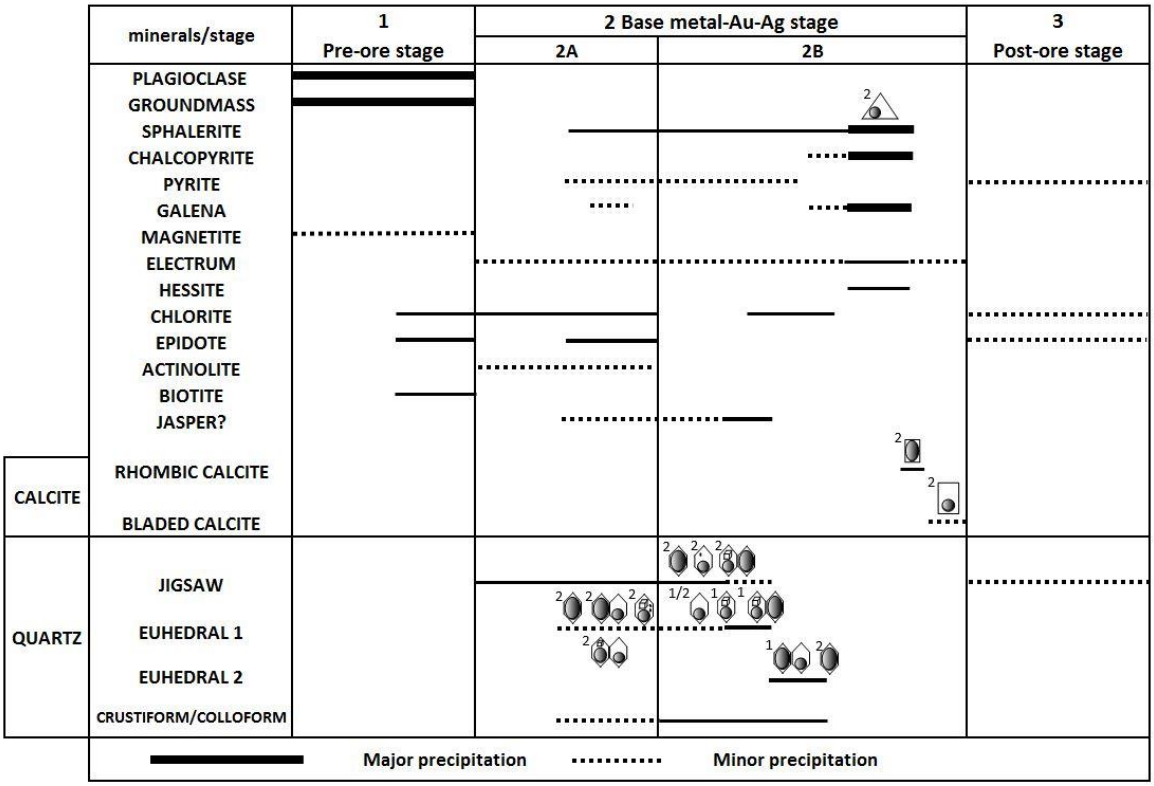

Figure 11. Paragenetic table of Maqui vein. Thick bars indicate higher abundances. Thin and dashed lines refer to lower abundances.

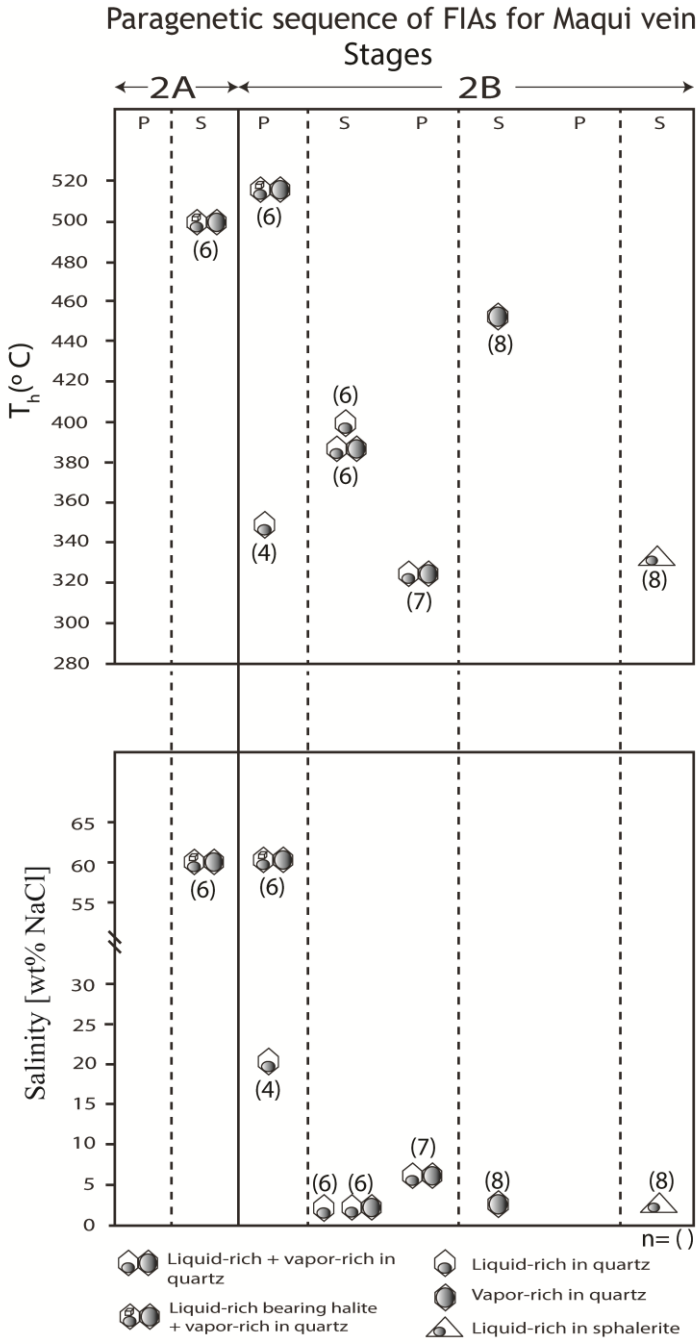

Figure 12. Paragenetic sequence of FIAs for Maqui vein.

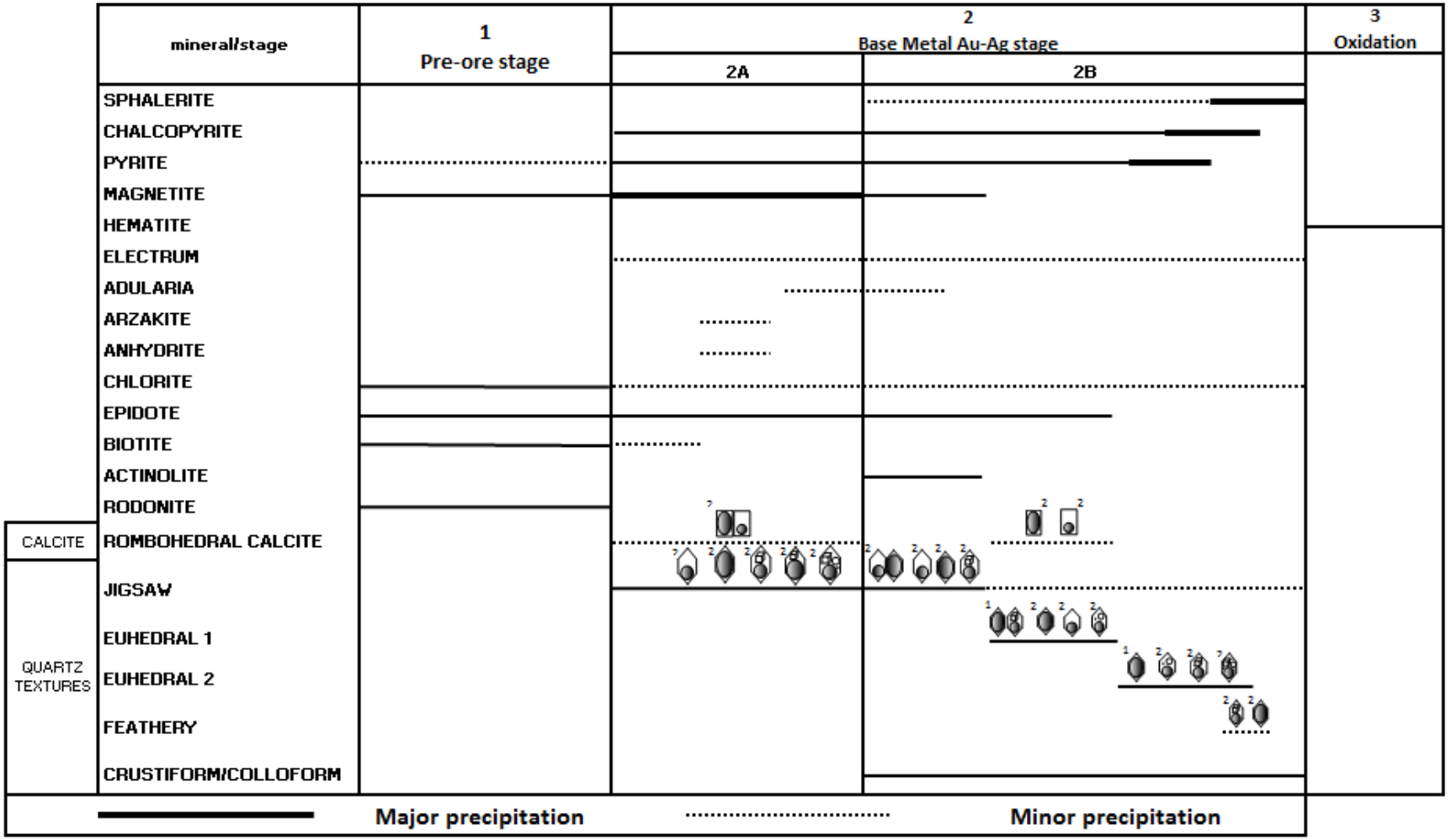

Figure 13. Paragenetic table of Lorena vein. Thick bars indicate higher abundances. Thin and dashed lines refer to lower abundances.

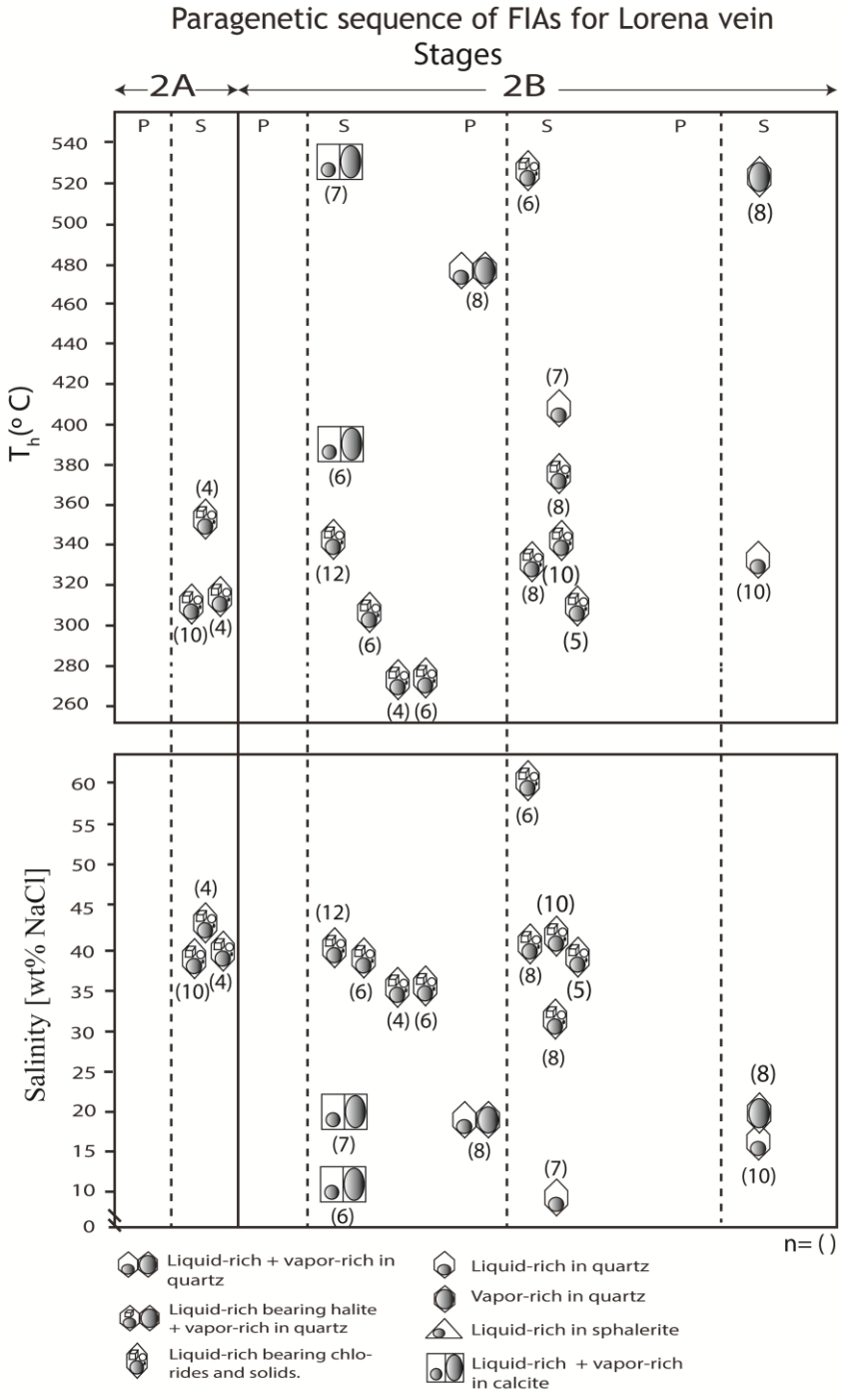

Figure 14. Paragenetic sequence of FIAs for Lorena vein.

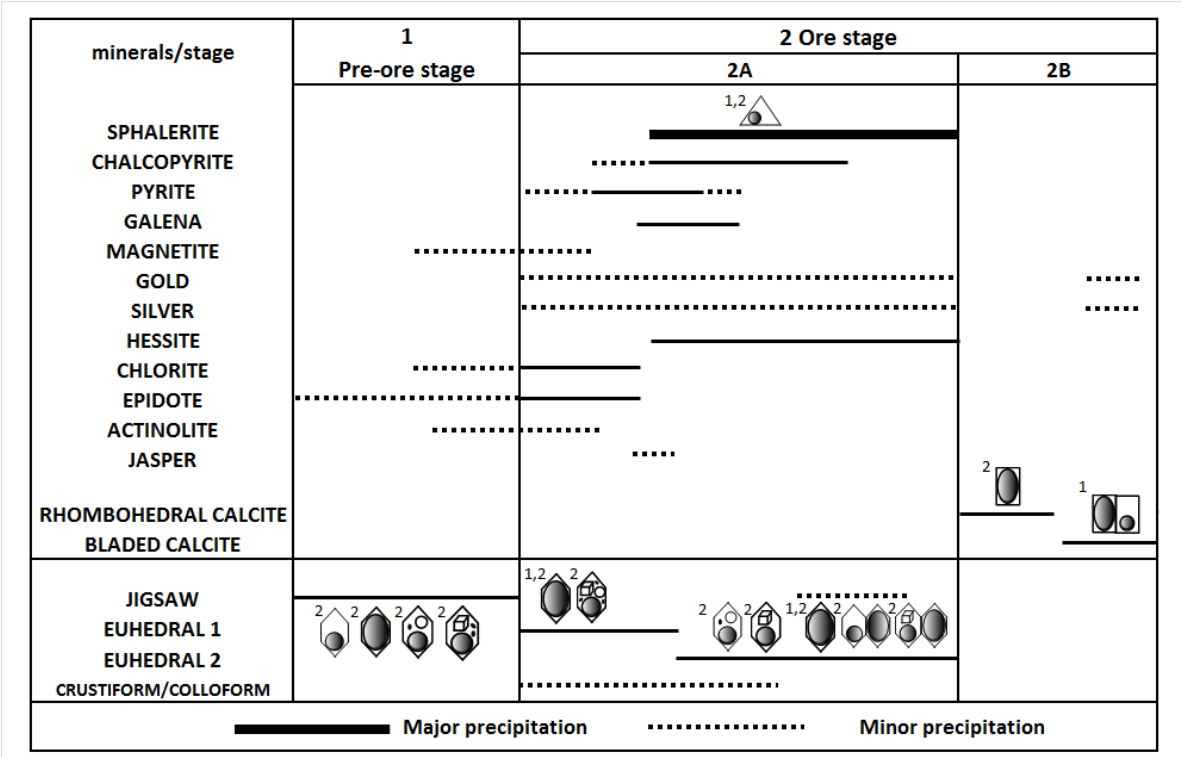

Figure 15. Paragenetic table of Chilco vein. Thick bars indicate higher abundances. Thin and dashed lines refer to lower abundances.

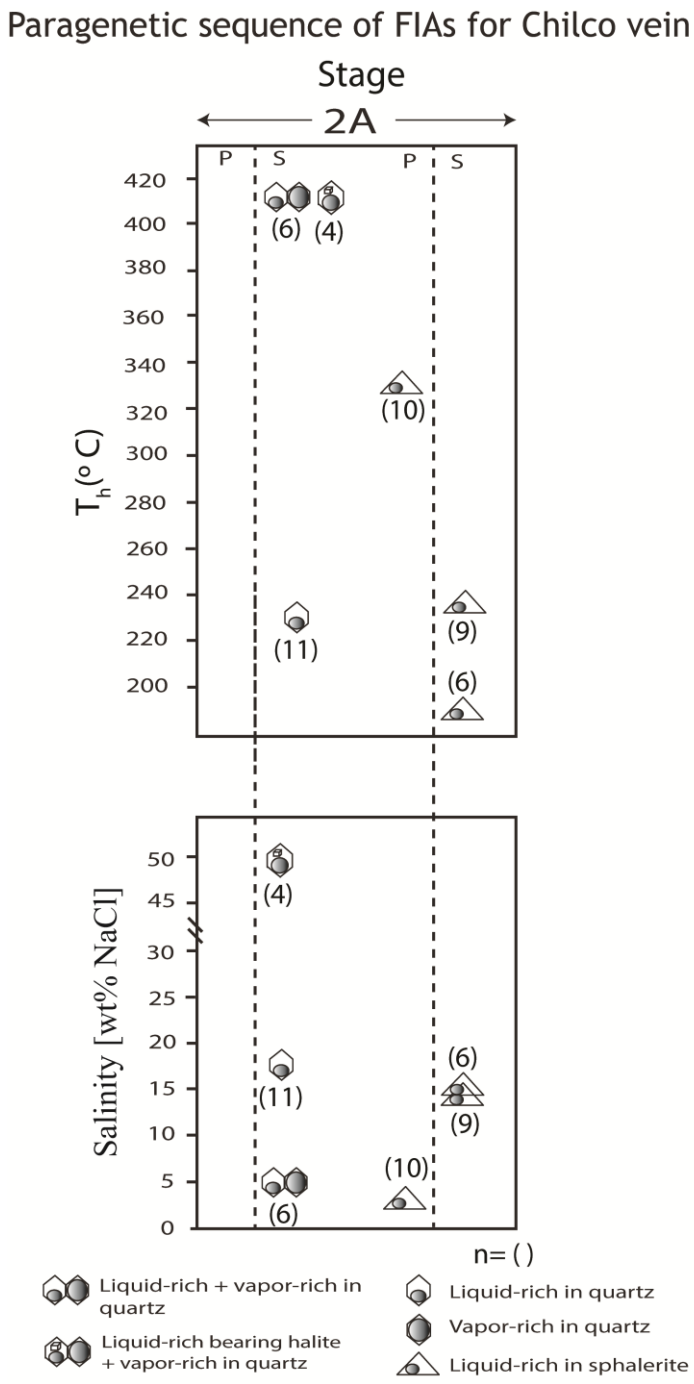

Figure 16. Paragenetic sequence of FIAs for Chilco vein.

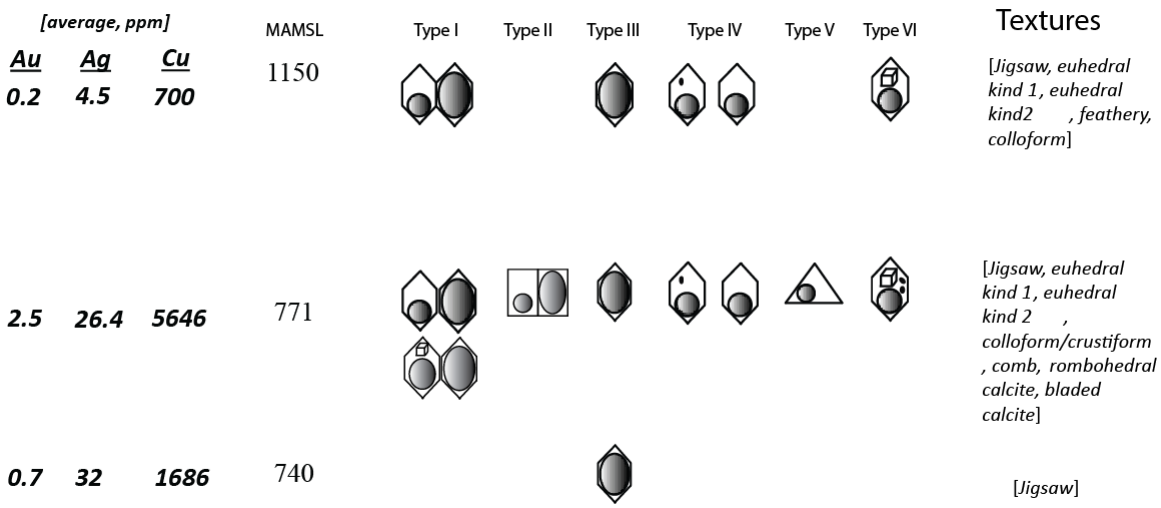

Figure 17. Vertical zonation of FIAs and quartz and calcite textures for Maqui Vein. Gold, Silver and Copper whole rock values are also shown per level (in meters above mean sea level).

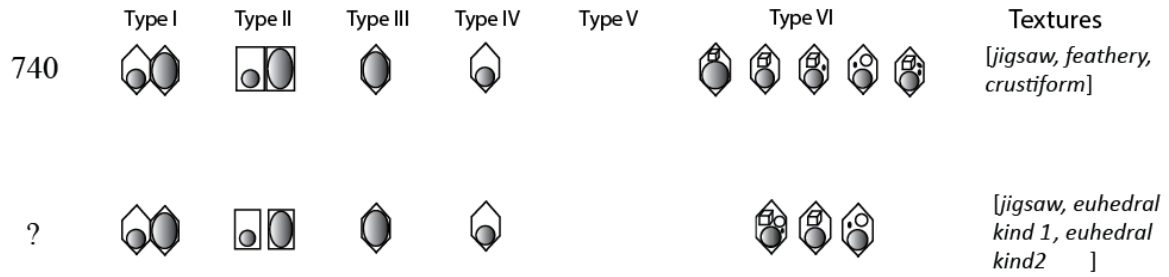

Figure 18. Vertical zonation of FIAs and quartz textures for Lorena Vein.

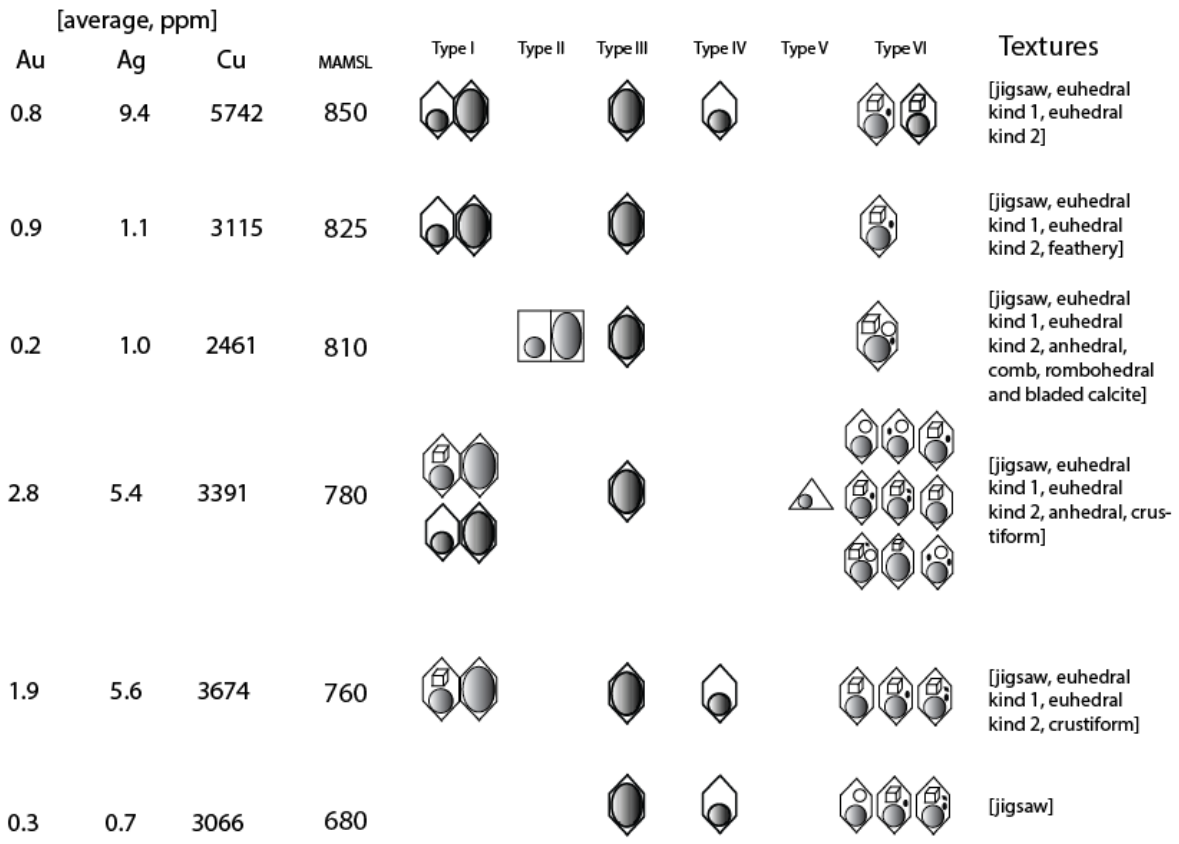

Figure 19. Vertical zonation of FIAs and quartz and calcite textures for Chilco Vein. Gold, Silver and Copper whole rock values are also shown per level (in meters above mean sea level).

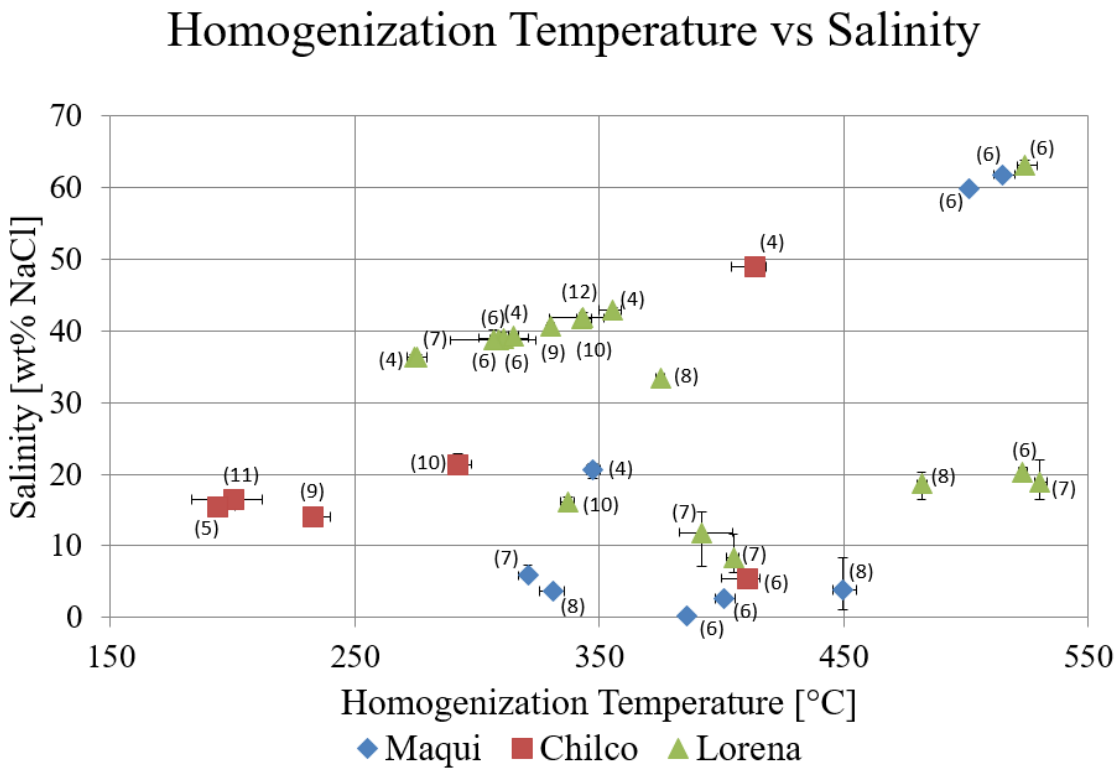

Figure 20. Homogenization Temperature [°C] vs Salinity [wt% NaCl] for FIAs from Maqui, Lorena and Chilco veins. Number of inclusions per FIA in brackets.

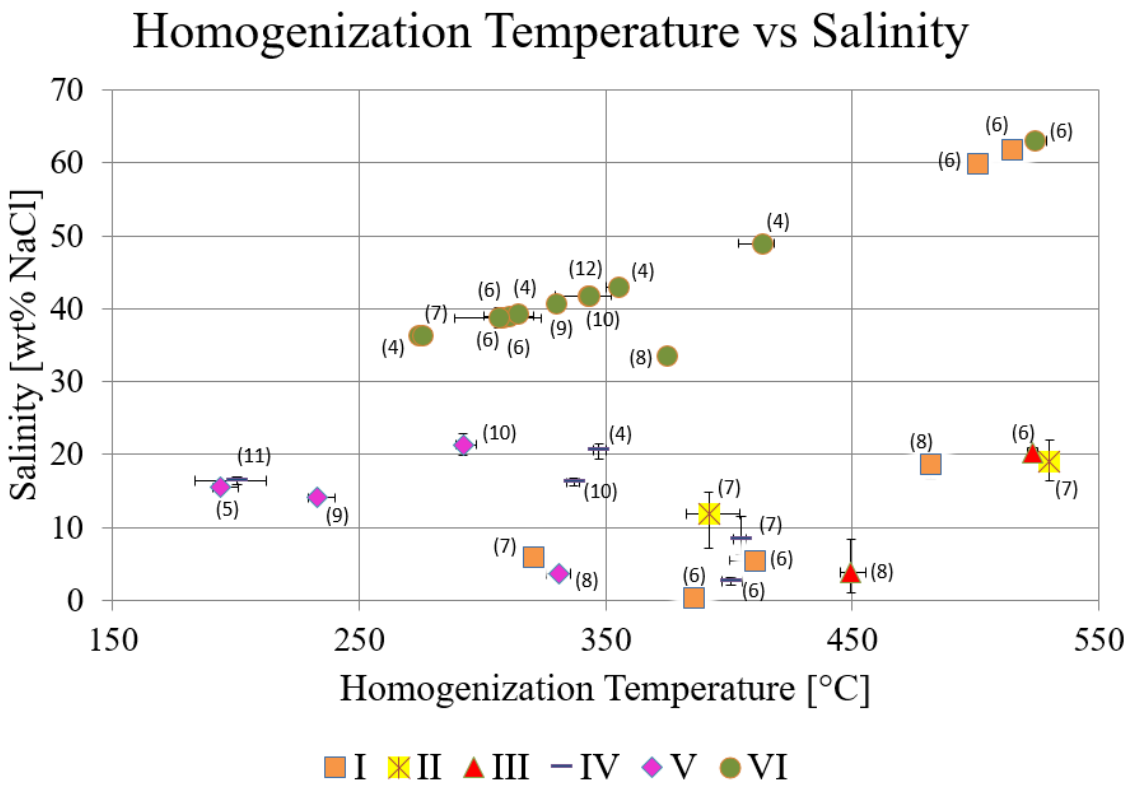

Figure 21. . Homogenization Temperature [°C] vs Salinity [wt% NaCl] for FIAs from Maqui, Lorena and Chilco veins classified by inclusion type following classification described in Figure 8. Number of inclusions per FIA in brackets.

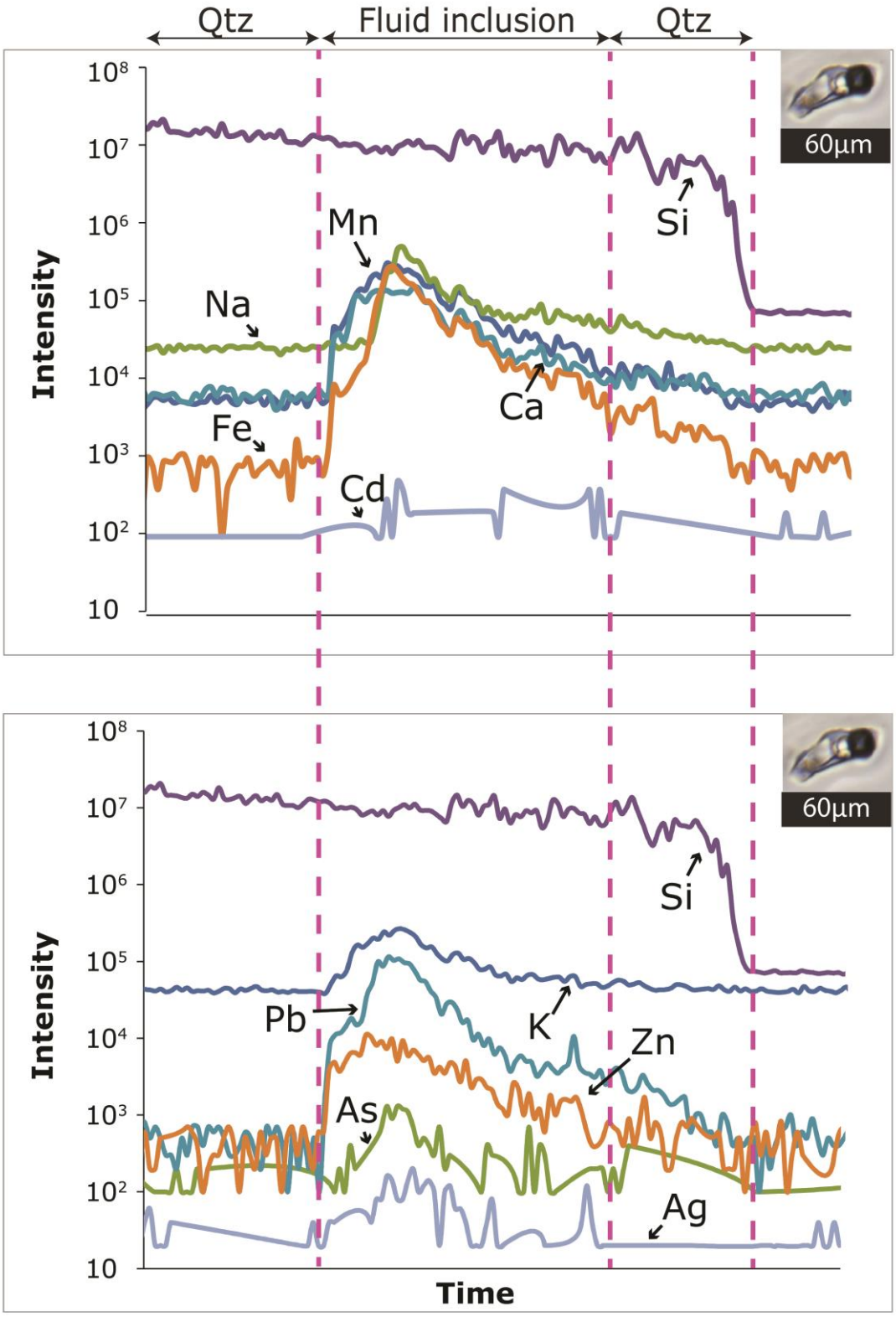

Figure 22. LA-ICP-MS signal from ablation of secondary fluid inclusion (Type VI) hosted in quartz. The inclusion contain 10 ppm of silver (Ag).

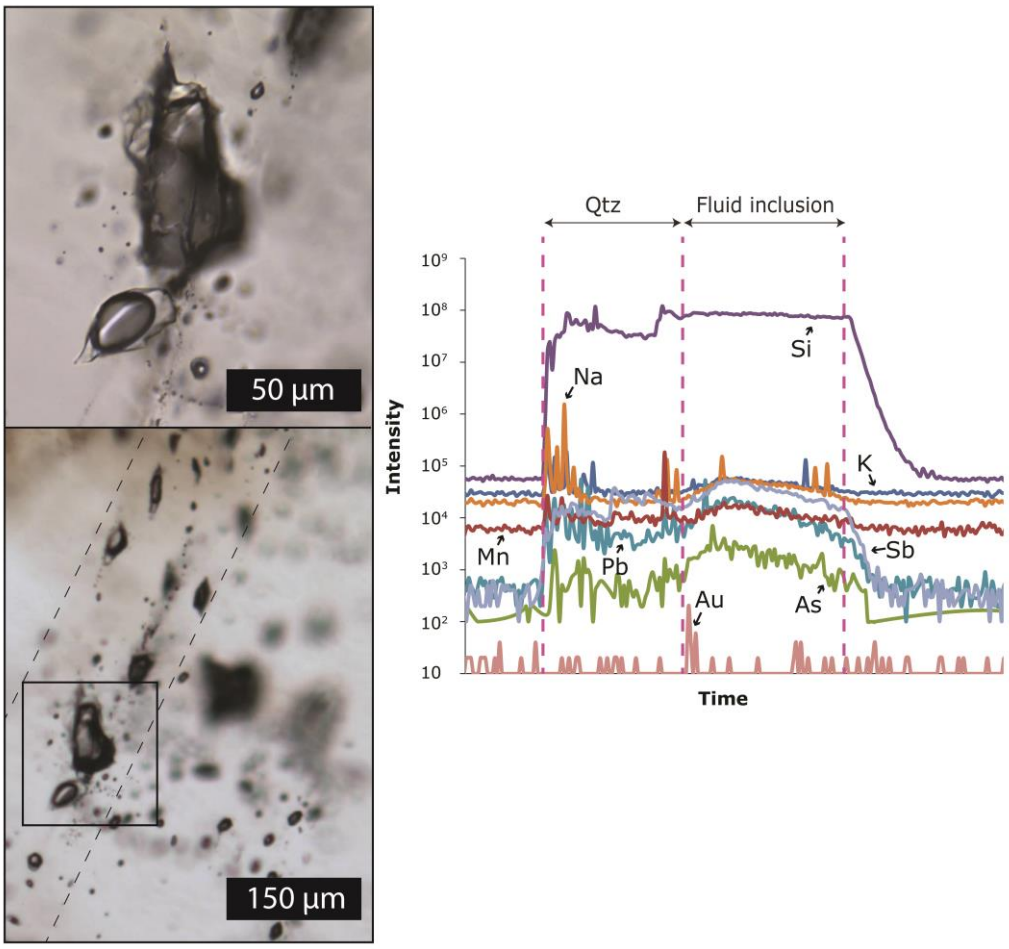

Figure 23. Left. Secondary vapor-rich fluid inclusion assemblage hosted in quartz (type III). Right. LA-ICP-MS signal from FI present in the assemblage.

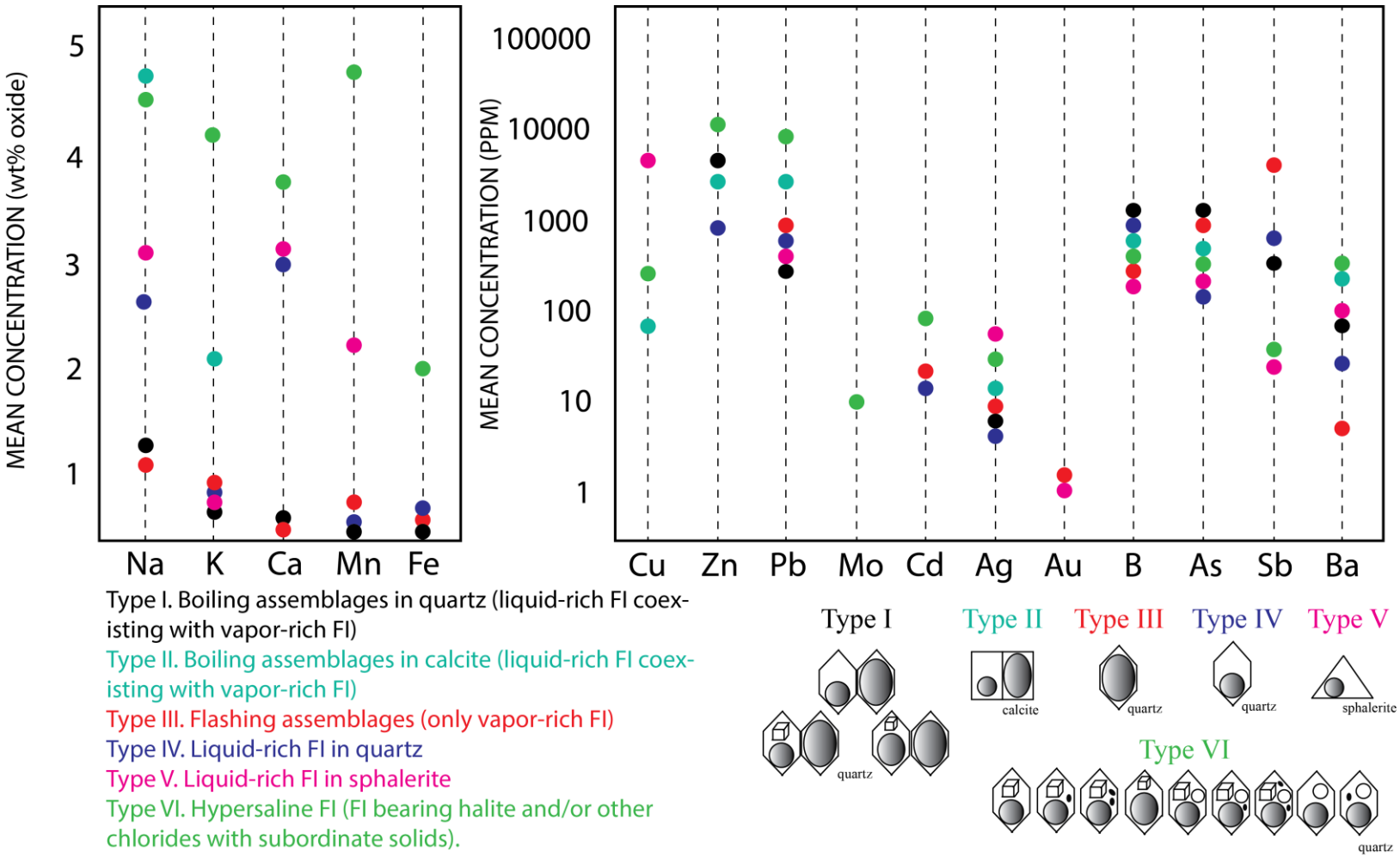

Figure 24. Summary of elemental content obtained by LA-ICP-MS for all six types of FIAs. Colored dots represent average content in ppm or wt% oxide.

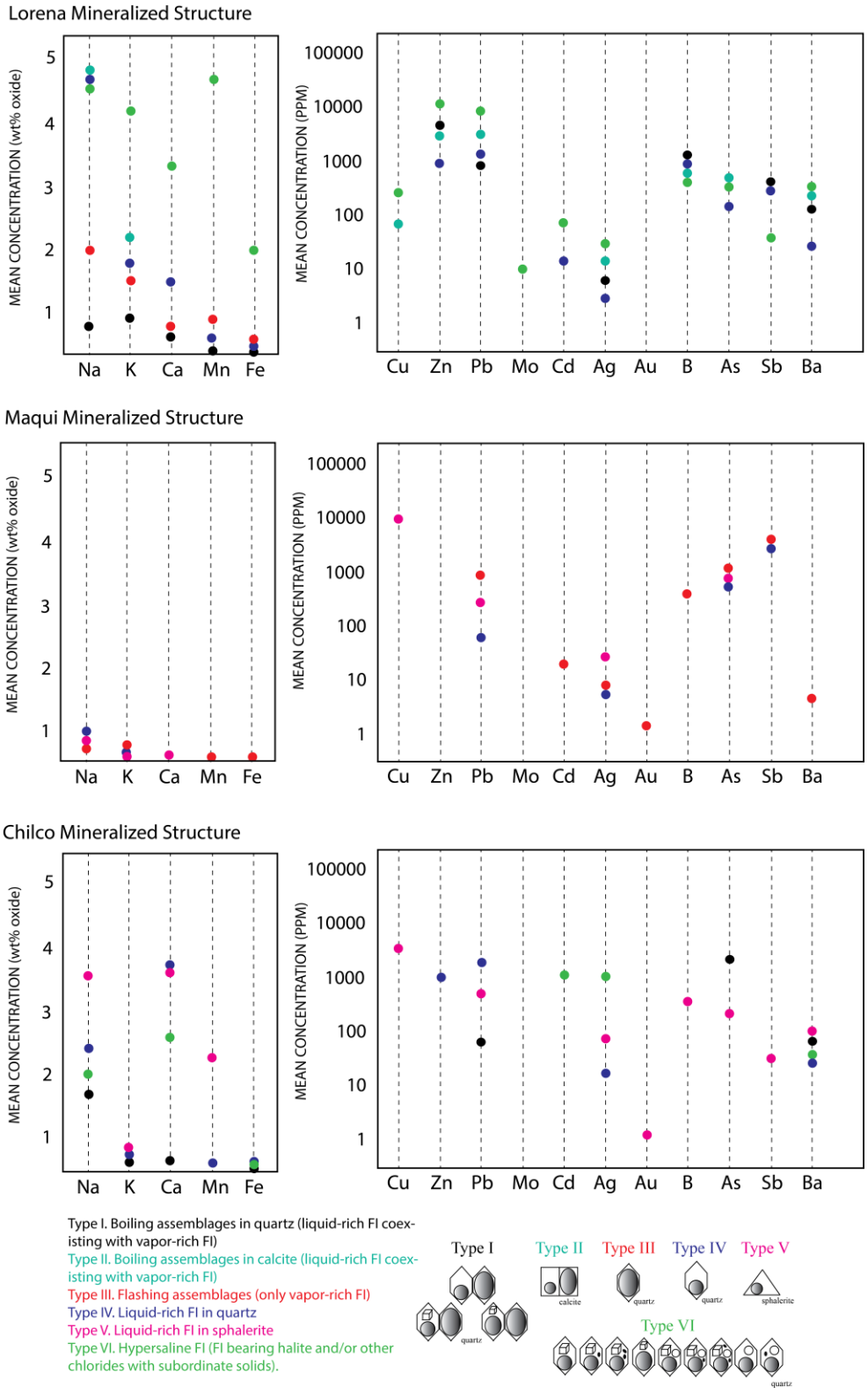

Figure 25. Summary of elemental content in fluid inclusions obtained by LA-ICP-MS for mineralized structures Lorena, Maqui and Chilco. Colored dots represent average content in ppm or wt% oxide.

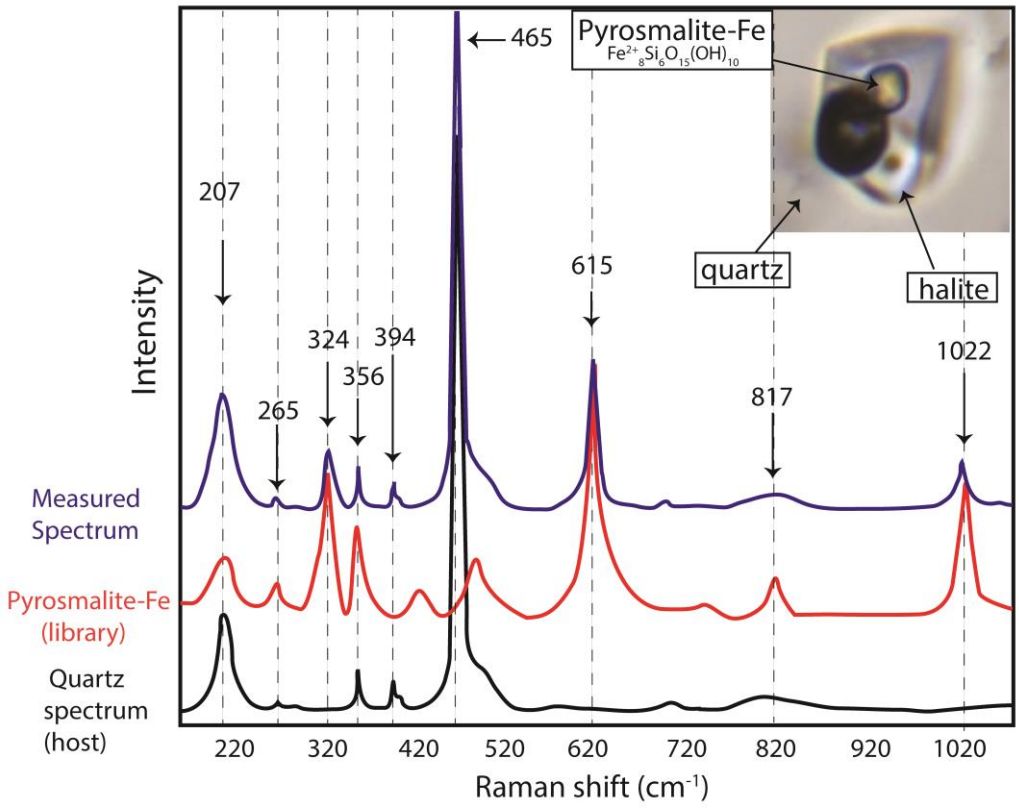

Figure 26. Raman spectrum of daughter mineral pyrosmalite-Fe inside a hosted in quartz liquid-rich FI bearing a halite crystal. Also quartz spectrum is shown. FI from sample 240910VQ1ZA (Lorena mineralized structure).

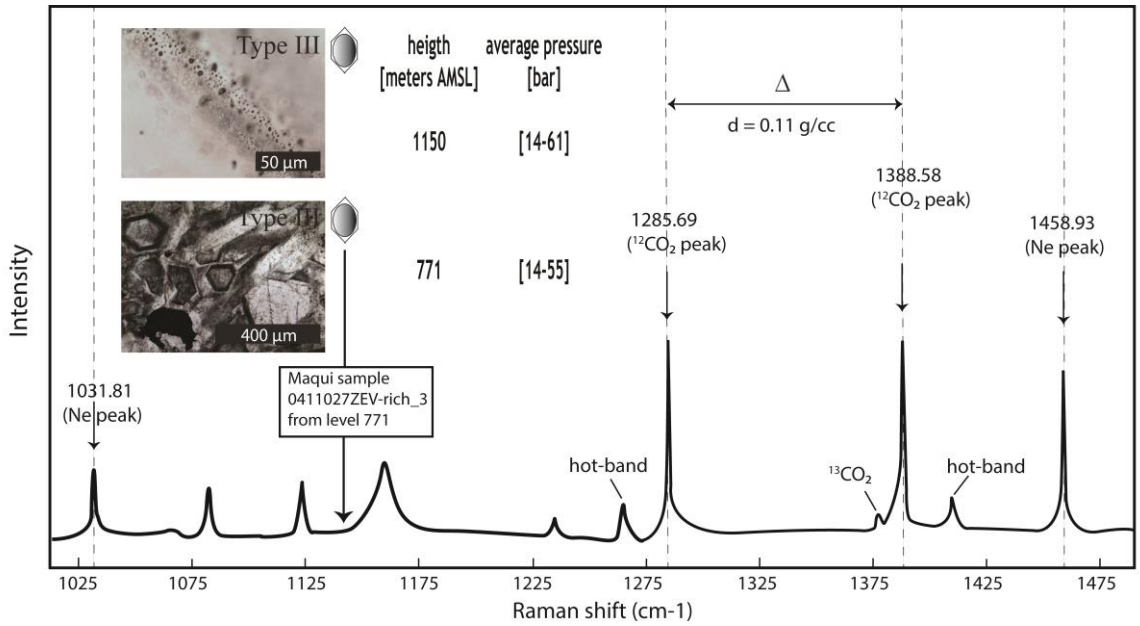

Figure 27. Raman spectrum of Carbon dioxide (CO2)-bearing fluids in Maqui structure. Calculated pressures related to CO2 density and to the splitting of the Fermi diad (Δ, cm-1) are also shown fo different levels. ΔCO2 is corrected by using ΔNe (Neon light) as a standard for calibration.

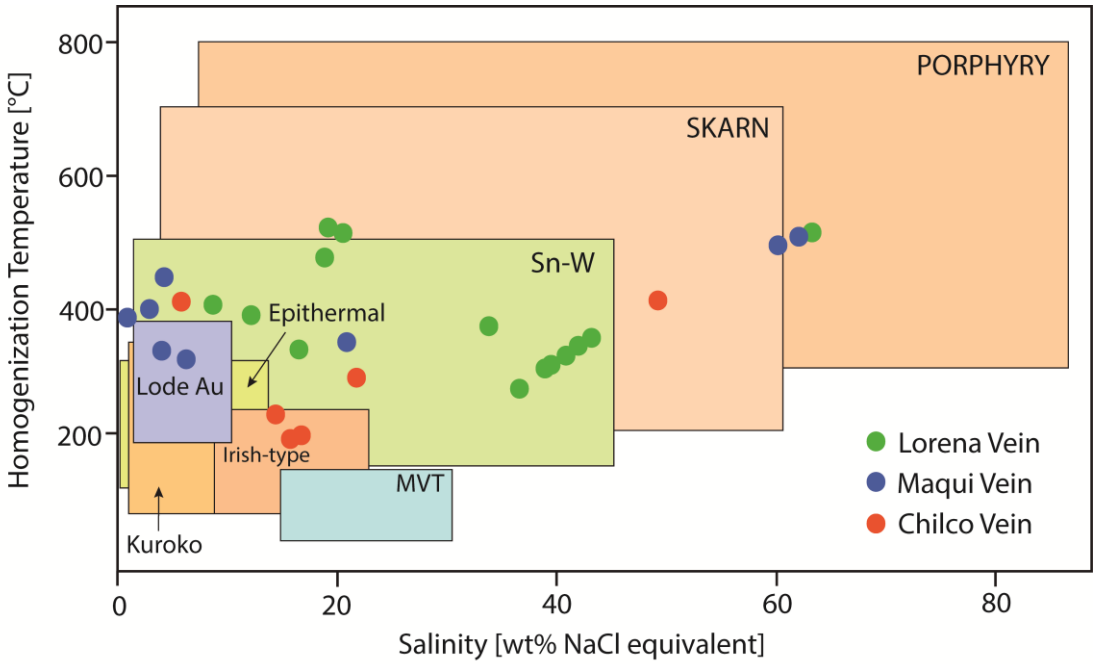

Figure 28. Th and salinities of the fluids from the Alhué mining district in comparison to typical ranges of ore-precipitating fluids projected in temperature-salinity fluids from Wilkinson (2001).

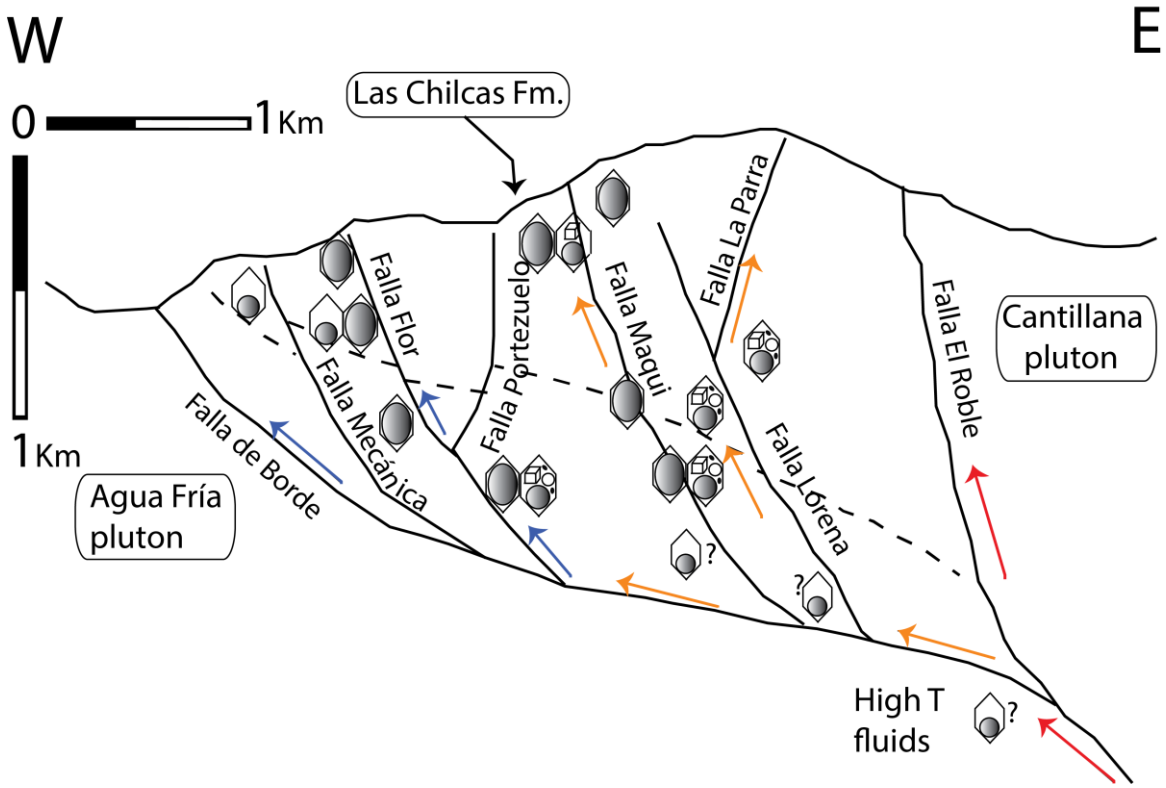

Figure 29. Spatial distribution of fluids in a general model of fluid`s migration in the Alhué Mining district. Modify after Matthews (2018).

Table 1. Generalized Jurassic to Late Cretaceous lithostratigraphic column for the Coast Range of Central Chile between 32°30' S and 34°S (after Vergara et al.. 1995).

Formation and Description	Thickness
Lo Valle Formation (Lower(?)-Upper Cretaceous) Continental volcanic and sedimentary. Continental (intra-montane) conglomerates and sandstones at the base of the unit. Acid to intermediate lavas and tuffs, intermediate to basic lavas, with minor intercalated sedimentary rocks.	750-3500 m
Veta Negra Formation (Lower Cretaceous) continental, partly marine (littoral) at the base. Basic to intermediate lavas and flows breccias, and eolian sandstones; scarce acid ignimbrites. Peperites and brackish-water sedimentary rocks at the base of the unit.	5000-15000 m
Las Chilcas Formation (Lower Cretaceous) Volcanic sequence interlayered with scarce continental sediments. Tuffs with andesitic and basaltic lava flows intercalations. No formal stratigraphy has been reported due to its lateral variation, lack of geochronological data and a complex structural architecture. 4 clear units have been described locally in the Alhué mining district: (1) Basal lithic-crystal tuff (2) Lower Andesites (3) Main Tuff and sedimentary unit (4) Upper Andesites.	1000-1500 m
Lo Prado Formation (Lower Cretaceous) marine (bathyal to littoral) and continental. *Upper member*: (1800-4500 m): acid ignimbrites and deltaic sedimentary rocks; subordinate basic lavas, partly peperites, and sublittoral clastic sedimentary rocks with limestone lenses and water-laid tuff intercalations. *Lower member*: (700-1800 m): Sublittoral-littoral conglomerates at the base of the unit, covered by bathyal volcaniclastic rocks (turbidites), limestones, and cherts. Water-laid tuffs and ignimbrites in the upper part.	3000-6000 m
Horqueta Formation (Upper Jurassic) continental. Basic to intermediate lavas and debris flows. Beach and/or eolian sandstones and acid lavas predominate in the lower part.	1800-4300 m
Cerro Calera Formation (Middle Jurassic) marine (littoral to sublittoral) and continental. Acid lavas, pyroclastic fall deposits (partly submarine) and ignimbrites, and marine clastic sedimentary rocks with minor limestone intercalations; subordinate basic lavas	350-1400 m

Formation and Description	Thickness
Ajial Formation (Lower – Middle Jurassic) marine (sublittoral to littoral). Acid lavas, pyroclastic fall deposits (partly submarine) and ignimbrites, and marine clastic sedimentary rocks with minor limestone intercalations; subordinate basic lavas.	750-2000 m
Quebrada del Pobre Formation (Lower Jurassic) marine (sublittoral to littoral). Marine clastic sedimentary rocks with limestone intercalations; scarce submarine acid lavas and ignimbrites, and basic lavas.	0-1250 m
Basement (upper Paleozoic) Tonalite, and microcline-bearing granodiorite and granite. Triassic marine sedimentary and volcanic rocks to the north of the studied area.	

Table 2. Summary of fluid inclusion studies conducted in the area. From left to right: Vein: mineralized structure in which the study was done. Fluid inclusion petrography: Petrographic description of FIAs at room temperature (L-rich: liquid rich inclusions; V-rich: vapor rich inclusions; L-rich+H: liquid rich with halite inclusions; L-rich+H.Solids: liquid rich inclusions bearing halite and some solids(one or more); L-rich+H.Sy: liquid rich inclusions bearing halite and sylvite. L-rich+CO2: liquid rich inclusions with two vapors in which one is CO2). Size: range of fluid inclusion´s sizes. Temperatures of homogenization (Th) reported in Celsius degrees and last melt temperutes (Tm) if reported. Salinities in wt% NaCl. Host crystal of the fluid inclusions described (qtz: quartz; sph: sphalerite). Boiling evidences found in the study (or inflicted from reported information). Comments of how the data was presented and reference of each study. MEM: Membrillo; P.V: Pedro Valencia; CAN: Cantillana. ROB: El Roble; MARI: MARISOL.

VEIN	FLUID INCLUSIONS PETROGRAPHY	SIZE [µM]	T_H [°C] REPORTED, T_M [°C] REPORTED	SALINITIES REPORTED [% NACL EQUIV]	HOST	BOILING EVIDENCES	COMMENTS / REFERENCE
MEM	V-rich (I); L-rich(I)	[1-6]	[115-320] in level 577; [140-300] in level 694; [120-340] in level 732.	[1-18] in level 577; [1-12] in level 694; [4-8] in level 732.	qtz	Crustiform texture. V-rich primary inclusions.	Fluid inclusion data grouped by mine levels. Piñana, 1993.
MEM	V-rich (I); L-rich (I); L-rich+H (I).	[20] (average)	[450] in level 668; [399] in level 488	[48] in level 668; [43] in level 488.	qtz	L-rich~V-rich.	Two T_h measurements. Harris et al., 2013.
PISCINA	V-rich (I); L-rich (I); L-rich+H (I).	[20] (average)	[442,342,344] in level 731; [399] in 728; [486] in 649.	[40.8,42.5,38.1] in level 731, [47.8] in 728; [58] in 649.	qtz	L-rich~V-rich.	Five T_h measurements. Harris et al, 2013
GARZA	V-rich (I); L-rich (I); L-rich+H (I).	[20] (average)	[361] in level 690; [296] in level 662.	[43] in level 690; [36] in level 662	qtz	L-rich~V-rich.	Two T_h measurements. Harris et al, 2013.
MAQUI	L-rich+H,Solids (sylvite?, calcite?, anhydrite?).	[4-15] (7, average)	[140-200], [240-320], [320-500]	[37.9-57.5] (just reported in one level, 909)	qtz	No described.	Fluid inclusion data grouped by Th range. Cotton, 1998. Cotton, 1999.
P.V. AND CAN.	L-rich L-rich+H L-rich+H, Solids	[3-30] (10, average)	[200-480] (in general). [268-295] (in central part of qtz crystal, inclusions without daughter minerals), [~400°C] (in edge of qtz crystal, inclusions containing daughter minerals, some does not homogenize) T_m: [240-380]	[<26 - >56]	qtz	Inclusions contain from 2 to 40% vapor. Radiating quartz crystals (pseudo-acicular?).	Homogenization temperature and salinity of the inclusions increase outward in the direction of cristal growth. Circular to elliptical daughter minerals are described in some inclusions. Pedro Valencia and Cantillana inclusions reported as one group. Cotton, 1998. Cotton, 1999. Alcázar, 2001.
ROB	L-rich L-rich+H,Solids	[7-40]	[168 – 475], (305, average). T_m: [250-279]	[34.6 – 36.5]	qtz	Sugary texture (jigsaw?)	Cotton, 1998.

VEIN	FLUID INCLUSIONS PETROGRAPHY	SIZE [µM]	T_H [°C] REPORTED, T_M [°C] REPORTED	SALINITIES REPORTED [% NACL EQUIV]	HOST	BOILING EVIDENCES	COMMENTS / REFERENCE
LORENA	L-rich L-rich+H L-rich+H,Solids V-rich	[10-40]	[139.9-397.1] (total data); [150-250] in level 740; [320-360] in level 795. T_m: [149-543]	[29-62] total data; [2-8] in level 740; [2-19] in level 795.	qtz	V-rich inclusions existence	Data obtained from L-rich, L-rich+H and L-rich+H,Solids inclusions. Sepúlveda, 2004
LORENA FAULT	L-rich L-rich+H L-rich+H,Solids V-rich	[9-22]	Th: [218-488] Tm: [255.6 – 408.7] (data from L-rich+H and L-rich+H,Solids inclusions).	[35-46.5] (In L-rich+H inclusions); [9-10] (in L-rich inclusions)	qtz	No described.	Data obtained from L-rich, L-rich+H and L-rich+H,Solids inclusions. Sepúlveda, 2004.
MARI	L-rich L-rich+H L-rich+H,Solids V-rich	[11-18]	T_h: [170 – 479] T_m: [270 – 468]	[35-52,5]	qtz	No described	Data obtained from L-rich, L-rich+H and L-rich+H,Solids inclusions. Sepúlveda, 2004.
PEUMO	L-rich V-rich L-rich+H L-rich+H,Sy L-rich+CO2	[5 - 40]	[233 – 411] in primary inclusions; [163 – 391] in secondary inclusions; [230-410] for fluid A; [200-400] for fluid B; [250-410] for fluid C.	[0.9 – 39] in primary inclusions. [4 -42] in secondary inclusions [0.9 – 10.7] for fluid A; [31 – 39] for fluid B. [15 – 25] for fluid C.	qtz and sph (no studies in the last)	V-rich existence.	Fluid inclusions data were classified under petrographic characteristics (primary/secondary FIAS and % volume of liquid inside inclusions) and reported. Herreros defined 3 main fluids in the vein A, B and C. Herreros, 2009

Table 3. Summary of Microthermometric data for fluid inclusions from Maqui, Lorena and Chilco veins.

Sample n°	vein	Host	FIA #	n°	FI Description	FI Type	Primary (P) / Secondary (S)	Th(V-L or L-V) range (°C)	Average Th(V-L or L-V) (°C)	Average Th (°C)	Tm range (°C)	Average Tm (°C)	Salinity range (wt% NaCl)	Average salinity (wt% NaCl)
241108Q1	Chilco	Sph	1	10	L-rich	V	P	289 to 294	292	292	-20.7 to -17.6	-18.6	20.7 to 22.8	21.4
241108Q2ZA	Chilco	Sph	2	9	L-rich	V	S	226 to 240	233	233	-10.1 to -9.5	-10.1	13.4 to 14.5	14.1
240910VQ1ZA	Lorena	Qtz	3	9	L-rich+IC	VI	S	264 to 268	266	330	329 to 332	330	40.5 to 40.8	40.6
240910VQ1ZB	Lorena	Qtz	4	10	L-rich+H,S1,S2	VI	S	265 to 271	268	343	341 to 347	343	41.6 to 42.1	41.7
240910VQ1ZC	Lorena	Qtz	5	6	L-rich+H,S1,S2	VI	S	267 to 276	270	309	306 to 312	309	38.6 to 39.1	38.8
240910VQ2	Lorena	Qtz	6	12	L-rich+IC,S1	VI	S	284 to 289	286	344	330 to 352	344	40.6 to 42.6	41.8
240910VQ3ZB	Lorena	Qtz	7	10	L-rich	IV	S	334 to 340	337	337	-12.9 to -11.8	-12.2	15.8 to 16.8	16.2
240910VQ3ZC	Lorena	Qtz	8	6	V-rich	III	S	521 to 525	523	523	-18.1 to -16.9	-17.1	19.6 to 21.0	20.3
240910VQ4ZB	Lorena	Qtz	9	8	L-rich + V-rich	I	P	480 to 484	482	482	-17.0 to -12.6	-15.1	16.5 to 20.2	18.6
240910VQ4ZC	Lorena	Qtz	10	8	L-rich+H,S1	VI	S	373 to 377	375	375	227 to 232	229.5	33.3 to 33.6	33.5
0411027ZA	Maqui	Sph	11	8	L-rich	V	S	326 to 336	331	331	-2.4 to -2.1	-2.2	3.5 to 3.9	3.6
0411027ZD1	Maqui	Qtz	12	6	L-rich+H + V-rich	I	S	381 to 386	383	501	500 to 502	501	59.8 to 60.1	59.9
0411027ZE1	Maqui	Qtz	13	6	L-rich+H + V-rich	I	P	405 to 424	414	515	511 to 520	515	61.3 to 62.5	61.8
240912Q1ZA	Lorena	Cal	14	7	L-rich + V-rich	II	S	528 to 533	530	530	-19.5 to -12.5	-15.5	16.4 to 22.0	19
240912Q1ZB	Lorena	Cal	15	7	L-rich + V-rich	II	S	383 to 405	392	392	-10.8 to -4.5	-8.2	7.2 to 14.8	11.9
240912Q2ZA	Lorena	Qtz	16	6	L-rich+H,S1,S2	VI	S	258 to 267	263	311	301 to 321	311	38.2 to 39.8	39.0
240912Q2ZB	Lorena	Qtz	17	4	L-rich+H,S1	VI	S	292 to 295	294	315	313 to 317	315	39.2 to 39.5	39.3
241117Q1ZA5	Chilco	Qtz	19	6	L-rich + V-rich	I	S	400 to 416	411	411	-3.5 to -3.3	-3.3	5.4 to 5.7	5.5
241117Q1ZC1	Chilco	Qtz	21	4	V-rich+H	VI	S	414 to 418	414	414	414 to 418	414	47.9 to 49.5	48.9
241117Q1ZE	Chilco	Qtz	22	11	L-rich	IV	S	183 to 212	200	200	-13.0 to -12.1	-12.5	15.9 to 16.8	16.4
2508163Q1Z2	Maqui	Qtz	23	4	L-rich	IV	P	345 to 350	347	347	-18.6 to -15.9	-17.5	19.4 to 21.4	20.6
2508163Q1Z6	Maqui	Qtz	25	6	L-rich	IV	S	400 to 405	401	401	-1.8 to -1.2	-1.5	2.1 to 3.1	2.6
250816Q1Z8	Maqui	Qtz	26	6	L-rich + V-rich	I	S	384 to 387	386	386	-0.3 to -0.1	-0.2	0.2 to 0.5	0.3
2508163Q2y3Z1	Maqui	Qtz	27	8	V-rich	III	S	445 to 455	450	450	-5.3 to -0.6	-2.3	1.1 to 8.3	3.9

Sample n°	vein	Host	FIA #	n°	FI Description	FI Type	Primary (P) / Secondary (S)	Th(V-L or L-V) range (°C)	Average Th(V-L or L-V) (°C)	Average Th (°C)	Tm range (°C)	Average Tm (°C)	Salinity range (wt% NaCl)	Average salinity (wt% NaCl)
241108Q2ZD	Chilco	Sph	29	5	L-rich	V	S	191 to 201	194	194	-11.9 to -11.1	-11.5	15.1 to 15.9	15.5
240912Q4ZA	Lorena	Qtz	30	6	L-rich+H,S1	VI	S	213 to 252	231	307	289 to 324	307	37.3 to 40.1	38.7
240912Q4ZB	Lorena	Qtz	31	4	L-rich+H,S1	VI	S	255 to 266	262	275	271 to 279	275	36.1 to 36.6	36.3
240912Q5	Lorena	Qtz	32	4	L-rich+H,S1	IV	S	251 to 259	255	356	350 to 359	356	42.4 to 43.3	42.9
240912Q6ZA	Lorena	Qtz	33	7	L-rich	IV	S	402 to 407	405	405	-7.9 to -3.9	-5.4	6.3 to 11.6	8.4
240912Q6ZB	Lorena	Qtz	34	6	V-rich+H	VI	S	359 to 384	369	524	521 to 529	524	62.6 to 63.8	63.1
2508162V2Q1ZA	Maqui	Qtz	35	7	L-rich + V-rich	I	P	318 to 326	321	321	-4.6 to -3.1	-3.6	5.2 to 7.3	5.9
240912Q4ZC	Lorena	Qtz	37	7	L-rich+H,S1	VI	S	240 to 245	244	276	271 to 279	276	36.1 to 36.6	36.4

Table 4. Elemental content of individual fluid inclusions. Results of LA-ICP-MS. All values are in ppm.

Sample n°	vein	host	FIA#	B	Na	K	Ca	Mn	Fe	Cu	Zn	As	Mo	Ag	Cd	Sb	Ba	Au	Pb
241108Q1	Chilco	Sph	1	537	42228	8181	36537					42		5			28		40
					35244	8372	37620					576		618			28		755
				609	35598	9922	37975					51		1194			31	3.8	
				401	32653	7581	40425					410		90			30		258
				471	32044	7853	39006					245		24			36		142
				524	34714	8268	35223					304		32			34		247
				99	21022	589	56809					1047		169			3		502
241108Q2ZA	Chilco	Sph	2	187	10410	3242	11582	23064		8903		118		12			155		751
				239	12412	4464	15397	15350		10797		133		12		12	199		1054
				245	14875	5363	17290	14000		4143		144		16		34	261		728
				274	15951	5397	18938	14159		312		169		15		31	282		784
				238	12406	4316	15644	21986		1664		137		20		29	226	0.3	660
				288	10192	6230	21389	13361		3911		148		21		38	299		1060
240910VQ1ZA	Lorena	Qtz	3		39544	31170	21817	33592	24266		9267	871		29	74		388		8672
					31981	37570	30473	33950	25939		9941						384		7794
					45639	32996	25257	31925	24134		9174			64			312		7002
240910VQ1ZB	Lorena	Qtz	4		50370	32841	20267	36702	21735		11229	437		24	63	65	292		8990
					65398	24785	18425	30008	23612		10699	455	8	25	47	35	119		5067
					51337	37288	19822	36174	17266		11458	368	10	24	57	55	349		9938
					70506	23800	15333	25648	21413		10812	679	10	34	73	45	234		13563
					46199	34184	15820	32308	27883		23747	732		31	30	69	123		1505
				277	60058	30353	12888	39187	16456	97	9971	246	9	22	62		291		9583
240910VQ1ZC	Lorena	Qtz	5		55920	26682	21902	29714	18847	384	6739	225	15	19	39		336		5733
					56284	27177	20265	28100	21178	277	7465	328		25	37		288		5527
					38651	34689	21752	35281	13198		16383			44			277		11541
					39792	29347	20645	26728	26689		15975			31			192		12378
					25253	30031	18668	34072	26363		21485	679			212		351		20565

Sample n°	vein	host	FIA#	B	Na	K	Ca	Mn	Fe	Cu	Zn	As	Mo	Ag	Cd	Sb	Ba	Au	Pb
240910VQ2	Lorena	Qtz	6		39025	44657	28500	30990	21142		7118	346		36	59		351		5336
					45264	51176	21807	31685	22177		7089	337		46	60		357		8283
					6982	28688	68160	22768	18766	488	23109	557		62	95		70		5288
					33133	37867	39263	30714	20335	507	12088			45	167		301		6280
					4037	40564	56847	25914	23140		21071	605		44	45		433		11136
					53950	46272	22062	30516	18745		5472	222		43	34		302		4939
240910VQ3ZB	Lorena	Qtz	7	887	34282	13751	11722	2586	216		294	293							169
				1016	35973	15836	9832	1539	132		196	266							
240910VQ3ZC	Lorena	Qtz	8		17714	17518	2725	8550	1458		1928	70		3	14	146	57		2470
					18143	12171	4192	6611	1761		2452	146		2		644	13		2954
					8988	8637	7343	5596	1224		1608	81				226	13		2054
240910VQ4ZB	Lorena	Qtz	9		4088	7727	2611	121	157					3		340	18		55
					5497	6909	2419	146	94							361	17		57
240910VQ4ZC	Lorena	Qtz	10		30693	23756	25535	40554	5125		10544	576		39	79		521		7999
					38332	17399	20816	38082	4469		15106	778					525		11148
					3402	39094	27532	53182	5860		13904	210			59		449		7409
					20157	38534	18777	39775	8934		13775	263		22	105		387		11464
0411027ZA	Maqui	Sph	11		5375	374	405			8494		862		25					312
					4076		1348			9536		533		22					218
					4891	640	311			8621		963		31					360
					4516		723			9309		769		21					204
240912Q1ZA	Lorena	Cal	14	1163	48362	21658					5078								4536
				1110	44709	20410					4577	361		8			677		3903
				1167	49013	22541					4256			11			814		5078

Sample n°	vein	host	FIA#	B	Na	K	Ca	Mn	Fe	Cu	Zn	As	Mo	Ag	Cd	Sb	Ba	Au	Pb
240912Q1ZB	Lorena	Cal	15	790	29427	14562				59	2661	393		6			423		2590
				834	34400	13551				76	2376	409		12			331		3320
					31323	14352					2315						210		2435
					29612	14993					2375						248		2400
				911	22501	23230					3327						79		2836
					30267	13518					3171	496		24			441		3172
240912Q2ZA	Lorena	Qtz	16		38801	31492	25563	29810	25688	346	7301	536		28			280		4578
				392	32119	38017	25146	30389	21842		10762	810		44	49		323		8251
				573	15442	43754	26195	35718	21461	85	19664	539		12	96	53	242		6692
				732	47839	30120	18804	30656	18686		9656	532		19	62	64	177		8129
241117Q1ZA5	Chilco	Qtz	19		14384	3309	3421										87		77
				804	13671	1959	2222		79			1299					20		39
					11527	2800	3331		300			2778					81		
241117Q1ZC1	Chilco	Qtz	21		436		174844		262					604	523		12		
					29978		18779							1424	1963		90		
241117Q1ZE	Chilco	Qtz	22		11960	2961	27659	1205	3111								22		171
					22022	2273	35188	502									43		
					20606	3925	21702	632	165		907			15			25		15226
2508163Q1Z6	Maqui	Qtz	25		7407	1433						620		9		2243			68
					7085	952						623		6		2303			52
2508163Q2y3Z1	Maqui	Qtz	27	345	1807	1549		505	468			1552				4674	3	1.5	837
				308	5211	4527		257	293			316		7		2051	8		525
				646	2035	1661		593	664			2441		9	17	7120	4	1.5	1242
241108Q2ZD	Chilco	Sph	29		34504	3943	21672							129			169		
					34288	4611	20964							289			196		
					35037	4226	20513							364			182		
					35502	3651	21648							116			193		
					35289	3380	22343							193			201		

Sample n°	vein	host	FIA#	B	Na	K	Ca	Mn	Fe	Cu	Zn	As	Mo	Ag	Cd	Sb	Ba	Au	Pb
240912Q4ZA	Lorena	Qtz	30	3218	10057	37455	23468	51896	3659		23683	927					377		15684
				509	51308	24467	21103	42235	4164		14054	243		19	82		411		7862
240912Q4ZB	Lorena	Qtz	31	771	6878	45193	25767	48531	5017		14138	269		4	70	14	512		10472
				493	9263	42197	22834	52732	8985		13999	407		11	53	32	407		9586
					48083	32352	20612	39163	22572		13850	582		26	113	68	275		11015
240912Q4ZC	Lorena	Qtz	37	448	22165	36844	25523	45209	5481		17084	246		14	54	14	167		3176
					35290	30208	18445	42018	8394		11474	364		11	81		386		9561
				363	34126	28678	19448	44761	9393		11058	315		14	62	22	362		10287
				550	28211	25671	20731	45138	12585		8225	309		9	57		635		8310
					44865	22060	15870	39525	10590		9826	403					301		8007
				366	12553	42550	19198	44863	5798		12287	270		7	106	20	1036		29975
				367	7301	45730	19466	49935	4577		17347	573		12	74	55	306		8582
				412	35464	31229	15598	36326	6123		12960	393		19	93	17	288		11118

Table 5. Ne and CO2 peaks measured in samples from Lorena. Maqui and Tribuna Este systems. ΔCO2 corrected. density (g/cm3) and pressure (psi) were calculated using equations 1.2 and 3 (in text).

Sample	System	Inclusion type	Ne measured	Ne measured	CO2 measured	CO2 measured	CO2 corrected	Density (g/cm3)	Pressure (Psi)	Pressure (Bar)
2508163Q2Y3	Maqui	Vapor-rich (Type III)	1031.67	1459.31	1286.31	1389.18	102.75	0.06	273.57	18.9
			1031.77	1459.32	1286.2	1389.22	102.93	0.12	584.35	40.3
			1031.77	1459.32	1286.2	1389.21	102.92	0.12	569.02	39.2
			1031.77	1459.32	1286.2	1389.21	102.92	0.12	569.02	39.2
			1031.74	1459.39	1286.39	1389.23	102.72	0.05	203.55	14
			1031.75	1459.43	1286.35	1389.97	103.49	0.32	890.05	61.4
241117Q1ZA1	Chilco	Vapor-rich+H (Type VI)	1031.89	1458.99	1286.3	1388.94	102.65	0.02	45.3	3.1
			1031.72	1458.03	1286.01	1388.75	102.94	0.13	612.28	42.2
0411027ZE	Maqui	Vapor-rich (Type III)	1031.84	1458.94	1286.33	1389.04	102.72	0.05	208.56	14.4
			1031.7	1458.95	1285.87	1388.69	102.8	0.07	362.59	25
			1031.81	1458.93	1285.69	1388.58	102.9	0.11	543.12	37.4
			1031.78	1458.9	1286.11	1388.8	102.7	0.04	152.63	10.5
			1031.73	1458.85	1285.16	1388.25	103.1	0.18	795.76	54.9
240910VQ3ZC	Lorena	Liquid-rich (Type IV)	1030.87	1458.01	1285.28	1387.95	102.67	0.03	94.59	6.5
			1030.79	1458.02	1285.19	1387.95	102.74	0.05	249.38	17.2

CAPÍTULO 4

DISCUSIONES

Las Figuras y tablas mencionadas en este capítulo corresponden a las citadas en el artículo científico del Capítulo 3.

Históricamente, el sistema hidrotermal del distrito minero de Alhué ha sido categorizado como un deposito epitermal de baja, intermedia y alta sulfidización (e.g. Piñana, 1993; Cotton, 1998; Herreros, 2009) así como también asociado a un sistema IRGS (*"intrusion related gold system"*) con afinidades mesotermales (Herreros, 2009; Harris et al 2013), cuerpo mineralizado tipo manto (Cotton, 1998), sistema tipo skarn rico en Zn-Pb-Ag (Cotton, 1998) y otros como por ejemplo un depósito de transición epitermal-mesotermal con alteración de sericita-adularia (Poblete, 2008). Existen en la literatura algunos ejemplos de depósitos con similares características como lo son la mina Groundhog en Nuevo México (Meinert, 1987; Hawksworth and Meinert, 1990) y las minas cerca del distrito mexicano San Francisco del Oro-Santa Barbara (Grant and Ruiz, 1988) en donde depósitos tipo skarn relacionados a pórfidos cupríferos son descritos (Cotton, 1998). En un intervalo reducido de sólo 300 metros de diferencia de cota las estructuras mineralizadas presentes en Alhué muestran un espectro que va desde cuerpos de afinidad mesotermal con minerales calcosilicatados a aquellas estructuras relacionadas sistemas de temperaturas bajas (epitermales) (Sillitoe, H.R., 2007). La transición de temperaturas mesotermales a epitermales presentes en Alhué puede ser observada no solo en las secuencias paragenéticas en donde calcita hojosa aparece al final de las etapas de mineralización (Figura 11 y Figura 15) pero también en la gran variedad de T_h que son obtenidas para un mismo sistema mineralizado (Figura 12, Figura 14, Figura 16, Figura 20 y Figura 28).

Algunas características particulares del deposito son: la presencia de mushketovita periférica, alteraciones sódico-cálcica (albita-epidota-actinolita) y potásica (feldespato potásico-biotita-magnetita), veta masivas de magnetita y la presencia de apatito y escapolita en algunas de las estructuras mineralizadas. El cuarzo podría ser por tanto considerado como un componente tardío en la formación de las estructuras mineralizadas que brechiza y cementa estructuras tempranas de minerales calcosilicatados y oxidos de hierro (Figura 4). El control principal de mineralización que presenta el depósito emplazado en la Fm. Las Chilcas corresponde al relacionado a la geología estructural (Figura 2). Fallas o estructuras de rumbo, normales e inversas son el target principal del distrito y pueden ser encontradas afectando a las 4 unidades principales del distrito: toba basal de líticos y cristales, andesitas inferiores, andesitas superiores, ignimbritas de tobas de cristales. Esta última secuencia pobremente mineralizada podría haber jugado un rol siendo el techo estéril de los clavos mineralizados presentes en el distrito. A una escala distrital, la Formación Las Chilcas corresponde a una zona de daño entre dos cuerpos de roca competentes (Intrusivos Cretácicos). Lo anterior hace posible la mineralización discontinua de estructuras de carácter distrital, como Maqui. La permeabilidad de esta zona de daño es relativamente alta por lo que los fluidos son más susceptibles de migrar a través de esta zona. Dilataciones co-

sismicas rápidas inducidas en ciertos sitios estructurales específicos como "*jogs*" dilatacionales y pliegues provocan reducciones localizadas y transitorias en la presión del fluido (Sibson, 2000). Consistentemente, presiones muy bajas fueron calculadas en arreglos de inclusiones fluidas ricas en vapor (asociadas a procesos de vaporización) alcanzando valores entre 3.1 – 61.4 [bares] (Figura 27, Tabla 5).

Evidencias teóricas, experimentales y observacionales de sistemas geotermales fósiles y actuales sugieren que los procesos de ebullición y/o vaporizaición son un mecanismo efectivo para precipitar oro y plata en sistemas hidrotermales (epitermales) (Brown, 1986; Seward et al., 2014). Se han encontrado características típicas de sistemas epitermales en cuanto a especiaciones mineralógicas, texturales y aquellas relacionadas a los arreglos de inclusiones fluidas en las muestras del distrito minero de Alhué. Por ejemplo, se han encontrado inclusiones fluidas ricas en líquido coexistiendo con inclusiones fluidas ricas en vapor en un mismo arreglo de inclusiones fluidas (Figura 9A, B and G) lo que significaría una prueba irrefutable de la presencia de ebullición en los fluidos del distrito (Bodnar et al., 1985; Goldstein and Reynolds, 1994). Similarmente, si la ebullición que ocurre es intensa (vaporización) tanto que poco o ningún líquido queda en el sistema, FIA compuestos de sólo inclusiones fluidas ricas en vapor se encontrarán (Figura 9E). Lo anterior es evidencia directa de que ebullición extrema (vaporización) ocurrió en los fluidos de Alhué. En síntesis, FIA asociados tanto a ebullición como a vaporización fueron encontrados durante la examinación petrográfica de las muestras de Lorena, Maqui y Chilco y documentados en secuencias paragenéticas de los tres sistemas en estudio (Figura 11, Figura 13, Figura 15). Cuando ocurre ebullición, las fases que precipitan suelen ser amorfas o de grano fino por lo que el atrapamiento de inclusiones fluidas primarias no es posible. Sin embargo, los fluidos en ebullición que al mismo tiempo precipitan fases amorfas o de grano fino pueden quedar atrapados como inclusiones fluidas de carácter secundario en fases previamente precipitadas que han cristalizado (o recristalizado) como granos más gruesos propicios para encapsular inclusiones fluidas. Debido a lo anterior, las inclusiones fluidas secundarias son una herramienta importante en el reconocimiento de fluidos que tuvieron ebullición, incluso si este mecanismo está siendo registrado por la ocurrencia de inclusiones que provienen de fluidos posteriores al que provocó la precipitación previa del mineral hospedante. La ebullición también condiciona la mineralogía y texturas minerales de un sistema hidrotermal debido a los cambios físicos y químicos que esta conlleva, incluyendo un decrecimiento abrupto de la temperatura, reducción de la cantidad de líquido disponible para acomodar componentes disueltos, pérdida de gases que llevan a cambios drásticos en la química del fluido y un incremento en el pH del fluido asociado a boiling (Moncada et al., 2017).

Las texturas descritas en este estudio son una probable consecuencia de la (re)-cristalización de silica amorfo o de la precipitación de calcedonia que responde a fluidos en ebullición. Proceso el cual es usualmente ligado a la precipitación de metales en sistemas hidortermales ricos en metales preciosos (Buchanan, 1979; Roedder, 1984; Bodnar et al., 1985; Brown, 1986; Simmons and Christenson, 1994; Etoh et al., 2002; Moncada et al., 2012). Muchas de las texturas que se encuentran en sistemas donde ocurrió ebullición fueron encontradas en las muestras del distrito minero Alhué (por ejemplo, textura mosaico,

plumosa, crustiforme, coloforme, peudo-acicular y calcita hojosa, Figura 7) siendo la textura en mosaico (*jigsaw*) en cuarzo la más común relacionada a ambientes de ebullición (47.8% de las muestras presentan esta textura, ver Figura 7A). La textura de mosaico (*jigsaw*) es una textura de recristalización caracterizada por agregados micro-cristalinos a cristalinos de cristales de cuarzo con bordes de grano inter-penetrados reconocibles solo a nicoles cruzados (Dong et al., 1995; Moncada et al., 2012). Esta textura es interpretada como el resultado de la (re)-cristalización de calcedonia masiva o sílice amorfo (Dong et al.,1995). Debido a su naturaleza, no se encontraron arreglos de inclusiones fluidas (FIA) primarios en este tipo de textura aunque si fue posible reconcer FIA secundarios que representan condiciones después de la (re)-cristalización de la calcedonia o sílice amorfo original.

En sistemas de agua pura, la solubilidad del cuarzo incrementa sistemáticamente con la temperatura hasta los ~370 °C, pero a temperaturas mayores, su solubilidad es retrograda (decrece con la temperatura). La presencia de sales alcalinas como NaCl, KCl reduce la solubilidad del cuarzo a bajas temperaturas pero la incrementa a temperaturas por sobre los 250°C (Williams-Jones, A.E. and Migdisov, A.A., 2013). Como resultado de lo anterior, un fluido sub-saturado en sílice puede alcanzar altos niveles de saturación provocando la precipitación abrupta de sílice amorfo. Con tiempo, el sílice amorfo puede recristalizar a sílice calcedónico y/o cuarzo (Fournier, 1985) para producir muchas de la texturas observadas en este estudio. Por ejemplo, textura en mosaico (*jigsaw*) caracterizada por cristales intercrecido de tamaño similar es un indicador de recristalización de sílice amorfo que precipitó desde una solución sobresatudara en sílice (Fournier, 1985).

Además de la textura mosaico de grano fino (*jigsaw*), otras texturas observadas en este estudio como la subhedral, plumosa (*feathery*), crustiforme, coloforme y pseudo-acicular corresponderían a procesos similares de precipitación de material desde fluidos sobresaturados en sílice o procesos de (re)-cristalización de calcedonia o cuarzo desde sílice amorfo. En cada muestra, la presencia de estas texturas fue descrita y usada para inferir si el proceso de ebullición ocurrió en la locación específica de la muestra en algún tiempo durante o posteriormente a la precipitación del material observado.

La presencia de adularia (observada en la secuencia paragenética de la estructura Lorena, ver Figura 13) en conjunto con la textura bandeada de cuarzo de tipo coloforme (Figura 7G) son consideradas evidencias directas de ebullición en tal estructura mineralizada. Un aspecto importante es que la fase electrum fue encontrada en cuarzo mosaico de grano fino implicando no solamente que la ebullición es reconocible a un nivel textural sino que además corresponde a un mecanismo eficiente de precipitación de oro y plata en las estructuras. Las texturas de ebullición fueron observadas en las secuencias paragenéticas de Lorena, Maqui y Chilco (Figuras 11, 13 y 15) y están siempre relacionadas a las etapas de mineralización independiente de la estructura. Además, un pulso epitermal relacionado a ebullición y temporalmente tardío se observa en las secuencias paragenéticas de Chilco y Maqui (Figuras 11 y 15) si se considera la presencia de calcite hojosa en las últimas etapas de mineralización (Figuras 7J, 11 y 15).

La pérdida de CO2 debido a la ebullición resulta en una rápida precipitación de calcita que favorece la formación cristales hojosos en lugar de romboédricos los cuales se forman comúnmente en crecimientos prolongados en el tiempo. Por lo tanto, la presencia de calcita hojosa corresponde a una fuerte evidencia de que efectivamente ocurrió ebullición en el sistema (Moncada et al., 2017). La presencia de texturas coloformes-crustiformes en cuarzo, feldespato potásico (adularia) y calcita hojosa indican la existencia de condiciones de ebullición que favorecen la precipitación de metales preciosos (Simmons and Browne, 2000) y dejan en evidencia la importancia de la ebullición en la precipitación de metales en en la muestras del distrito minero de Alhué. Además de las evidencias en texturas y fases minerales que involucran ebullición, y las observaciones realizadas en arreglos de inclusiones fluidas que respaldan este proceso (FIA tipos I y II en Figura 8), una gran variedad de FIA fueron descritos para las muestras de cada uno de los sistemas en estudio. Inclusiones fluidas ricas en líquido hospedas en cristales de cuarzo y esfalerita (FIA tipos IV y V en Figura 8 respectivamente) y FIA relacionados a fluidos hipersalinos portadores de cloruros y sólidos opácos (hasta 3) dentro de las inclusiones (tipo VI en Figura 8) son descritos en las estructuras de Lorena, Maqui y Chilco. Estos tipos de FIA (IV, V y VI) son también bastante comunes en las muestras del distrito y podrían contener evidencia de procesos no relacionados a ebullición o vaporización que pudieron haber mineralizado de igual manera el sistema con metales base y preciosos. Algunos hechos importantes a mencionar respecto a lo anterior son: (1) Los FIA tipo V (primarios) fueron encontrados (en algunos casos) relacionados a mineralización diseminada de calcopirita y pirita (sulfuros orientados según la orientación del arreglo ver Figura 9D) implicando que la precipitación de sulfuros estuvo directamente relacionado a inclusiones fluidas que representaban un fluido sin ebullición (proponiendo entonces que ni ebullición ni flashing fueron los mecanismos responsables en precipitar calcopirita, pirita, esfalerita, oro y plata). (2) Los FIA tipo VI presentan cristales hijos correspondientes principalmente a halite (aunque también se documentó la presencia bastante común de cloruros redondeados como silvita o cloruros de hierro) y sólidos (Figura 9C, H, I y J). En este tipo de inclusiones polifásicas (que contienen vapor, líquido y algunas veces más de dos sólidos a temperatura ambiente) ferropirosmalita, el extremo rico en hierro de la serie de pirosmalitas [$(Fe,Mn)_8Si_6O_{15}(OH,Cl)_{10}$] fue inferido a partir de espectros Raman. Usando espectroscopía Raman, dos bandas distintivas a los 615 cm^{-1} y 1022 cm^{-1} fueron identificadas y relacionadas al mineral en cuestión (Figura 26). Las inclusiones tipo VI (*L-rich+IC,S1*) que contenien ferropirosmalita ocurren en muestras de abundante cuarzo que contienen abundante mineralización de sulfuros. Durante experimentos de calentamiento, la ferropirosmalita se comporta de manera estable sin decrecimiento en tamaño hasta los 570°C (temperatura máxima ocupada en este estudio). Estas temperaturas altas de homogenización podrían corresponder a temperaturas de fluidos mineralizantes previos a la deposición de la mena (Adshead, 1996). Un hecho importante es que mediante el estudio microanalítico de LA-ICP-MS en inclusiones fluidas singulares (pero pertenecientes a un FIA en particular) se observó que las inclusiones tipo VI contienen las más altas concentraciones de hierro (~1000s to ~10000s ppm) consistentemente con la presencia de ferropirosmalita. Además, la

estructura mineralizada Lorena, en donde este tipo de inclusiones con ferropirosmalita en su interior era más abundante, es la estructura más rica en hierro de las tres estructuras en estudio. El hierro (roca total) en esta estructura presenta correlaciones positivas con Ag (roca total) y con la salinidad de las inclusiones. Lo anterior es consistente también con las señales transientes de LA-ICP-MS observadas para este tipo de inclusiones (tipo VI) en donde *peaks* notorios en Na, K, Mn, Ca, Fe, Ag, Pb, Zn, As, Cd fueron observados (Figura 22).
FIA tipo VI que homogenizan por desaparición de halita son comunes en todas las estructuras del distrito en estudio (Lorena, Maqui y Chilco) como pasa en muchos depósitos de origen hidrotermal, incluyendo pórfidos cupríferos (Bodnar and Beane, 1980), skarns (Baker and Lang, 2003) y yacimientos de hierro-cobre-oro (IOCG) (Niiranen et al., 2007).

Mediciones microtermométricas fueron realizadas en los seis tipos de FIA definidos previamente (ver Figura 8). En términos microtermométricos, las inclusiones fluidas fueron clasificadas por su comportamiento al calentarlas y considerando su fase anfitriona (cuarzo, calcita, esfalerita) y su origen genético (primario o secundario). Debido a la gran varieriedad de FIA presentes en las muestras del distrito minero de Alhué (Figura 8) existe una amplia variedad de T_h y salinidades observadas y reportadas a toda escala: distrital, por estructura y en una misma muestra (Figuras 20 y 21). Figura 28 muestra rangos estadísticos observados a escala global de fluidos precipitadores de mena para distintos tipos de yacimientos en términos de T_h y salinidad tomados de Wilkinson (2001) y muestra aquellas T_h y salinidades calculadas para las distintas estructuras del distrito minero Alhué (Lorena, Maqui y Chilco). Los datos son dispersos consistentemente con lo dicho anteriormente por lo que no se observa una tendencia ni agrupación en particular.

La variación en las temperaturas de homogenización (T_h) y salinidades en las estructuras (Maqui por ejemplo) refleja la diversidad de fluidos formadores de mena pero también podría reflejar la inclusión de datos (FIA) que no refieren a procesos de mineralización metálica. En estudios históricos de inclusiones fluidas, los autores acuerdan que la amplia distribución de T_h encontrada en las distintas estructuras mineralizadas (y también dentro de una misma estructura) indica la presencia de diferentes y múltiples eventos hidrotermales para cada estructura y por lo tanto cada una debe ser estudiada como un sistema aparte considerando variaciones sustanciales en los fluidos. La concentración de oro determinada por los análisis LA-ICP-MS en inclusiones fluidas sólo estuvo por encima del límite de detección de en tres FIA de dos muestras (muestra 241108 de Chilco y muestra 2508163 de la estructura Maqui) y correspondían a arreglos primarios y secundarios de los FIA tipo V y III respectivamente. En la muestra 241108 de Chilco, FIA primario y secundario asociados a inclusiones ricas en líquido hospedadas en cristales de esfalerita (tipo V) mostraron valores de 0.13 ppm de oro. En la muestra 2408163, FIA secundario del tipo III (inclusiones fluidas ricas en vapor hospedado en cuarzo) demostró valores de 1.5 ppm promedio de oro. Las salinidades de los FIA tipo V que poseían oro disuelto se calcularon entre los 14.1 y los 22.1 % en peso de NaCl equivalente. Debido a la naturaleza de este tipo de inclusiones, complejos clorurados deben ser un componente activo en el transporte de oro para la estructura de Chilco y sus mecanismo de precipitación deben ser distintos a los de

ebullición y/o flashing (pudiendo ser estos enfriamiento y/o mezcla) aunque FIA del tipo I, II (ebullición) y III (vaporización) son bastante comunes en esta estructura y por lo tanto deben estar participando de cierta manera en la precipitación de oro (Figura 19). Las inclusiones ricas en vapor hospedadas en cuarzo (tipo III) que transportaban oro en solución fueron observadas en un FIA correspondiente a una muestra de la superficie de la estructura Maqui (muestra 2508163). Este FIA de baja salinidad (2.8 a 3.9 % en peso de NaCl equivalente) está relacionado a concentraciones menores de oro consistentemente con la pérdida esperada de este metal precioso en una columna referente a un fluido en ebullición. En este tipo de fluidos H_2S es fuertemente fraccionado a la fase vapor disminuyendo como consecuencia la actividad de HS^-, provocando la precipitación de oro e implicando que HS^- también corresponde a un ligante importante a considerar en el distrito minero de Alhué. El distrito minero tiene, como se dijo anteriormente, un control estructural dominante. La "Falla de Borde" o "Falla Agua Fría" corresponde a una falla transtensiva con una alta importancia en la migración de fluidos profundos que mineralizan el sistema hacia cotas superiores. Esta falla ha sido interpretada de datos aeromagneticos como el límite entre el Plutón Agua Fría (Cretácico Inf.) al oeste y una cuenca rellena con una sucesión volcánica correspondiente a la Fm. Las Chilcas al este (Matthews, S. 2018). Esta falla tiene un carácter distrital a regional debido a su extensión (ver Figura 2) y naturaleza y podría haber sufrido una inversión durante su historia evolutiva. Figura 29 muestra un modelo general en donde fluidos de alta temperatura, probablemente productos de la desvolatilización de magmas máficos emplazados en la corteza profunda, ascienden y alcanzan condiciones someras de subsuelo mediante la utilización de este sistema de fallas interconectado observable en todas las áreas del distrito. A escala local, los procesos de ebullición y vaporización son mecanismos efectivos en la precipitación de metales preciosos y base en el distrito, aunque otros procesos no deberían ser descartados debido a la evidencia propuesta en este estudio.

CAPÍTULO 5

CONCLUSIONES

El distrito minero de Alhué tiene un control estructural fuertemente marcado y que domina sobre la mineralización Algunas de sus características peculiares son: la presencia de mushketovita perférica, alteraciones calcosódica (albita-epidota-actinolita) y potásica (feldespato potásica-biotita-magnetita, especialmente en la parte más suroriental del distrito), vetas de magnetita masiva y apatito y escapolita como fases mayores de ganga en algunas de las estructuras mineralizadas hacen consistente esta idea. El dominio estructural es el control principal y dominante de la mineralización. Dilataciones co-sismicas inducidas en ciertos sitios estructurales específicos como "*jogs*" dilatacionales, pliegues y puntos de encuentro entre estructuras provocan reducciones localizadas y transitorias en la presión del fluido que gatillan la acción de mecanismo de precipitación como ebullición y/o vaporización. Evidencias en texturas minerales y arreglos de inclusiones fluidas respecto a estos dos mecanismos de precipitación mineral fueron reportados en las tres estructuras mineralizadas en estudio (Maqui, Lorena y Chilco) pero podrían no ser la únicas participando activamente en la mineralización de metales preciosos y base en el distrito. La presencia de oro y plata en ambos, arreglos de inclusiones fluidas ricas en vapor hospedados en cuarzo (FIA tipo III) y arreglos de inclusiones fluidas ricas en líquido hospedados en esfalerita (FIA tipo V) implica que el oro es efectivamente transportado como complejo clorurado y sulfurado dependiendo del sistema. Aunque la secuencia paragenética de ciertas estructuras como Chilco muestras texturas de ebullición tardías en la etapa de mineralización (calcita hojosa), los datos sugieren que el oro está siendo transportado como complejo clorurado y precipitando por mecanismos distintos a los de ebullición y/o vaporización (probablemente enfriamiento o mezcla de fluidos). El enfriamiento puede ser un mecanismo efectivo en sistemas donde el oro es transportado como complejo clorurado pero la ebullición y/o la vaporización no puede ser del todo descartadas debido a la presencia de texturas e inclusiones fluidas que existe en la estructura Chilco. El oro en Maqui fue encontrado en arreglos de inclusiones fluidas ricas en vapor con valores entre 1.48 a 1.56 ppm. Complejos sulfurados son probablemente los transportadores de oro para este sistema debido a la naturaleza de los fluidos que reportan el oro. Los mecanismos de ebullición y/o vaporización tendrían un rol más protagónico en la precipitación de oro en ciertos sitios estructurales favorables (trampas de mena) como "*jogs*" dilatacionales por ejemplo para esta estructura. La estructura mineralizada correspondiente a Lorena representa la zona más profunda más profunda estudiada y contiene fluidos con una salinidad calculada superior a las otras estructuras estudiadas (Maqui y Chilco). Estos fluidos tienen cristales hijos en su mayoría correspondientes a halita y, en algunos casos, a otros cloruros y sólidos (transparentes y/o opácos). Además, las más altas temperaturas de homogenización fueron medidas en muestras de Lorena alcanzado valores de hasta 533°C lo que es concordante con temperaturas de fluidos que se encuentran más próximos a su fuente. Cristales hijos como ferro-pirosmalita dentro de arreglos de inclusiones fluidas en Lorena

dejan en evidencia fluidos ricos en hierro que mineralizan las estructuras más profundas. Las texturas de cuarzo observadas en las muestras del distrito minero Alhué corresponden a mosaico ("*jigsaw*"), subhedral prismático, plumosa ("*feathery*"), crustiforme, coloforme y pseudo-acicular son producidas por la directa precipitación desde fluidos sobresaturados en sílice (o bien por la recristalización de calcedonia o cuarzo desde sílice amorfo) lo cual es usualmente relacionado a la deposición de metales preciosos en sistemas hidrotermales. La presencia o ausencia de estas texturas fue utilizada en este estudio para inferir si el mecanismo de ebullición ocurrió o no en la locación de la muestra al mismo tiempo o posteriormente a la deposición del material original. En las tres localidades de Maqui, Lorena y Chilco se encontró evidencia de texturas mienrales y de arreglos de inclusiones fluidas que hacen referencia a procesos de ebullición y/o vaporización. Ebullición y vaporización como mecanismo de precipitación no pueden ser descartados para ningún sistema debido a la evidencia encontrada y son considerados relevantes para las estructuras en donde se muestra un gran espectro de evidencias (Maqui por ejemplo). Dado que existe una gran variabilidad respecto a la presencia de más o menos arreglos inclusiones fluidas que sugieren ebullición/vaporizaición, Maqui puede ser considerada una estructura con mayor contenido de FIA relacionados a ebullición/vaporización seguido por Lorena y finalmente Chilco y por tanto los mecanismos de precipitación mineral que respectan a estos procesos pudieron haber sido más protagónicos en Maqui y Lorena respecto a Chilco. Las texturas de ebullición pueden ser observadas en las tres secuencias paragenéticas y están relacionadas siempre a etapas de mineralización metálica. Electrum en cuarzo mosaico ("*jigsaw*") de una de las muestras de Lorena (240909) es un hecho importante en la demostración de que la ebullición efectivamente precipito metales preciosos como oro y plata en el distrito minero de Alhué. Inclusiones fluidas ricas en líquido hospedadas en cuarzo o esfalerita (FIA tipos IV y V) y arreglos de inclusiones que contienen cloruros y sólidos (hasta 3) relacionadas a fluidos hipersalinos (FIA tipo VI) fueron también descritos en las tres estructuras. Estos tipos de arreglos de inclusiones fluidas (FIA tipos IV, V y VI) presentan evidencia de mecanismos de precipitación no relacionados a ebullición y/o flashing que mineralizaron también el sistema. Algunos hechos importantes a mencionar respecto a lo anterior son: (1) Los FIA tipo V (primarios) fueron encontrados (en algunos casos) relacionados a mineralización diseminada de calcopirita y pirita (sulfuros orientados según la orientación del arreglo, ver Figura 9D) implicando que la precipitación de sulfuros estuvo directamente relacionado a inclusiones fluidas que representaban un fluido sin ebullición (proponiendo entonces que ni ebullición ni flashing fueron los mecanismos responsables en precipitar calcopirita, pirita, esfalerita, oro y plata). (2) Los FIA tipo VI presentan cristales hijos correspondientes principalmente a halita (aunque también se documentó la presencia bastante común de cloruros redondeados como cloruros de potasio o hierro) y sólidos (Figura 9C, H, I and J) implicando que la mineralización de Mn, Fe, Zn, Pb, Cd y Ag (elementos presentes en microanálisis LA-ICP-MS realizado en arreglos de inclusiones fluidas tipo VI en muestras de Lorena) es una respuesta a mecanismos de precipitación distintos a los de ebullición. Ferropirosmalita, el extremo rico en hierro de la serie de pirosmalitas [$(Fe,Mn)_8Si_6O_{15}(OH,Cl)_{10}$] fue inferido a

partir de espectros Raman hecho en FIA tipo VI que consistentemente mostraron valores altos de hiero (~1000s to ~10000s) medidos mediante LA-ICP-MS. FIA tipo VI que homogenizan por desaparición de halita son comunes en todas las estructuras del distrito en estudio (Lorena, Maqui y Chilco) como pasa en muchos depósitos de origen hidrotermal, incluyendo pórfidos cupríferos, skarns y yacimientos de hierro-cobre-oro (IOCG). En téminos microtermométricos, la gran variabilidad de temperaturas de homogenización y salinidades calculadas a toda escala: distrital, dentro de una misma estructura y en una misma muestra, correspondería a la gran diversidad de condiciones en las que se formó el distrito minero así como también, a una variabilidad en los procesos que gatillaron la mineralización y en los componentes geoquímicos actuando en cada una de las locaciones. Sin embargo, podría deberse también, al estudio de arreglos de inclusiones fluidas que no estuvieron involucradas directamente el proceso de mineralización metálica del distrito. Autores de estudios anteriores acuerdan que esta amplia distribución en temperaturas de homogenización encontrada en las distintas estructuras mineralizadas así como también dentro de una misma estructura indica la presencia de etapas múltiples de mineralización hidrotermal que mineralizaron las estructuras de manera desigual. Como se dijo anteriormente, la naturaleza estructural del distrito corresponde al control primordial de la mineralización en donde fallas transtensivas de carácter distrital como la falla “Agua Fría” hicieron posible la migración de fluidos hasta alcanzar condiciones someras de subsuelo y en donde los mecanismos de ebullición/vaporización pudieron haber ocurrido en conexión directa con paleo-sismos que gatillaron progresivamente la precipitación de oro y plata en el sistema durante un largo periodo de tiempo. Los mecanismos de ebullición y vaporización fueron efectivos en la precipitación de metales en el distrito pero otros mecanismos como enfriamiento y/o mezcla de fluidos no deberían ser descartados debido a la presencia presentada en este estudio.

BIBLIOGRAFÍA

Adams, S. F., 1920. A microscopic study of vein quartz. Economic Geology, v. 15, p. 623-664.

Adshead, N.D., 1996. Extended abstract, MIC'96. Townsille 1-4.

Aguirre, L., 1985. The Southern Andes, In: Nairn, A. E. M., Stehli, F. G., and Uyeda, S., (eds), The Ocean Basins and Margins: The Pacific Ocean, Volume 7A. New York, Plenum Press, p. 265–376.

Alcázar, P., 2001. Geología y estimación de reservas de Sistema de vetas Valeria, distrito minero Alhué región metropolitana. Memoria para optar al título de geólogo. Universidad de Chile. 100 p.

Araya, J., 2001. Informe geológico y evaluación de recursos distrito minero Alhué. Memoria de Título. Universidad de Chile, Santiago, Chile. 160 p.

Becker, S.P., Eichhubl, P., Laubach, S.E., Reed, R.M., Lander, R.H., Bodnar, R.J., 2010. A 48 m.y. history of fracture opening, temperature and fluid pressure: cretaceous Travis Peak Formation, East Texas basin. Bulletin of the Geological Society of America 122 (7/8), 1081–1093.

Bodnar, R. J., 2003a. Introduction to fluid inclusions, *in* Samson, I., Anderson, A., and Marshall, D., eds., Fluid Inclusions: Analysis and interpretation: Mineralogical Association of Canada, Short Course 32, p. 1-8.

Bodnar, R. J., 2003b. Reequilibration of fluid inclusions, *in* Samson, I., Anderson, A., and Marshall, D., eds., Fluid inclusions: Analysis and interpretation: Mineralogical Association of Canada, Short Course 32, p. 213–230.

Bodnar, R. J.; Beane, R. E., 1980. Temporal and Spatial Variations in Hydrothermal Fluid Characteristics during Vein Filling in Preore Cover Overlying Deeplly Buried Porphyry Copper-Type Mineralization at Red Mountain, Arizona. Economic Geology, Vol. 75, pp. 876-893.

Bodnar, R. J., Reynolds, T. J., and Kuehn, C. A., 1985. Fluid- inclusion systematics in epithermal systems. Reviews in Economic Geology, 2, p. 73-97.

Brown, K.L., 1986. Gold deposition from geothermal discharges in New Zealand. Economic Geology 81 (4), 979–983.

Buchanan, L. J., 1979. The Las Torres Mines, Guanajuato, Mexico: Ore controls of a fossil geothermal system. Unpublished Ph. D. dissertation, Colorado School of Mines, Golden, Colorado, 138 pp.

Buchanan, L. J., 1981. Precious metal deposits associated with volcanic enviroments in the Southwest. Arizona Geological Survey Digest, 14: 237-262.

Carter, W.D., 1963. Unconformity marking the Jurassic-Cretaceous boundary in the La Ligua area, Aconcagua Province, Chile. U.S. Geological Survey Proffesional Paper 450-E. p. E61-E63.

Corvalán, J., 1974. Paleozoic crystalline basement complex of central Chile. IAVCEI - International Symposium on Volcanology. Guide book D-6. Santiago-Chile: Departamento de Geología. Universidad de Chile. 1l pp.

Cotton, W. B., 1998. Geology and Ore Deposits of the Maqui Vein, Alhué Mining District, Coast Range of Central Chile. MS, University of Colorado.130 p.

Cotton, W. B. III, Atkinson, W. W. Jr, Sharaky, A. M., 1999. Geology and ore deposits of the Maqui vein, Alhué mining district, Coast Range of Central Chile. Geological Society of America, Annual Meeting, Denver, Colorado, USA, Abstract 52241.

Clark, J.R. and Williams-Jones, A.E., 1990. Analogues of epithermal gold.silver deposition in geothermal well scales. Nature, 346(6285): 644-645.

Diaz, S., 1986. Geología Económica y Prospección Geoquímica del área de la Mina La Leona, distrito minero Chancón, VI Región. Memoria para optar al Título de Geólogo. Universidad de Chile. 196 p.

Dong G, Morrison, G., Jaireth , S., 1995. Quartz textures in epithermal veins, Queensland; classification, origin and implication. Economic Geology. 90(6): 1841-1856.

Etoh, J., Izawa, E., Watanabe, K., Taguchi, S., Sekine, R., 2002. Bladed quartz and its relationship to gold mineralization in the Hishikari low-sulfidation epithermal gold deposit, Japan. Economic Geology 97 (8), 1841–1851.

Fournier, R.O., 1985. The behavior of silica in hydrothermal solutions. Reviews in Economic Geology 2, 45–61.

Frezzotti, M.L., Tecce, F., Casagli, A., 2012 Raman spectroscopy for fluid inclusión analysis. Journal of Geochemical Exploration. 112. 1-20.

Fuentealba C., 2002. Geología y Mineralización de Oro en el Distrito Minero de Alhué, Cordillera de la Costa de Chile Central. Memoria para optar al Título de Geólogo. Universidad de Chile. 96 p.

Gammons CH., Yu Y, Williams-Jones A.E., 1997. The disproportionation of gold chloride complexes at 25 to 200°C. Geochimica et Cosmochimica Acta 61: 1971-1983

Gana, P. and Wall, R., 1997. Evidencias geocronológicas ^{40}Ar-^{39}Ar y K-Ar de un hiatus Cretácico Superior – Eoceno en Chile central (33°-33°30'S). Revista Geológica de Chile. Vol. 24. No. 2. p. 145-163.

Ganerod, G.V.; Braathen, A.; Willemoes-Wissing, B., 2008. Predictive permeability model of extensional faults in crystalline and metamorphic rocks; verification by pre-grouting in two sub-sea tunnels, Norway. Journal of structural Geology. 30. 993 – 1004.

Grant, G. and Ruiz, J., 1988. Pb-Zn-Cu-Ag deposits of the Granadena mine, San Francisco del Oro-Santa Barbara district, Chihuahua, Mexico. Economic Geology. Vol. 83. Pp.1683-1702.

Gropper, J., 2011. Franjas metalogénicas de edad Jurásica y Cretácica en la cordillera de la costa de Chile central, entre los 32° y los 35° 20' de latitud sur. Memoria para optar al título de geólogo. Universidad de Chile.

Goldstein, R.H., Reynolds, T.J., 1994. Systematics of fluid inclusions in diagenetic minerals: SEPM Short Course Notes, 31, p. 213.

Harris, J., Matthews, S., Perez, M., 2013. Informe técnico campaña de exploración 2008-2012. Proyecto Chancón – Membrillo. Región metropolitana y libertador Bernardo O´higgins, Chile. Informe preparado por Yamanca Gold Inc. Inédito. 178 p.

Hawksworth, M. and Meinert, L., 1990. Alteration and Fluid inclusion study of the Groundhog vein system, Central Mining District, New Mexico. Economic Geology. Vol. 85, pp 1825-1839.

Hedenquist, J. W., Arribas, A. and Eliseo, G.-U., 2000. Exploration for epithermal gold deposits. Society of Economic Geologists Reviews, 13: 245-277.

Henley, R. W., and Hughes, G. O., 2000. Underground fumaroles: "Excess heat" effects in vein formation. Economic Geology, 95, 3, p. 453-466.

Herreros, D., 2009. "Caracterización geológica y antecedentes microtermométricos de la veta Peumo Distrito Valencia, Región Metropolitana, Chile. Memoria de título. Universidad de Concepción. Departamento de Geología. 106 p.

Herrington, R.J., Wilkinson, J.J., 1993. Colloidal gold and silica in mesothermal vein systems. Geology, v. 21, p. 539-542.

Hervé, F., Godoy, E., Parada, M. A., Ramos, V., Rapela, C., Mpodozis, C., and Davidson, J., 1987. A general view on the Chilean-Argentinian Andes, with emphasis on their early history, in Monger, J. W. H., and Francheteau, J., eds., Circum-Pacific orogenic belts and the evolution of the Pacific basin: Washington, D. C., American Geophysical Union, Geodynamic Series, v. 18, p. 97–113.

Hervé, F., Munizaga, F., Parada, M.A., Brook, M., Parkhurst, R., Snelling, N., Drake, R., 1988. Granitoids of the Coast Range of Central Chile: Geochronology and geologic setting: Journal of South American Earth Sciences, v.1, p. 185-194.

Iglesias Patrimoniales Chile, 2014. Historia de Iglesias Patrimoniales. http://iglesiaspatrimoniales.cl/iglesia-de-alhue-historia (acceso 13 de Agosto, 2018).

Johnson JW, Oelkers EH, Helgeson HC, 1992. SUPCRT92: A software package for calculating the standard molal thermodynamic properties of minerals, gases, aqueous species, and reactions from 1 to 5000 bar and 0 to 1000°C. Computers & Geosciences 18: 899-947

Lamadrid, H.M., Moore L.R., Moncada, D., Rimstidt J.D., Burrus, R.C., Bodnar, R.J., 2017. Reassessment of the Raman CO_2 densimeter. Chemical Geology. 450. 210-222.

López-Escobar, L., Frey, F., Oyarzún, J., 1979. Geochemical Characteristics of Central Chile (33-34°S) Granitoids. Contributions to mineralogy and petrology, 70, 439-450.

Lemmlein, G.G., 1929. Sekundäre Flüssigkeitseinschlüsse in Mineralen. Z. Kristallogr. 71, 237-256.

Levi, B., 1969. Burial metamorphism of a Cretaceous volcanic sequence west from Santiago, Chile: Contributions to Mineralogy and Petrology, v. 14, p. 39-49

Levi, B., Aguirre, L., Nystrom, J.O., Padilla, H., Vergara, M., 1989. Low-grade regional metamorphism in the Mesozoic-Cenozoic volcanic sequences of the Central Andes: Journal of Metamorphic Geology, v. 7, p. 487-495.

Levi,B., Padilla, H, Nyström, J., Vergara, M., 1988. Facies de Alteración Regional en las secuencias volcánicas Mesozoicas y Cenozoicas de Chile Central. Revista Geológica de Chile, Vol. 15, Nº 1. Servicio Nacional de Geología y Minería.

Lindgren, W., 1933 Mineral deposits, 4th edition, New York, McGraw-Hill, 930 pp.

Lindgren, W. and Bancroft, H., 1914. The ore deposits of the Republic mining district: U.S. Geological Survey Bulletin. 550, 147p.

Matthews, S., 2017a. Geología Distrital Florida. Informe inédito. Yamana Gold Inc.

Matthews, S., 2017b. Metamorfismo y alteración. Informe inédito. Yamana Gold Inc.

Matthews, S., 2018. Geología del Distrito Minero Alhué. Presentación inédita. Yamana Gold Inc.

Moncada, D., Baker, D., Bodnar, R.J., 2017. Mineralogical, petrographic and fluid inclusion evidence for the link between boiling and epithermal Ag-Au mineralization in the La Luz area, Guanajuato Mining District, México, Ore Geology Reviews.

Moncada D., Mutchler, S., Nieto, A., Reynolds, T.J, Rimstidt, J.D., Bodnar, R.J., 2012. Mineral textures and fluid inclusion petrography of the epithermal Au-Ag deposits at Guanajuato, Mexico: Application to exploration. Journal of Geochemical Exploration 114, p 20-35.

Meinert, L., 1997. Application of skarn deposit zonation models to mineral exploration. Explor. Mining Geol. Vol. 6. No 2. Pp. 185-208.

Munizaga, F. and Vicente, J.C., 1982. Acerca de la zonación plutónica y del volcanismo miocénico en los Andes de Aconcagua (lat. 32-33°S): Datos radiométricos K-Ar: Revista Geológica de Chile. Vol. 16. p. 3-21.

Muñoz-Cristi, J, 1964. Estudios petrográficos y petrológicos sobre el Batolito de la Costa de las provincias de Santiago, y Valparaíso. Inst. Geol. Univ. Chile. Publ. No. 25, 93 pp.

Nasi, C., 1981. Estratigrafía del Jurásico y Cretácico de la Cordillera de la Costa al sureste de Melipilla (Chile Central). Memoria de título (Inédito), Departamento de Geología Universidad de Chile,. 246 p.

Nasi, C., 1981. Estratigrafía del Jurásico y Cretácico de la Cordillera de la Costa al sureste de Melipilla (Chile Central). Memoria de título (Inédito), Departamento de Geología Universidad de Chile,. 246 p.

Nasi, C., Thiele, R., 1982. Estratigrafía del Jurásico y Cretácico de la Cordillera de la Costa al sur del río Maipo, entre Melipilla y Laguna de Aculeo (Chile Central). Revista Geológica de Chile Nº 16 p. 81-99.

Niiranen, T.; Poutiainen, M.; Manttari, I. Geology., 2007. Geochemistry, fluid inclusion characteristics, U-Pb age studies on iron oxide-Cu-Au deposits in the Kolari región, northern Finland. Ore Geology reviews. Volume 30. Issue 2, pages 75-105.

Ogryzlo SP., 1935. Hydrothermal experiments with gold. Economic Geology 30: 400-424.

Pincheira, M., Frutos, J., Hernádez, L., Zamarreño, J., 1994. Antecedentes mineralógicos texturales en la mineralización estratoligada del distrito Punta del Cobre, Chile. VII Congreso Geológico Chileno, Concepción, Chile, Vol. 2, p. 873-877.

Piñana, X., 1993. Mineralización epitermal de oro distrito minero “El Membrillo de Alhué”. Memoria para optar al título de geólogo. Universidad de Chile. 113 p.

Piracés, R., 1976. Estratigrafía de la Cordillera de la Costa entre la Cuesta El Melón y Limache, Provincia de Valparaíso. Chile. Primer Congreso Geológico chileno, Actas, v.1, p. 65-82.

Poblete, J., 2008. Geología, Alteración y mineralización en los prospectos Au-Ag Las bellas y Don Bernardo, comuna de Alhué, región metropolitana. Memoria para optar al título de geólogo. Universidad de Chile. 104 p.

Rodriguez, M., Campos, E., Barra, F., 2000. Antecedentes mineralógicos y microtermométricos del yacimiento Manto Verde, distrito minero Punta del Cobre, Norte de Chile. 5p. Inédito.

Roedder, E., 1984. Fluid Inclusions. Mineralogical Society of America. Reviews in Mineralogy, vol 12. 644p.

Rogers, A.F., 1917. A review of the amorphous minerals: Journal of Geology. v. 25. p. 515-541

Romero, N., Mundaca, P., 1997. Geología del Distrito Minero Alhué. Informe Inédito S.L.M. LAS CENIZAS. 55 p.

Sander, M. V. and Black, J. E., 1988. Crystallization and recrystallization of growthzoned vein quartz crystals from epithermal systems, implications for fluid inclusion studies. Economic Geology, 83, 5, p. 1052-1060.

Scambelluri, M.; Piccardo, G.; Philippot, P.; Robbiano, A.; Negretti, L., 1997. High-salinity brines from recycled seawater in deeply subducted serpentiinite. Earth Planet. Sci. Lett. 148. 485-499.

Seward, T.M., Williams-Jones, A.E. and Migdisov, A.A., 2014. The Chemistry of Metal Transport and Deposition by Ore-Forming Hydrothermal Fluids. In: 42 H.D.H.K. Turekian (Editor), Treatise on Geochemistry (Second Edition). Elsevier, Oxford, pp. 29-57.

Schrader, F.S., 1923. The Jarbidge mining district, Nevada: U.S. Geological survey Bulletin 741, 86 p.

Sepúlveda, F., 2004. Caracterización geológica y antecedentes microtermométricos de la veta Lorena, distrito minero Alhué, región metropolitana, Chile. Memoria para optar al título de geólogo. Universidad de Chile. 85 p.

SERNAGEOMIN., 2003. Mapa Geológico de Chile: versión digital, publicación geológica digital, No 4, Santiago, Chile, Servicio Nacional de Geología y Minería, escala 1:1000 000.

Seward, T.M., 1973 Thio complexes of gold and the transport of gold in hydrothermal ore solutions. Geochimica et Cosmochimica Acta 37: 379–399

Shaub, B.M., 1934. The cause of banding fissure veins: A:merican Mineralogist, v. 19, p. 393-402.

Sibson, R.H., 2000. Fluid involvement in normal faulting. Journal of Geodynamics 29. 469-499.

Sillitoe, R. H., 2007. Comments on the Alhué, Jerónimo, Esperanza and Encrucijada Gold Properties, Chile. Internal. Internal Meridian Report: Unpublished.

Simmons, S.F. and Browne, P.R.L., 2000. Hydrothermal minerals and precious metals in the Broadlands-Ohaaki geothermal system: Implications for understanding low-sulfidation epithermal environments: Economic Geology, 95: 971−999.

Simmons, S.F., Christenson, B.W., 1994. Origins of calcite in a boiling geothermal system. American Journal of Science 294 (3), 361–400.

Simmons, S.F., White, N.C. and John, D.A., 2005. Geological Characteristics of Epithermal Precious and Base Metal Deposits. Economic Geology 100th Anniversary Volume, Economic Geology; One Hundredth Anniversary Volume, 1905-2005: 485-522.

Stefánsson, A., Seward T.M., 2004. Gold(I) complexing in aqueous sulphide solutions to 500°C at 500 bar. Geochimica et Cosmochimica Acta 68: 4121-4143

Streckeisen, A., 1976. To each plutonic rock its propert name. Earth Science Reviews, 12: p.1-33.

Thomas, H., 1958. Geología de la Cordillera de la costa entre el Valle de la Ligua y la Cuesta Barriga. Instituto de Investigaciones Geológicas, boletín Nº 2, 86 p.

Van den Kerkhof, A.M., Hein, U.F., 2001. Fluid inclusion petrography. In: Andersen, T., Frezzotti, M.-L., Burke, E.A.J. (Eds.), Lithos. Special volume in honour of Jacques Touret: Fluid inclusions: Phase relationships- methods- applications, pp. 27–47.

Vergara, M., Levi, B., Nystrom, J.O., and Cancino, A., 1995. Jurassic and Early Cretaceous island arc volcanism, extension, and subsidence in the Coast Range of central Chile, GSA Bulletin, v. 107, no. 12, p. 1427-1440.

Vergara, M. and Drake, R., 1979a. Edades K/Ar en secuencias volcánicas continentales postneocomianas de Chile Central, su depositación en cuencas intermontañas restringidas: Asociación Geológicas Argentina. Revista XXXIV. Vol. 1. p. 42-52.

Vergara, M. and Drake, R., 1979b. Eventos magmáticos plutónicos en los Andes de Chile Central. II Congreso Geológico Chileno (Arica). Vol. 1. p. F19-F30.

Vikre, P.G., 1985. Precious metal vein systems in the National District, Humboldt County, Nevada. Economic Geology, 80(2): 360 -393.

Wall, R, Gana, P, Gutiérrez, A., 1996. Mapa Geológico del área de San Antonio-Melipilla. Regiones de Valparaíso, Metropolitana y del Libertador Bernardo O'Higgins. Servicio Nacional de Geología y Minería (Chile). Mapa geológico N° 2, escala 1:100.000. 20 p.

Huizenga, J.M., and Parker, A.G., 2017. Hydrothermal Au mineralisation caused by fluid decompression and cooling in dilatational cavities. In: EGRU Contribution (69), p. 57. From: FUTORES II Conference: future understanding of tectonics, resources, environment and sustainability, 4-7 June 2017, Townsville, QLD, Australia.

Wilkinson, J.J., 2001. Fluid inclusions in hydrothermal ore deposits. Lithos 55, 229-272.

Williams-Jones, A., Bowell, R., Migdisov, A., 2009. Gold in solution. Elements 5(5):281-287.

Wright, R.B., Wang, C.H., 1973. Density effect on the Fermi resonance in gaseous CO2 Raman scattering. J. Chem. Phys. 58, 2893–2895.

Wright, R.B., Wang, C.H., 1975. Effect of density on the Raman scattering of molecular fluids. II. Study of intermolecular interactions in CO2. J. Chemical Physics. 61, 2707–2710.